UNDERSTANDING HOW CHANGES IN DISTURBANCE REGIMES AND LONG-TERM CLIMATE SHAPE ECOSYSTEM AND LANDSCAPE STRUCTURE AND FUNCTION

by

JAMIE LEE WRIGHT

A DISSERTATION

Presented to the Environmental Studies Program and the Division of Graduate Studies of the University of Oregon in partial fulfillment of the requirements for the degree of Doctor of Philosophy

June 2022

DISSERTATION APPROVAL PAGE

Student: Jamie Lee Wright

Title: Understanding How Changes in Disturbance Regimes and Long-Term Climate Shape Ecosystem and Landscape Structure and Function

This dissertation has been accepted and approved in partial fulfillment of the requirements for the Doctor of Philosphy degree in the Environmental Studies Program by:

Scott Bridgham	Chairperson
Lucas CR Silva	Advisor
Krista McGuire	Core Member
Matt Polizzotto	Core Member
Daniel Gavin	Institutional Representative

and

Krista Chronister	Vice Provost for Graduate Studies

Original approval signatures are on file with the University of Oregon Division of Graduate Studies.

Degree awarded June 2022

© 2022 Jamie Lee Wright

This work is licensed under a Creative Commons
Attribution-Noncommercial-NoDerivs (United States) License.

DISSERTATION ABSTRACT

Jamie Lee Wright

Doctor of Philosophy

Environmental Studies Program

June 2022

Title: Understanding How Changes in Disturbance Regimes and Long-Term Climate Shape Ecosystem and Landscape Structure and Function

Long-term and anthropic climatic change intersecting with disturbances alters ecosystem structure and function across spatiotemporal scales. Quantifying ecosystem responses can be convoluted, therefore utilizing multiproxy approaches clarifies consequent responses beyond correlations. Throughout the Holocene, climate continuously changed, contributing to increasing drought duration in some regions, such as the Pacific Northwest (PNW) (early Holocene) of the United States (also late Holocene wetting), and more intense precipitation in others, like South America (mid to late Holocene). A dominant dictating force in terrestrial system compositions is climate (e.g., temperature and precipitation), which is observed through reoccurring biotic patterns existing across the globe (i.e., 'biomes').

Some biome distribution schematics designate biomes based on a shifting relationship between temperature and precipitation in which biomes can transition into others consequently mirroring climatic change. However, shifts in biomes are instigated on a lower level, such as the ecosystem scale where ecosystems dynamically respond to internal and exogenous forces. Consequently, ecosystems are perpetually fluctuating where multiple regimes can coexist under the same environmental conditions in which

feedbacks, perturbations, and regime resiliency can either reinforce ecosystem statuses or contribute to shifts.

My dissertation aims to elucidate ecosystem responses to climatic and disturbance changes specifically looking through a lens of carbon sequestration and stability. Understanding the persistence of carbon within an ecosystem is more prudent than ever given our current climate crisis. My research spans different hemispheres and time periods, where I utilize different approaches in each chapter to quantify ecosystem responses from varying angles. In Chapter II, I quantify how forest and savanna ecosystems have changed over the late Holocene across a large ecoregion (i.e., Brazil's Cerrado) using stable and radiocarbon isotopes within the soil. In Chapter III, I transition to a landscape scale in the PNW where I investigate how fire in tandem with post-fire management influence soil carbon stability and soil fungal community composition. Chapter IV encompasses the ecosystem level within the PNW, where I use a single sediment core and a multiproxy approach to reconstruct biogeochemical shifts throughout the Holocene in response to climatic and disturbance changes. My dissertation possesses previously published and unpublished coauthored research.

CURRICULUM VITAE

NAME OF AUTHOR: Jamie Lee Wright

GRADUATE AND UNDERGRADUATE SCHOOLS ATTENDED:

University of Oregon, Eugene
University of California, Davis

DEGREES AWARDED:

Doctor of Philosophy, Environmental Sciences, Studies, and Policy, 2022, University of Oregon
Bachelor of Science, Environmental Sciences and Management, 2017, University of California, Davis

AREAS OF SPECIAL INTEREST:

Soil Geochemistry
Carbon Stability and Sequestration
Ecosystem Ecology
Data Visualization

PROFESSIONAL EXPERIENCE:

Graduate Research Fellow, University of Oregon, 2018-2022

Graduate Teaching Fellow, University of Oregon, 2017-2021

Research Assistant, Horwath Biogeochemistry and Nutrient Cycling Lab, Department of Land, Air and Water Resources, University at California, Davis 2012-2013

GRANTS, AWARDS, AND HONORS:

Soderwall Foundation Research Grant (2021)

Marthe E. Smith Memorial Science Scholarship (2021- 2022)

Hill Fund Graduate Award (2020 - 2021;2019 - 2020)

David S Easly Memorial Award (2020 - 2021; 2021-2022)

General University Scholarship (2020 - 2021)

New Phytologist Trust travel grant (2019)

Barker Research Support (2018)

Promising Scholar Award (2017 - 2018)

Graduated with highest honors from University of California, Davis (2017)

Outstanding Senior Award (2017)

UC Davis Dean's List (2013 - 2017)

Luther and Marie Davis Scholarship (2016 - 2017;2014 - 2015)

Steindler Agricultural and Environmental Science Scholarship (2015 - 2016)

H. J. Heinz Scholarship (2015 - 2016)

LAWR Opportunity Fund Scholarship (2014 - 2015)

Beeghley-Merritt Scholarship (2013 - 2014)

PUBLICATIONS:

Wright, **J.L.**, Bomfim, B., Wong, C. I., Marimon-Júnior, B. H., Marimon, B. S., & Silva, L. C. R. (2020). Sixteen hundred years of increasing tree cover prior to modern deforestation in Southern Amazon and Central Brazilian savannas. Global Change Biology, 1–33. https://doi.org/10.1111/gcb.15382

Silva, L. C. R., Corrêa, R. S., **Wright, J.L.,** Bomfim, B., Hendrix, L., & Gavin, D. G. (2021). A New Hypothesis for the Origin of Amazonian Dark Earths. Nature Communications, 12(1). https://doi.org/10.1038/s41467 020-20184-2

ACKNOWLEDGMENTS

This research would not have been possible without the help of my coauthors, colleagues, and mentors. Ecosystem ecology brought me a unique experience where I had the privilege to work with countless brilliant scientists and wonderful technical support persons that allowed me to execute the research that inspires me. I would like to express explicit appreciation to Barbara Bomfim and Lucas Silva for their mentorship and assistance in helping me develop as a scientist. I would also like to thank all the members of my dissertation committee who were always willing to help when I had questions. In addition, the SPA lab members have been an invaluable asset over the years. Lastly Kaye L. Shek and Natalie J. Kozlowski were some of my biggest collaborators, and I cannot imagine doing my research without either of you.

This dissertation would have never come to fruition without the support of my loved ones who continuously reminded me that life is happening all around me and that I am a part of it as well.

TABLE OF CONTENTS

LIST OF FIGURES

Figure Page

CHAPTER II

CHAPTER III

CHAPTER IV

LIST OF TABLES

Table Page

CHAPTER III

CHAPTER I

INTRODUCTION

The Holocene provides a unique opportunity to study diverse ecosystems' responses to dramatic changes in climate and disturbance regimes. Throughout the Holocene, an epoch succeeding the last glacial period of the Pleistocene, (Roberts, 1998) climate continuously fluctuated, contributing to increased drought duration in some regions, such as the Pacific Northwest (PNW) of the United States in the early-Holocene (Nelson et al., 2011) and late-Holocene wetting. While causing more intense precipitation in others, like South America in the mid- to late- Holocene (Marchant & Hooghiemstra, 2004; Smith & Mayle, 2018). Climate is a dominant dictating force in terrestrial system compositions (e.g. temperature and precipitation), which is observed through reoccurring biotic patterns existing across the globe (i.e. 'biomes'(Freeman et al., 2013)). Some biome distribution schematics designate biomes based off a shifting relationship between temperature and precipitation (Whittaker, 1975) in which biomes can transition into others consequently mirroring climatic change. However shifts in biomes are instigated on a lower level, such as the ecosystem scale where ecosystems are 'dynamic regimes' (Scheffer st al., 2001; Scheffer & Carpenter, 2003) susceptible to change. Dynamic regimes build upon the theory of 'alternative stable states' in that it encompasses the idea that an ecosystem can transition into different regimes in response to internal and exogenous forces. However, regimes remain in constant fluctuation and are therefore never truly 'stable'. Multiple regimes can coexist under the same environmental conditions, referred to as bistable states, in which positive and negative feedbacks, internal and external perturbations, and regime resiliency can either reinforce regime statuses or contribute to regime shifts (Scheffer et al., 2001).

Regime shifts at the ecosystem level consequently influence regional cycles, such as carbon, that may scale up to affecting global cycles. Understanding the interaction between ecosystem dynamics and carbon cycling specifically remains imperative since carbon possesses a substantial role in both climate destabilization and stabilization. Currently, uncertainty in how much carbons soils and vegetation hold limits our understanding of the global carbon cycle and ability to quantify and predict carbon changes (Schlesinger & Bernhardt, 2013). This is important for a future climatic change, land-use changes, and disturbances, which contribute to ecosystem regime shifts, will likely amplify uncertainty. Looking into the past allows for a unique opportunity to observe interactions between climatic change and ecosystem dynamics, such as carbon. My research is divided into two distinct systems; tropical and temperate, to study paleolandscape-climate interactions in efforts to better understand their future interactions and their relation to carbon and nutrient cycling.

Dissertation Research

The objective of my dissertation is to understand how ecosystems have dynamically changed throughout the Holocene and their consequences for ecosystem function – specifically through a lens of carbon stability and sequestration. To achieve this objective, I collected samples from Northern and Southern hemispheres and varying spatiotemporal scales.

Multiple regimes have existed within Brazil's Cerrado ecoregion throughout the Holocene where forests and savannas coexist. Within this system, moisture as well as edaphic properties play crucial roles in a forest's ability to maintain a forest. On the other hand, adjacent savannas are more influenced by perturbation's, in that fire frequently influences reinforces savanna presence but does not penetrate the adjacent forests (Silva et al., 2008). Previous research has found evidence that the boundary between these two regimes within the area has fluctuated

throughout the Holocene, (Silva et al., 2008) thus the interaction of feedbacks, perturbations, and resiliency is likely stronger in one regime with respect to the other. In Chapter II of my dissertation, I build on this study with coauthors where we reconstructed vegetation cover over the past 1,600 years using stable and radiocarbon isotopes in the soil. Chapter II is titled "Sixteen hundred years of increasing tree cover prior to modern deforestation in Southern Amazon and Central Brazilian savannas" and is published in *Global Change Biology* (2020). This publication is coauthored by me, Barbara Bomfim, Corrine Wong, Ben H. Marimon-Júnior, Beatriz S. Marimon, and Lucas C.R. Silva. Our objective was to elucidate if previously reported expansion of woody vegetation was a localized phenomenon or if it represents a broader process caused by climate dynamics throughout the region.

In the Northern hemisphere – specifically the PNW – climate has shifted from drier and warmer conditions to wetter and cooler ones. However, anthropic forcing has shifted the trajectory of climate to promote more sporadic climate patterns. This shift contributes to increased drought, and shifting disturbance regimes, specifically more frequent and sever fires. Although extensive fire suppression throughout the Western United States (WUS) helped retain carbon on the landscape over the past 70 years, it also has predisposed these forests to high-severity wildfire especially in the face of climatic change and increased drought frequency. Chapter III of my dissertation is titled "Forest Soil Carbon Dynamics 20 Years After a Catastrophic Wildfire". This work is coauthored by me, Katherine L. Shek, Sydney Katz, Krista McGuire, and Lucas C.R. Silva. We sampled soils from fire-affected landscapes across the Rogue River-Siskiyou National Forest – where nearly 500 thousand acres burned in the 2002 Biscuit Fire. The objective was to understand how soil carbon stability and fungal community composition have changed in response to a catastrophic wildfire. Here, we hypothesized that (1)

TOC stocks will decrease along a fire intensity and management gradient, where low severity fires will have higher TOC stocks than unburned and moderate/high burn severity systems, (2) soil carbon will have higher "stability" in regions with lower fire severity and without post-fire management and (3) fungi composition will shift from ECM fungi dominance to saprotrophic across a fire severity and management gradient.

As aforementioned, climate has shifting dramatically throughout the Holocene in the PNW mirrored by ecosystems transitions/shifts. It is prudent to understand how ecosystems have responded to climate and disturbances to better understand how these systems will change in the face of rapid and anthropic climate change. Chapter IV is titled "Elucidating Ecosystem Productivity and Terrestrial Development in the Pacific Northwest" and is coauthored by me, Natalie J. Kozlowski, Dan G. Gavin, and Lucas C.R. Silva. Our objective here was to use a multiproxy approach of biological and geochemical indicators to first detangle how the surrounding terrestrial ecosystem responded to the intersection of climatic and disturbance shifts, and second, to quantify lake productivity changes along the same axis.

CHAPTER II

SIXTEEN HUNDRED YEARS OF INCREASING TREE COVER PRIOR TO MODERN DEFORESTATION IN SOUTHERN AMAZON AND CENTRAL BRAZIL SAVANNAS

From Wright, J.L., Bomfim, B., Wong, C. I., Marimon-Júnior, B. H., Marimon, B. S., & Silva, L. C. R. (2020). Sixteen hundred years of increasing tree cover prior to modern deforestation in Southern Amazon and Central Brazilian savannas. Global Change Biology, 1–33. https://doi.org/10.1111/gcb.15382

Contributions

J. L. Wright analyzed the data and wrote the manuscript. All coauthors contributed to the collecting of the samples and lab analyses of data acquired prior to July 2018. All authors contributed greatly to reviewing this manuscript prior to publication and provided insight and direction on figures and statistics.

Introduction

Over the past decade more than 200 million hectares of forested land were deforested (Austin et al., 2017) with approximately 40% of that deforestation occurring in Brazil's Amazon and Cerrado ecoregions (Levy et al., 2018). Earth system models suggest that tropical forest cover loss of this magnitude, if continued, will alter water and carbon cycles and climatic patterns (Garcia et al., 2016). For instance, atmospheric moisture increases significantly with forest cover due to tree transpiration, a process that favors continuous rainfall recycling (Spracklen et al., 2012), and buffers drought impacts regionally (Staal et al., 2018). Although this forest-atmosphere feedback can be used to predict linkages between changes in primary productivity and tree cover, and between tree cover and precipitation (Sternberg, 2001), many uncertainties surround the past and future of tropical ecosystems as a stabilizing climatic force. These

uncertainties are, at least in part, rooted in a lack of empirical data to parameterize scenarios before and after deforestation became a dominant planetary force (Silva & Lambers, 2018). In the present study, we address some of these uncertainties by measuring proxies to estimate long-term changes in forest-savanna distributions and carbon-water relations in a region of global significance, the Amazon-Cerrado transition of central Brazil.

The Amazon-Cerrado transition spans a broad climatic and ecological gradient, with tree cover increasing as moisture increases from seasonally dry savanna-dominated landscapes towards the Amazon monsoon core (Elias et al., 2019). At one end of the transition, Amazon rainforests dominate under the influence of the South American Summer Monsoon (SASM). At the other end of the transition, under more seasonal precipitation, different types of ecosystems coexist including grasslands, savannas, and riparian forests. Throughout the region, vast areas of relatively undisturbed vegetation (i.e. mostly protected from direct human impact until very recently (Freitas et al., 2018) allow for the study of connections between climate variability and ecosystem processes, such as water use and carbon accumulation in biomass and soils. For example, sharp forest–savanna ecotones (i.e. boundaries within a few meters), which are commonly found in the region, have been shown to shift with long-term changes in precipitation (Silva et al., 2008). At local scales, such sharp ecotones are also maintained by fires, which occur regularly in savannas but do not typically penetrate into dense forests (Hoffmann et al., 2012). At regional scales, fire frequency and intensity are influenced by precipitation. Thus, if sufficiently widespread, changes in precipitation can cause biome scale rearrangements as well as incremental expansion of tree cover outward from local forest-savanna transitions.

Due to high primary production, the expansion of woody vegetation in savannas can significantly increase carbon stocks aboveground and belowground (Silva 2017; Abreu et al.,

2017; Duarte-guardia et al., 2019). However, this is not always the case because many savanna species tend to invest a significantly greater portion of their net carbon gain toward belowground biomass (Miranda et al., 2014; Veldman et al., 2015). Beyond carbon sequestration, increasing tree cover in forests and savannas can increase precipitation due to increased transpiration (Spracklen et al., 2012; Zemp et al., 2017). Therefore, understanding long-term changes in tree cover is critical for understanding the future of essential ecosystem carbon and water cycling functions, as well as the role of those ecosystems in supporting high levels of biodiversity and endemism that characterize the region (Abreu et al., 2017; Brannstrom et al., 2008).

Previous studies have found a trend of forest expansion into savannas in Brazil since the mid Holocene, which has been interpreted as an indication of increased precipitation (Silva et al., 2008; Silva, 2014). Those studies were performed using a few strategically selected sites which indicated that tree cover increased near riparian forest margins as well as in some upland savannas. However, it remains unclear if this expansion of woody vegetation was a localized phenomenon or if it represents a broader process caused by climate dynamics throughout the region. To answer this question, we reconstructed forest and savanna tree cover across paleolandscapes using radiocarbon (^{14}C) dating and stable carbon isotope signatures ($\delta^{13}C$) of soil organic matter (SOM). This approach is based on two assumptions: (i) that the average age of SOM increases with depth through the soil profile, such that each profile represents a chronological sequence of vegetation inputs (Schmidt et al., 2011; Trumbore, 2000); and (ii) that differences in stable carbon isotope ratios between savanna and forest biomass occur due to marked differences in the relative abundances of trees and grasses and lead to unequivocal SOM isotope signatures from either ecosystem (Victoria et al., 1995; J. C. von Fischer et al., 2008). Based on these assumptions we moved beyond local reconstructions to generate current and paleo data from 83 different sites,

which allowed us to develop regional maps that relate SOM isotope signatures and spatial changes in ecosystem cover through time.

Materials and Methods

Study region

Our study region spans latitudinally from Pará State to Goiás State (4°S to 16°S) and longitudinally from eastern Tocantins State to central Mato Grosso State (46 °W to 56 °W) in Brazil (Figure 1). Annual precipitation ranges from 1250 mm to 2500 mm, with precipitation amounts and distribution varying significantly across the study region (Figure 1 A). Eastern and southern sites are characterized by strong seasonality (i.e. wet summers and dry winters) whereas more constant precipitation inputs persist near the monsoon core, at the northern and western sites (Ward et al., 2019). A less important temperature gradient exists throughout the study region with respect to the precipitation gradient, in which mean annual temperature ranges from 22 to 26 °C (Figure 1B). Across the region we gathered vegetation and soil data from 46 forests, 26 savannas, and 10 transitions (i.e. sites classified as forest-savanna ecotones) from a combination of published (Silva et al., 2010; Silva et al., 2008) and new sampling locations (Supplemental Table 1). Soil taxonomy was determined at order level using the Brazilian soil classification system and converted to the nearest matches in the USDA system (Soil Survey Staff, 2014). We controlled for recent changes in land use and vegetation cover when choosing sampling sites. First, we excluded sites that displayed distinct signs of human disturbance (e.g. deforestation, non-native species, or grazing). Second, we relied on local expert collaborators to identify and exclude any sites where the floristic composition and vegetation structure could not be classified as typical of native forests and savannas. Finally, all selected sampling locations correspond to legally protected public or private land where forests and savannas appeared to be

at steady conditions, with no major changes in vegetation cover or land conversion, detectable in ~20 years of satellite images (Didan, 2015; AppEEARS Team, 2019).

Ecosystem cover

To characterize ecosystem cover we measured leaf area index (LAI) in forests and savannas throughout the region using a combination of standard ground-based and satellite-based measurements (Ladd et al., 2013). A negative relationship between current LAI and $\delta^{13}C_{SOM}$ is to be expected because trees and other C_3 woody plants discriminate more against the heavier ^{13}C carbon isotope relative to ^{12}C than do C_4 grasses (Smith & Smith, 2015), which dominate in this region and give rise to unequivocally distinct $\delta^{13}C_{SOM}$ signatures. Previous research has found a significant linear relationship between topsoil $\delta^{13}C_{SOM}$ values and LAI (Ladd et al., 2014), which allows for reconstructing past tree canopy cover using deep $\delta^{13}C_{SOM}$ signatures. Although input and decomposition rates vary significantly with ecosystem type, as well as soil properties and microbial community composition, there is no overlap between SOM carbon isotope signatures from tree- and grass-dominated systems in our region (Ladd et al. 2014). Here, we build on that finding by adding 83 new sites to improve the quantitative inference of tree cover from $\delta^{13}C_{SOM}$ values. Our data confirm expectations and show a significant decline in $\delta^{13}C_{SOM}$ with increasing LAI measured using ground-based measurements and Moderate Resolution Imaging Spectroradiometer (MODIS) 15A2 and MCD15A3H (accessed 2019-08-20 from https://doi.org/10.5067/MODIS/MCD15A3H.006) (Appendix 1).

Ground-based LAI measurements were taken with a 180° hemispherical lens to estimate total tree cover per area of ground cover across all vegetation types captured from approximately 1 m above the soil surface at forested sites, which typically lack grass cover, and at approximately 1 m height and at the soil surface for savanna sites to incorporate grass cover.

Ground-based LAI calculations were done using the open source Gap Light Analyzer (GLA) software (Frazer, 1999), where the blue color plane was used as a threshold to better distinguish between sky and vegetation. The LAI estimates obtained in this way represent total tree cover rather than green leaf area per se, such that our values of LAI include stem area, as well as leaf area. In forests, C_4 grasses are non-existent, but when tree cover declines C_4 grasses dominate open ecosystems, therefore, the resulting relationship between ground- and MODIS-derived LAI is unambiguous ($R^2 = 0.91$; p-value < 0.0001) and tree cover can be inferred from SOM carbon isotope ratios (Figure 2).

Soil sampling

Soil samples were collected from forest (n = 46), savanna (n = 26), and forest-savanna transition zone (n = 10) ecosystems. At each site, up to five soil profiles were collected near the LAI measuring location (when measured with ground-based technique). The regions with fewer sample sites are within the Amazon ecoregion where forests have persisted since at least the mid-Holocene (Smith & Mayle, 2018). The exact location and number of profiles sampled at each site are shown in Supplemental Table 1. The majority of soil profiles extended to a depth of approximately 100 cm. At some sites, we were capable of sampling down to 200 cm depth. At few locations, shallower profiles were collected where the bedrock was reached before a 100 cm depth. Soil samples were retrieved in 5 to 10 cm increments, sieved, air-dried and homogenized by depth of collection within each site. This effort resulted in 742 individual samples which were subsequently prepared for analysis of total organic carbon content and stable isotope ratios. A representative number of samples were selected for determination of radiocarbon activity as follows.

Soil carbon: Age-depth model and vegetation reconstruction

To determine changes in ecosystem cover, we used stable carbon isotope signatures ($\delta^{13}C_{SOM}$ given in permille (‰) units), which compare the proportion of ^{13}C to ^{12}C in SOM of each sample relative to an internationally accepted standard (Vienna PeeDee Belemnite). For this analysis, bulk SOM samples of all 742 individual samples were ground and homogenized after the removal of undecomposed plant material, powdered using an automated ball mill and manually encapsulated in 5x8 mm tin capsules (sample size approximately 0.25 to 0.70 mg). Isotopic ratios were determined by dry combustion gas chromatography coupled with continuous-flow isotopic-ratio mass spectrometry (GC-IRMS 20-20/ANCA-NT; Europa, Crewe, UK, at the University of California, Davis Stable Isotope Facility), measured with expected standard deviation <0.2‰. Carbon content per sample was calculated to optimize aliquot amounts for radiocarbon dating. Soil samples were prepared following standard procedures, air-dried and passed through a 2 mm sieve in which aliquots were ground using a ball mill in preparation for $\delta^{13}C$ analysis and ^{14}C dating. Approximately 800 mg of bulk soil were sent to the University of California, Irvine Keck Carbon Cycle Accelerator Mass Spectrometer Facility, where a precision of ~1% on samples with 100 µg or more of carbon is routinely achieved.

To determine changes over time, we measured radiocarbon (^{14}C) activity in 43 strategically selected depths from soil profiles sampled in forests (n = 20), savannas (n = 11), and forest-savanna transitions (n = 12) considered representative of each ecosystem and soil type. This effort resulted in calibrated radiocarbon dates for profiles sampled in about one third of all sampled sites (26 out of 83). Only a few sites were suspected of containing carbonates (3 out of 83) based on pH, a one-way ANOVA showed no significant difference (p-value = 0.83) between acid treated and non-treated $\delta^{13}C_{SOM}$ aliquots of those samples. We found that three riparian sites (likely seasonally flooded) had current SOM ^{14}C signatures at deep layers (≥ 80 cm). Those sites

were removed from the analysis. No statistical differences were found on the basis of soil type (p-value >0.05) using an ANCOVA test. We used the same test for ecosystem types and found that only forest-savanna transitions possessed statistically different regression slopes from other ecosystems. Therefore, we chose to use a single regression including forests and savannas even though we found high site-specific variation around the age-depth mean (as shown in the Figure 3). Consequently, the average age of vegetation change reported here should be understood as a regional approximation rather than a precise date for shifts within sites, which require local analysis and interpretation as each site. A linear age-depth regression explains most of the variance in SOM age across sites ($R^2 = 0.73$; p-value < 0.0001; Figure 3). The vast majority of soil profiles surveyed extended to at least 80 cm depth and yielded sufficient SOM for isotopic analysis (Figure 4). For this reason, 80 cm was used as the reference depth/age for comparison of past vegetation cover across the region (Figure 5). At the selected depth, the average age across sites is 1,595 years before present and the standard error of the mean is 404 years (Figure 3), hereafter referred to as ~1,600 years for simplicity.

The results reported here represent isotopic ratios and radiocarbon activities of organic carbon pools. To ensure that inorganic carbon was not included in the analysis, soil pH was measured in samples suspected of possessing carbonates, which are rare in Oxisols but common in some dolomite outcrops near the north-easternmost sites (Silva et al., 2010). Potential presence of carbonates (pH>5) was identified for three sites (Site 79, 81, 82; Supplemental Table 1). Samples from those sites were treated with hydrochloric acid (HCl) and resubmitted for analysis of radiocarbon and stable isotope ratios. The samples were subsequently put into an oven until the HCl solution evaporated. The samples were repeatedly washed with DI water to bring the pH above 4.0. Some samples were centrifuged to separate fine particles from solution

in order to minimize sample loss. The samples for carbon stable isotope analysis were treated with 1 M HCl to remove carbonates. Two milliliters of the 1 M HCl solution were added to each sample of approximately 0.25 to 0.70 mg in a glass vile, in which samples were placed in an oven until the HCl solution evaporated. To determine if there was a significant difference between acid treated and non-treated soil samples for stable isotope analysis ($\delta^{13}C_{SOM}$ values), a one-way ANOVA was performed. Two standards were acid-washed using the same procedure applied to soil samples. The standards included a modern and a 'dead' sample in which the modern sample came from deciduous tree leaves and the dead was anthracite coal. These standards were used to make background corrections when analyzing soil samples' ages (Santos et al., 2019). The samples for radiocarbon dating were treated with 0.1 M HCl.

Spatial interpolation and regional analysis

To reconstruct paleolandscapes across the study region, interpolation maps were generated using ordinary kriging, as in previous geostatistical studies of soil data (e.g. Elbasiouny, et al., 2014; von Fischer et al., 2008). This approach allows predictions of unknown spatial data to be determined with minimum variance and removed bias under the following assumptions: variation in the data is random and stationary (Oliver & Webster, 2014). The method fits a variogram model to the data, in which a variogram is the semivariance as a function of the data's direction and distance separation. The only input data was $\delta^{13}C_{SOM}$ with their corresponding coordinates. Since no other variable was interpolated, ordinary kriging was used instead of alternative kriging methods.

Maps were first made for the current environment using topsoil data (0-10 cm), intermediate layers (i.e. 30 cm, 50 cm, 70 cm) and down to a depth of 80 cm. Then a change 'heat map' for its difference relative to current conditions was developed (i.e. topsoil minus 80

cm layer). We used a depth of 80 cm for two reasons. First, on the basis of $\delta^{13}C_{SOM}$ signatures it was apparent that significant changes in vegetation cover happened across most sites at age corresponding to that depth (i.e. ~1,600 years ago). Second, the majority of sites had profiles that would go to that depth or beyond. The heat map of change was generated by subtracting the intermediate layer at 80 cm from topsoil so that the direction of change would correspond with forest or savanna $\delta^{13}C_{SOM}$ signatures (i.e. negative values represent increasing tree cover and positive values indicate decreasing tree cover). Averages were used when sites had multiple samples from the same depth interval. One of the study sites (Site 56, Supplemental Table 1) located deep within the Amazon was removed when generating the interpolation maps due to its distance from other clustered sites, which decreased the robustness of the interpolation maps. Notably, that site has been relatively 'stable' meaning that its $\delta^{13}C_{SOM}$ profile signatures have been that of a dense forest for the past several thousand years which does not affect our analysis of change in tree cover at other locations since ~1,600 years ago.

In some regions of our interpolation map, fewer data points exist and the spatial variance increases in those regions, but tree cover increased in the vast majority of sites regardless of variance within and across ecosystem. To evaluate the robustness of the underlying variogram we used goodness-of-fit analysis for each kriging map applying different common variograms (i.e., exponential, spherical, Gaussian). To quantify goodness-of-fit, each models' root mean square error (RMSE) values were quantified after performing cross-validation on each model type. The variogram model that fit the data the best was the exponential model based on cross-validation and RMSE values (2.8, 3.4, 3.6 for topsoil, intermediate, and change layer). For simplicity, we only present the best models selected through this approach. A one-way ANOVA was run between the observed and fitted groups generated from kriging, displayed that the

observed and fitted values were not statistically different (p-value = 0.90, p-value = 0.39, p-value = 0.43), consequently indicating that the ordinary kriging model fits our data.

To investigate whether climate (regional and local) matched tree cover we used previously reported oxygen (Ward et al., 2019) and strontium (Wortham et al., 2017) data from speleothems. Oxygen data was collected throughout Brazil, as observed in Figure 1 of Ward et al., 2019 and strontium data locations are shown in Figure 1, denoted by blue stars. Oxygen isotope ratios ($\delta^{18}O$) reflect regional SASM intensity and strontium isotope ratios ($^{87}Sr/^{86}Sr$) reflect soil moisture and rock dissolution (Wortam et al., 2017; Ward et al., 2019). Speleothem isotope ratios where normalized (z=(x-mean)/stdev) within each site to allow for trends to be compared across sites. To better interpret the average regional change in vegetation cover over space and time, we used a mixing model (Parnell 2020) to quantify C_3- versus C_4-derived contributions to the bulk $\delta^{13}C_{SOM}$ signatures between topsoil (10 cm) and an intermediate depth (80 cm) of known age (Supplemental Figure 1). Source values for $C_3$and C_4 vegetation were based on typical grassland and forest signatures measured across the region (-27‰ and -12.5‰; respectively). A Tukey HSD test was performed to determine at what depth differences in $\delta^{13}C_{SOM}$ signatures became significant within each ecosystem relative to the topsoil (0-10 cm).

Soil carbon: Stocks and relationship to changes in vegetation

To better understand whether and how changes in forest and savanna cover influence soil carbon stocks, we quantified soil carbon concentrations at each study site profile and soil depth. To better estimate the timing of vegetation change and its resulting effects on soil carbon stocks, bulk density (g/cm^3) from a subset of typical forest, savanna, and transition ecosystems were supplemented by radiocarbon and stable isotope datasets from previously published studies conducted in central Brazil (Silva et al., 2008; 2010; 2013). To match the analysis of ecosystem

cover (described above) we report carbon stocks down to 80 cm at all sites. The relative contribution of C_3 and C_4 plants to SOM across sites are shown in Supplemental Figure 1. A mixed-effects model was applied to test the significance of fixed effects (ecosystem type, soil order, and paleovegetation) as well as random effects (sampling site nested within ecosystem type) on soil carbon stocks (Supplemental Figure 2). The geographic location and basic description of ecosystem and soil types at all sites are shown in Supplemental Table 1.

Results

Current ecosystem cover and $\delta^{13}C_{SOM}$

In Figure 2 we show a linear regression describing the relationship between LAI and topsoil $\delta^{13}C_{SOM}$ to be significant ($R^2 = 0.23$; p-value < 0.0001; error = 2.15) which is consistent with previous studies of this kind (Ladd et al., 2014). However, when we applied a non-parametric function (locally weighted regression) to our data, the relationship improved and possessed a lower model error ($R^2 = 0.30$; error = 2.06). In either scenario, carbon isotopic signatures become more negative (i.e. representative of increasing tree cover or woody vegetation dominance) as LAI values increase. Conversely, increasingly positive carbon isotopic signatures are found with declining LAI and dominance of herbaceous plants, which in this region means increasing dominance of C_4 grasses.

Soil carbon: Age-depth model and vegetation reconstruction

In Figure 4 we show all $\delta^{13}C_{SOM}$ data by profile and site. The vast majority of sites show trends within profiles that indicate a gradual change in carbon isotopic signatures due to woody vegetation expansion or densification. Least square regressions are used to describe significant changes in $\delta^{13}C_{SOM}$ within each sampled profile (grey lines) in forests, savannas, and transition zones. The proportion of our sites that can be linked to changes in vegetation cover (Figure 5) is

based on a four permille threshold for ecosystem stability, which excludes enrichment or depletion from diagenetic fractionation. Based on those criteria we quantified a major shift in paleovegetation cover in which 7.7% (five) of the sites' $\delta^{13}C_{SOM}$ values became more positive (i.e. moving towards grass-dominated signatures), 24.6 % (16) remained stable (less than plus or minus two permille), and 67.7% (44) became more negative (i.e. moving towards tree-dominated signatures) moving up the soil profile.

The rate of vegetation change was significantly different (p-value <0.001) among ecosystem types, but the coefficient of variation for changes in vegetation within forest, savanna, and transition sites was high (74.0%, 55.0%, and 281%, respectively). Despite large variability among sites, a consistent increase is woody vegetation cover was observed for the vast majority of forest and savanna ecosystems. Figure 4 (a-c) shows the rate of vegetation change for each soil profile down to a depth of 200 cm, in which depth averages (the black points), individual soil profile linear regressions (grey lines - if significant with a p-value <0.05, are included within each plot). Depth averages per ecosystem type are included in Supplemental Table 3. The proportions of C_3 and C_4 plants contribution to SOM was calculated using a stable isotope mixing model for topsoil (current) and deep soil (70-80 cm; old) for all forest and savanna ecosystems (Supplemental Figure 1). A Tukey HSD test showed that $\delta^{13}C_{SOM}$ isotopic signatures became statistically different from current values at depths ranging from 30 to 50 cm at most forests and savannas. At transition zones, current $\delta^{13}C_{SOM}$ isotopic signatures did not differ significantly from other depths. A mixed-effects model (Supplemental Figure 2) including the random effect, sampling site nested within ecosystem, performed better than other models that included no random effects. The fixed effects of depth, ecosystem type and their interactions had significant effects (p-value <0.05) on the response variable ($\delta^{13}C_{SOM}$). Soil order did appear to

have a significant effect (p-value >0.05) on $\delta^{13}C_{SOM}$, however, soil order improved the overall model when included. Model quality comparisons were derived from the Akaike Information Criteria (AIC) in which smaller values indicate better model fit.

Spatial interpolation and regional analysis

The $\delta^{13}C_{SOM}$ kriging maps for topsoil (0-10 cm), intermediate layers, and deep soil (70-80 cm), and their difference heat map between 80 cm and topsoil (Figure 5) showed that the vast majority of sites (67.7% of all sampled profiles) followed a trend of woody vegetation expansion and densification over time. The few instances in which tree cover declined (7.7% of all sampled profiles) were associated with dry conditions in savannas on rock outcrops at the easternmost sampling sites, which as shown in Figure 1, are characterized by warm and dry climate. The topsoil map (Figure 5a) represents current ecosystem cover as a function of C_3 vs C_4 abundance, with $\delta^{13}C_{SOM}$ ratios consistent with typical forest and savanna isotopic signatures (ranging from -29‰ to -18‰). The deep soil layer at 80 cm selected for mapping (Figure 5a), representing past ecosystem cover ~1,600 years ago, shows a landscape dominated by more positive $\delta^{13}C_{SOM}$ ratios (i.e. less negative values that are characteristic of savannas and grasslands) ranging from -26‰ to -13‰. The intermediate depths, which have been converted to years before present, suggest that the trend of woody vegetation expansion and densification has been a gradual shift over time rather than an abrupt transition, which is often characteristic of anthropic interventions. Using the linear model presented in Figure 2 the observed changes in $\delta^{13}C_{SOM}$ ratios can be converted to units of LAI (Supplemental Table 4). We only used our linear regression to convert $\delta^{13}C_{SOM}$ ratios to LAI, since it is consistent with previous studies (Ladd et al., 2014).

Topsoil soil $\delta^{13}C_{SOM}$ is known to reflect differences in vegetation cover across biomes, especially in tropical regions where the isotopic difference between tree- and grass-dominated

system reaches its maximum value (Ladd et al 2014). As expected, we found a significant negative relationship between LAI and current $\delta^{13}C_{SOM}$ ratios, which serve as a baseline from which past ecosystem dynamics can be retraced. The heat map of change (Figure 5b) shows the marked shifts in $\delta^{13}C_{SOM}$ raw data in which different colors indicate the magnitude and direction of vegetation change over time. Blue regions represent -13‰ to -3‰ shifts, which are indicative of changes towards woodier vegetative signatures. Whereas warmer colors (i.e. orange-red, red) represent 3‰ to 6‰ shifts, which indicate areas where forests have receded or been replaced with mixed grass-shrub vegetation or grasslands. The raw isotopic ratios of SOM also incorporate changes in the isotopic composition of atmospheric CO_2 due to the emission of fossil fuels over the past century (known as the Suess effect). However, changes in $\delta^{13}C$ ratios of CO_2 have been small for most of the Holocene (<1.5‰ over the past 10,000 years; (Hare et al., 2018) and affected both tree and grass biomass $\delta^{13}C$ signatures in similar ways. We can therefore rule out this pre-depositional process as an explanation for long-term changes in $\delta^{13}C_{SOM}$ observed here, which happened before anthropogenic CO_2 emissions became a significant planetary force. Although it is difficult to distinguish between processes that occur after SOM deposition, post-depositional changes occur primarily in the topsoil as litter decomposes, typically leading to a <2‰ fractionation (Krull et al., 2002). To be conservative, we only present interpolated $\delta^{13}C_{SOM}$ maps in which shifts greater than ±2‰ occurring at depths from 30-50 cm or deeper in the soil profile. As a result, the yellow to yellow-green colors in the interpolation maps indicate regions of relatively 'stable' ecosystem states; that is, those in which $\delta^{13}C_{SOM}$ varied between -2‰ and 2‰ within any given profile.

Variation in the reconstructed changes in tree cover and woody vegetation expansion are consistent with local to sub-regional hydroclimate variability, inferred from speleothem

strontium ratios which indicate increasing soil moisture and rock dissolution near most, but not all, soil sampling sites (i.e. a general shift to more negative Z-scores characteristic of wetter conditions; Figure 5c). The steepest and most consistent increase in moisture conditions, inferred from strontium isotopes, was observed for the Tamboril site in central Brazil. No clear trend in hydroclimate was observed for the Paraiso cave, suggesting stable moisture regime at our northernmost site in the Amazon region. All other cave sites showed some degree of increasing moisture with significant sub-regional variability, oscillating between the trends displayed in the Tamboril and Paraiso records. The regional record of monsoon intensity, inferred from speleothem oxygen isotope ratios, showed a less consistent signal of increasing precipitation, with larger variability than the local trends in hydroclimate throughout the region for most of the Holocene (Supplemental Figure 3).

Soil carbon: Stocks and relationship to vegetation cover

Carbon stocks decreased significantly with depth (p-value < 0.001) as observed in Figure 6a. There was also a significant difference in carbon stocks (to a depth of 80 cm) among ecosystem types (Figure 6b). The mixed-effects model applied to carbon stocks per depth indicated that the fixed effects of paleovegetation (i.e. from ~1,600 years ago) had significant effects (p-value < 0.05) on carbon stocks per depth only within past savannas, where increasing tree cover had a positive effect on carbon storage. Soil type was not a significant predictor of SOM carbon isotope ratios (Supplemental Figure 2), but it was a strong predictor of carbon stocks (Figure 6c), even though we found a significant random effect (sites nested within present ecosystem type) indicating that variation in carbon stocks depended on sampling location.

Discussion

There have been many studies about the effects of deforestation at the Amazon-Cerrado transition, but little is known about long-term variation in tree cover and climate before modern deforestation. Here, we show that a widespread process of increasing tree cover prior to modern deforestation. Our findings are supported by isotopic data which display a general trend of woody vegetation expansion and densification over at least the past 1,600 years in forest- and savanna-dominated landscapes. Overall, the spatial pattern observed amounts to a regional process of woody vegetation expansion that happened either through forest encroachment into savannas or through densification of tree cover in previously grass-dominated systems. Our data indicate an increase in precipitation during the mid- to late-Holocene transition, which is consistent with independent climate reconstructions from lake sediment pollen and charcoal (Behling, 1998; Bird et al., 2011; Sternberg, 2001; Sande et al., 2019) and from speleothem carbonate oxygen and strontium records (Cruz et al., 2005; Vuille et al., 2012; Ward et al., 2019; Wortham et al., 2017). Specifically, our analysis of SOM across 83 study sites supports the hypothesis of increasing tree cover due to increasing moisture inferred from speleothem-based reconstructions that reflect spatial and temporal variation in climate across the region.

Regarding the timing of forest or woody savanna expansion, our SOM ^{14}C data represent the most recent changes in vegetation out of a range of possible ages. Soil develops from two directions, with mineral weathering occurring primarily in deep layers near the parent material and new organic inputs occurring primarily near the soil surface. However, current inputs can also occur within and beyond the rhizosphere (e.g. via root exudates and rhizodeposition). Given that recent addition of carbon into the deeper soil matrix can occur, calibrated ^{14}C dates of bulk organic matter represent an average age of vegetation input for any given depth. This

interpretation is consistent with several previous studies, which showed a general trend of savanna systems (having a C_4 signature) being replaced with forests (having a C_3 signature) as inferred from SOM (Berhe et al., 2012; Sanaiotti et al., 2002; Trumbore, 2009). Large variance is to be expected within and across ecosystems because, although differences in molecular composition of tree- and grass-derived litter and their relative contributions to SOM are not expected to affect soil carbon stability, other environmental and biological factors can affect carbon turnover (Schmidt et al., 2011). Therefore, the estimated ~1,600 years of woody vegetation expansion should be understood as the mean minimum age of SOM associated with ecosystem change, which probably began earlier as suggested as suggested in previous case studies (e.g. Silva 2014), triggered by mid-to-late Holocene changes in the regional monsoon intensity (Wortham et al 2017; Ward et al., 2019).

Forests in the Amazon region have expanded further in some areas over the past few decades due to fire suppression and/or agricultural land-abandonment (Rosan et al., 2019). Our data indicate that a natural trend of forest expansion and densification of savannas has occurred over a much longer time period, as predicted from feedbacks between increasing precipitation, decreasing fire disturbance, and increasing tree cover (Sternberg 2001). Notably, woody vegetation expansion occurred despite increasing pre-Columbian human populations and associated disturbances (Souza et al., 2018) during the late Holocene. The genome-based population reconstructions in this region show continuity of ancient peoples and practices beginning ~5,800 years before present with "a striking pattern of continuity with present-day people" beginning ~2,000 years ago (Posth et al., 2018) – i.e. the same period when speleothem isotope records suggest a shift towards wetter conditions due to increased monsoon intensity, although with major variability for local hydroclimates among surveyed sites (Ward et al., 2019).

From our map of vegetation change it is clear the dominant trend has been tree cover expansion and densification in both savanna and forest ecosystems since the late-Holocene, however, a few areas exist where vegetation remained relatively stable. Interestingly, transition zones did not show a consistent shift over time. This suggests that the woody vegetation expansion at forest-savanna boundaries might have been more strongly affected by disturbances (recent and old) at those sites. Humans are currently affecting vegetative cover in this region through land-use change and fire suppression, in some cases, and increasing the frequency of fire disturbance for rangeland expansion, in other cases (Andreoni & Londoño, 2019). Therefore, the long- and short-term drivers of woody vegetation expansion and current deforestation make the results from transition zones difficult to ascribe to a single process. For example, although woody vegetation expansion and densification appear to be the dominant response to climate variability over the past 1,600 years, a trend of decreasing tree coverage towards our easternmost sites also exists. Woody vegetation cover may have declined in this sub-region due to the prevalence of dry deciduous or semi-deciduous tree species. Unlike evergreen tropical forests, deciduous or semi-deciduous dry forests in this sub-region are adapted to low moisture of nutrient rich rock outcrops (Dexter et al., 2018). Under such conditions, increasing regional precipitation can decrease tree dominance and increase grass productivity, favoring the expansion of savannas (Silva et al., 2010).

Total carbon stocks did not vary consistently among ecosystem types, even though we found statistically significant differences between some forest and savannas due to a significant effect of soil order on carbon storage and outlier riparian zone profiles. The presence of gallery and riparian forests in our study region is contingent on soil moisture as well as soil nutrient inputs. During the mid-Holocene climatic conditions in South America shifted to becoming

wetter (Marchant & Hooghiemstra, 2004) and shifts in the SASM intensity might have caused sediment and nutrient flows that favored forest expansion. In other regions, forest-savannas landscape mosaics can persist for millennia regardless of fluctuations in precipitation due to feedbacks that involve fire disturbance, nutrient limitation, and herbivore population density (Pausas & Bond, 2020). However, climate-driven increases in tree cover could still be recorded until the mid-1980s in open landscapes of central Brazil, even in sandy soils with low water retention capacity at the southeastern edge of the Amazon region (Marimon et al., 2006). In addition to hydrological feedbacks that favor increasing tree cover, positive feedbacks between forest expansion and soil fertility would also be necessary to allow forest expansion because nutrient stoichiometries are fundamentally different between forests and savannas (Flores et al., 2019). Therefore, multiple factors must be considered to explain past and predict future woody vegetation expansion including climatic change, disturbances (e.g. floods and fires), and nutrient deposition from exogenous sources (e.g. atmospheric deposition and landscape translocation).

Most of the reconstructed increases in tree cover, evidenced here coincides with increasing density of pre-Columbian populations in southern Amazonia (estimated to vary between 500,000 and one million inhabitants from 1250 to 1500 AD (Souza et al., 2018). This is important because it reveals that increasing pre-Columbian population densities apparently did not cause forest loss at the regional scales. Our findings are consistent with case studies of paleovegetation in other areas of the Amazon region (e.g. Lombardo et al., 2019; Silva et al., 2014; Smith & Mayle, 2018), but contradict a common assumption of human-driven expansion of open ecosystems in the region since the mid Holocene. Recent anthropological findings could reconcile this apparent contradiction. Plant domestication dates back to >10,000 years ago in western Amazonia (Lombardo et al., 2020), however, the emergence of complex societies that

relied on intensive land use in central Amazonia is much more recent (Capriles et al., 2019). Across the central and eastern Amazon basin human activity can be divided into three main phases: a pre-cultivation period (>6000 years ago); an early-cultivation period (6000–2500 years ago); and an intensive cultivation period (2500–500 years ago) (Maezumi et al., 2018). Our observation of increasing tree cover coincides with the chronology of intensification in sedentary settlements during the late Holocene, which probably resulted in an overall decline in deforestation and fire use across the region prior to European contact. On the other hand, current deforestation is interrupting a historical increase in tree cover in forests and savannas, which would have been further accelerated by the recent stimulation of tree growth due to increases in atmospheric CO2 (Silva & Lambers 2020). Moreover, current deforestation is also likely to change the regional climate by decreasing rainfall. Indeed, a recent increase in legal and illegal deforestation has followed the Brazilian Forest Act revision, with as of yet unquantified consequences for ecological and climatic stability (Freitas et al., 2018). Positive feedbacks between deforestation rates, warming climates, and declining precipitation could lead to a "deforestation-generated degradation of the hydrological cycle" (at 20-25% deforestation threshold) beyond which large sections of the Amazon forest would be replaced with savannas unless major reforestation and conservation efforts can be implemented (Nobre & Lovejoy, 2018).

Conclusion

We found that woody vegetation expansion has been occurring throughout the Amazon-Cerrado region since ~1,600 years prior to modern deforestation. In addition to increasing tree covers near forest-savanna ecotones, most forests and savannas have experienced significant densification of tree cover, with grass cover expanding only in a few locations characterized by

dry climates and poorly developed soils. Several biophysical and biogeochemical mechanisms may have contributed to forest expansion and densification of woody vegetation in savannas, including positive feedbacks between tree cover and precipitation which can dampen fire disturbance and promote nutrient accumulation, which favor the persistence of closed canopies (Bomfim et al., 2019, 2020; Silva & Lambers, 2020). The observed incremental expansion forests into savannas could have significant impacts on carbon-water relations, potentially affecting the balance between precipitation and evapotranspiration (Garcia et al., 2016). However, we did not observe a clear effect of changes in vegetation on soil carbon stocks. Future studies should focus on the mechanisms driving the permanence of carbon derived from woody vegetation expansion, informed by soil and climate records throughout the region. The next phase of understanding will come from the integration of plant, soil, and atmospheric data to understand the influence of human activity on ecosystem-climate feedbacks as a path towards improving carbon sequestration and water conservation.

Acknowledgements

We thank all of our collaborators for providing samples, field support, and data analyses. We acknowledge Roberto Ventura Santos, Flavio Fernandes, and Toby Maxwell, for help with field surveys. This research was supported by the National Science Foundation Grant No. 1602958 and by CNPq (PPBio-457602/2012-0 and PELD-441244/2016-5) collaborative research grants.

Figure 1 Study sites, current ecosystems, and climate: A) mean annual precipitation (mm) over the time period 1981-2010. Blue stars indicate cave sites where paleoclimate records were derived from speleothems. B) mean annual temperature (°C) over the time period 1981-2010. C) study region displaying 83 sites sampled for this study within the Amazon-Cerrado region. The yellow line within the study region delineates the ecoregions – Amazon to the Northwest and Cerrado to the Southeast. Shapes and colors correspond to forest, savanna, or forest-savanna transitions. Climate map adapted from INMET, 2019.

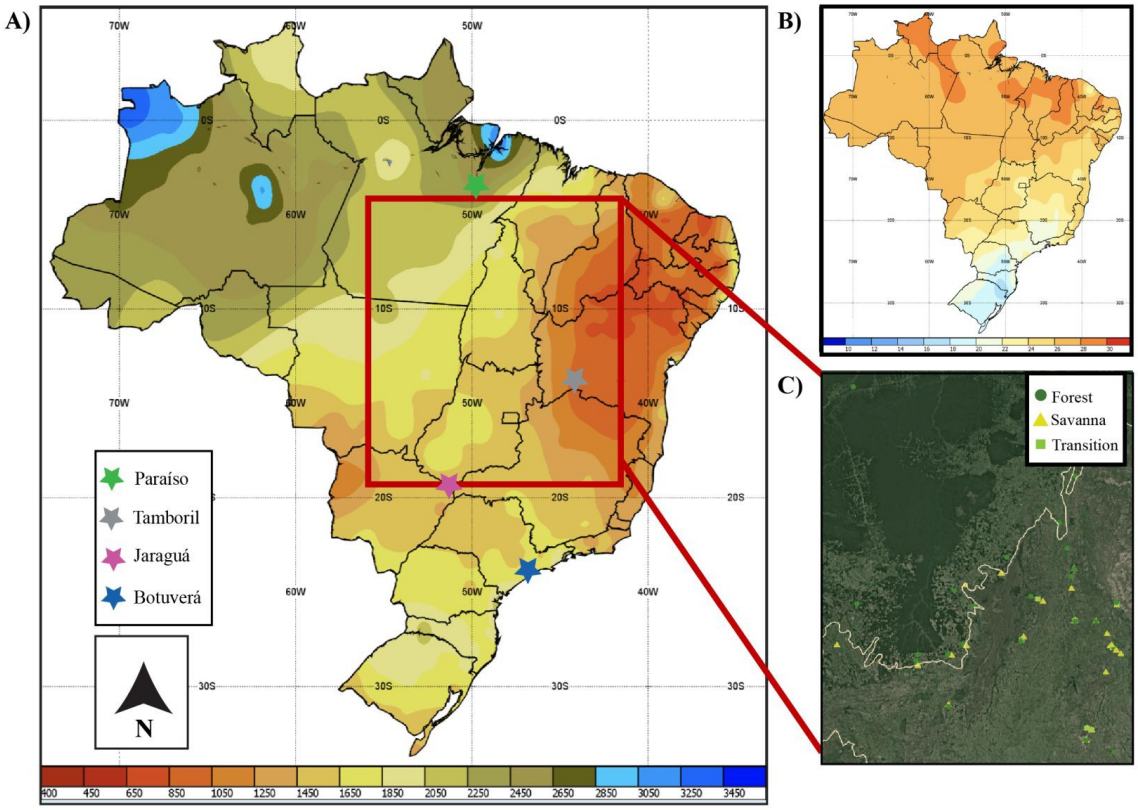

Figure 2 Relationship between topsoil soil organic matter carbon isotope signatures ($\delta^{13}C_{SOM}$) and ground- based or satellite-derived leaf area index (LAI; Supplemental Table 2). Less negative $\delta^{13}C_{SOM}$ values correspond to C4 grass dominance. More negative $\delta^{13}C_{SOM}$ values correspond to C_3 woody vegetation dominance. Shapes and colors correspond to current ecosystem type. The black line displays a significant linear regression between $\delta^{13}C_{SOM}$ and LAI ($R^2 = 0.23$; p-value < 0.0001). The dashed black line displays non-linear regression between $\delta^{13}C_{SOM}$ and LAI ($R^2 = 0.30$). Previously published data (represented by black points) adapted from Ladd et al., 2014.

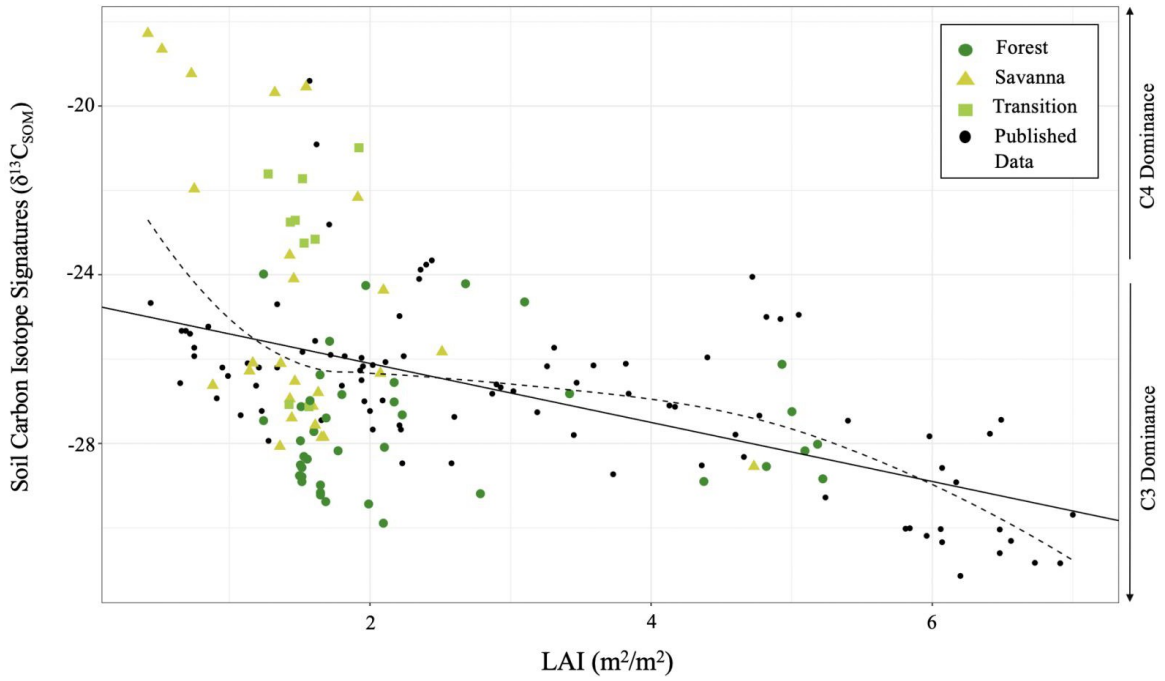

Figure 3 Age-depth model displaying relationship between soil depth and calibrated radiocarbon years before present. Ecosystem type (i.e. forest, savanna, transition) are distinguished using different colors and shapes in which standard deviations represent analytical uncertainty.

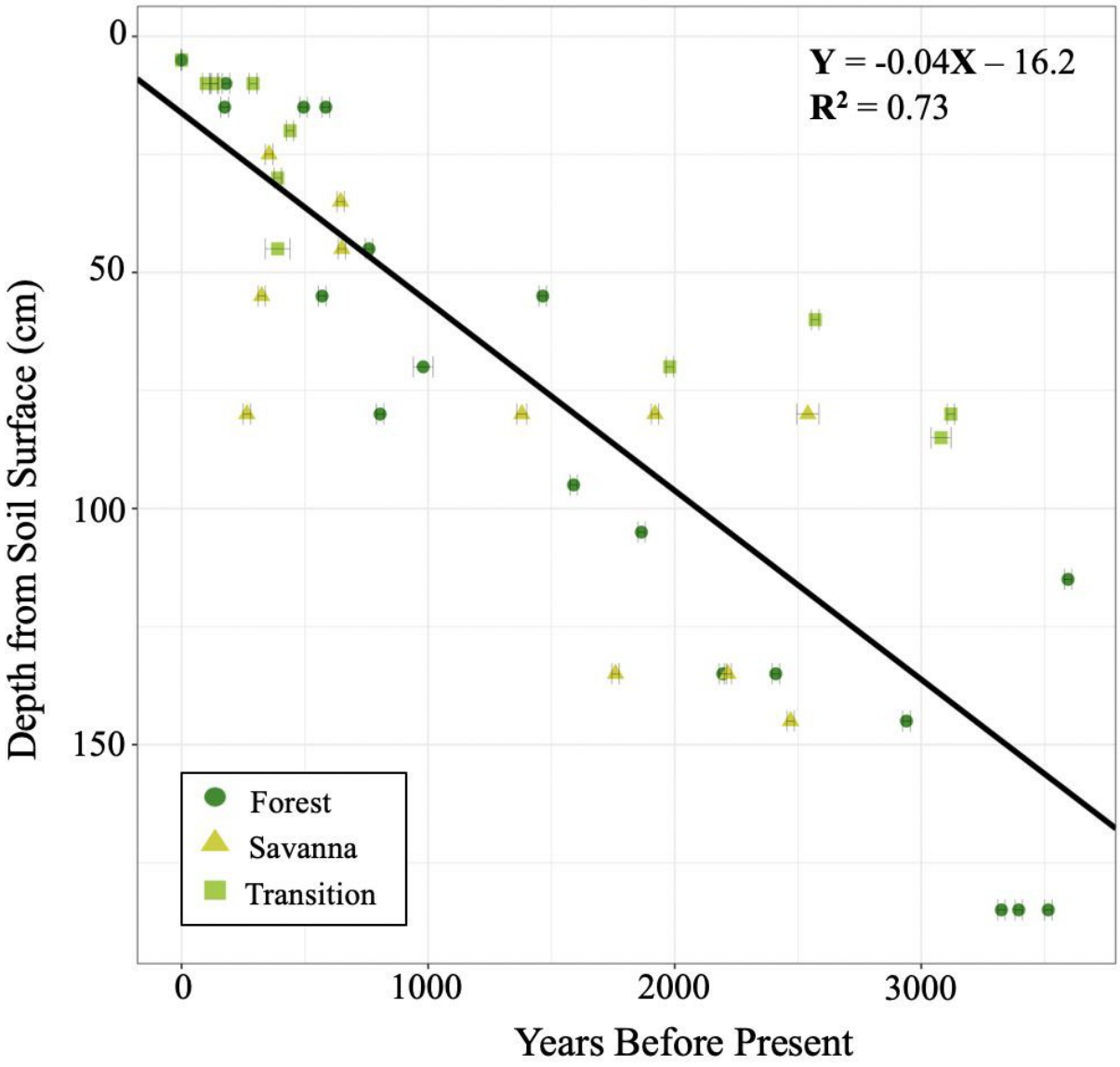

Figure 4 Soil organic matter carbon isotope ratios ($\delta^{13}C_{SOM}$) across depths for (A) forest, (B) savanna, and (C) forest-savanna transitions. Figures to the right show the proportion of data points for each soil depth. Grey lines represent significant linear regressions (p-value <0.05) between soil depth and $\delta^{13}C_{SOM}$ within each soil profile. Red-dashed lines indicate the depth of 80 cm selected for vegetation reconstructions across all sites. Black points represent averages per depth. The majority of regressions indicate increasing woody cover over time.

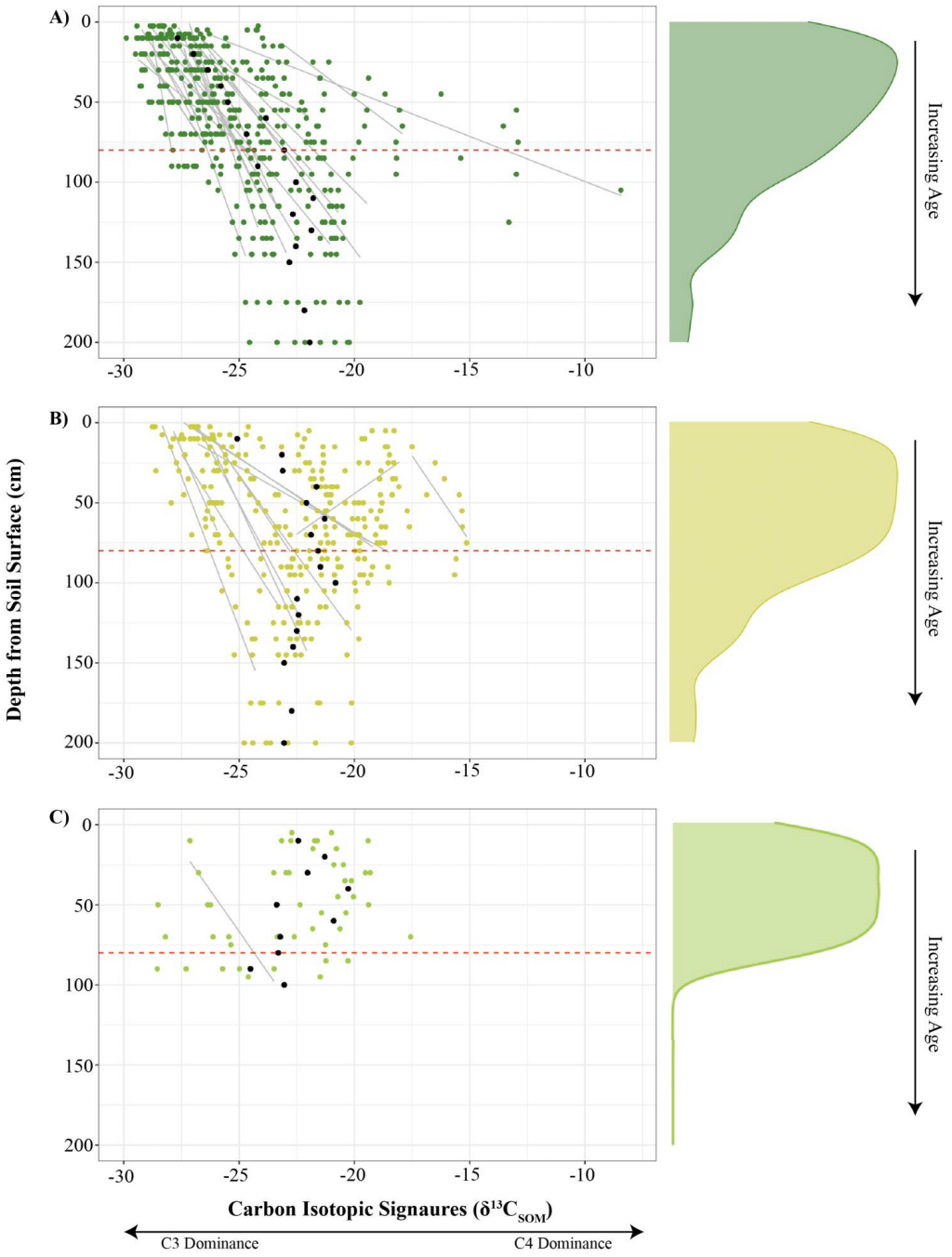

Figure 5 Changes in $\delta^{13}C_{SOM}$ at (A) varying depths across study sites, where the x-axis is longitude and the y- axis is latitude, and depth has been converted to age; (B) vegetation change heatmap where blue represents woody vegetation expansion, yellow represents no change, and red represents grass expansion; and (C) strontium isotope ratios, adapted from Ward et al. 2019, as a proxy for soil moisture and rock dissolution, indicating a shift towards wetter conditions. Different colors within each location represent different speleothem samples collected within the same cave site (Figure 1).

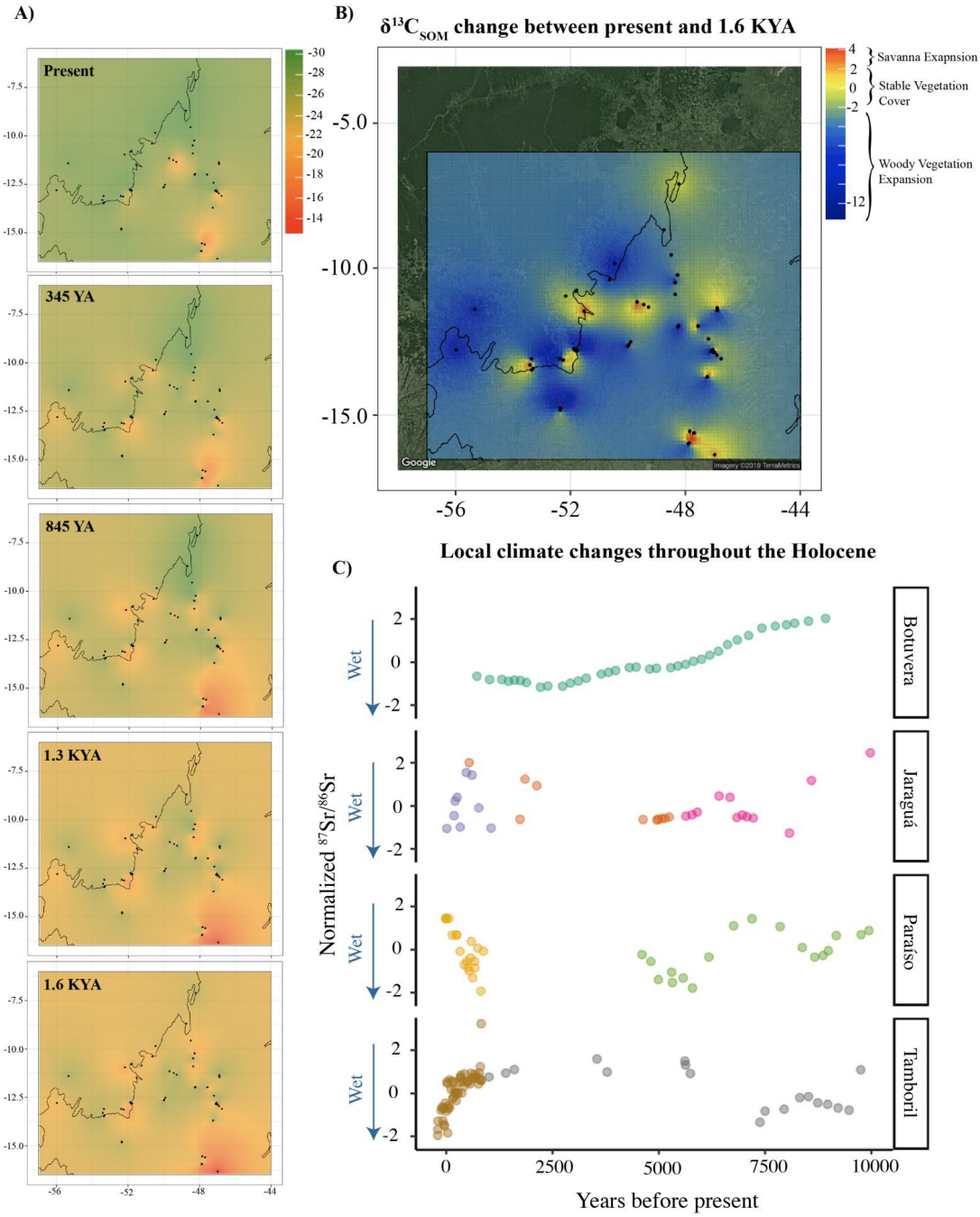

Figure 6 Variation in soil organic carbon stocks for each ecosystem and soil depth. Minor differences were found for average carbon stocks across ecosystems, although notable outliers exist within forests and forest- savanna transitions. A mixed-effects model indicates that soil order and woody vegetation expansion significantly affected soil carbon content only in savannas, where woody vegetation expansion had a positive effect on carbon stocks. A significant random effect of sampling location also exists for all ecosystem types.

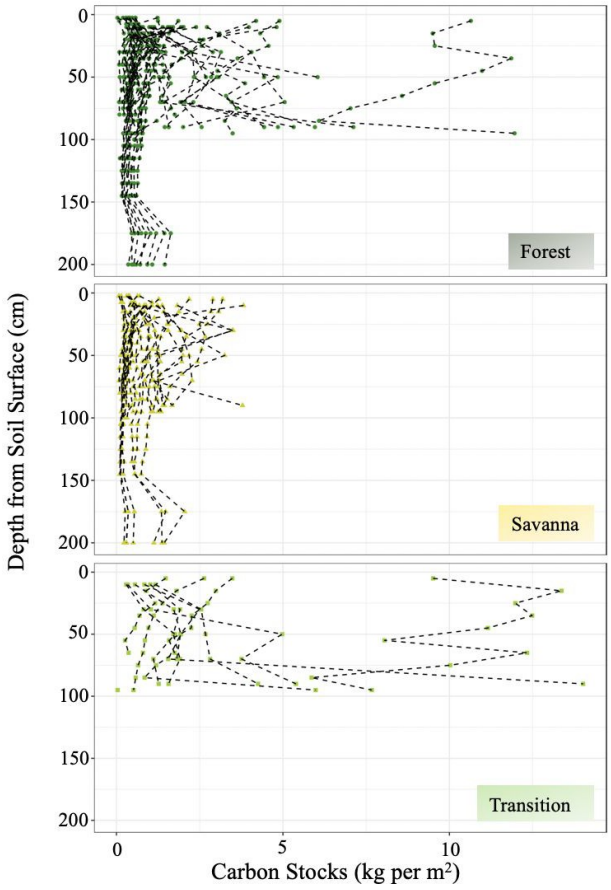

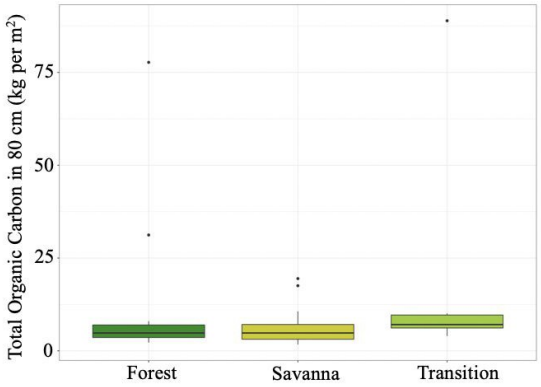

	stock		
Predictors	*Estimates*	*CI*	*p*
(Intercept)	1.10	-0.43 – 2.64	0.162
d13C	-0.08	-0.11 – -0.05	**<0.001**
Histosol	-2.71	-4.64 – -0.78	**0.010**
Inceptisol	-1.78	-3.46 – -0.10	**0.045**
Oxisol	-2.96	-4.39 – -1.53	**<0.001**
Plinthite soil	-1.80	-3.26 – -0.34	**0.020**
Ultisol	-2.41	-3.89 – -0.92	**0.003**
grassland	-0.06	-1.69 – 1.58	0.946
savanna	0.76	0.20 – 1.33	**0.012**
transition	0.16	-0.37 – 0.69	0.560
Random Effects			
σ^2	0.45		
Marginal R^2 / Conditional R^2	0.241 / 0.591		

CHAPTER III

FOREST SOIL CARBON DYNAMICS 20 YEARS AFTER A CATASRTOPHIC WILDFIRE

Contributions

This chapter in coauthored by Jamie L. Wright, Katherine L. Shek, Sydney Katz, Krista McGuire, and Lucas C.R. Silva. I was responsible for data collection and sample analyses where Katherine L Shek executed all microbial analyses. I am responsible for data analyses and writing the manuscript, where again Katherine L Shek contributed to microbial data analyses.

Introduction

Although extensive fire suppression throughout the Western United States (WUS) has helped to retain carbon on the landscape over the past century (Keyser & Westerling, 2019), it also predisposes forests to high-severity wildfire. The frequency and severity of wildfires is now expected to increase across the WUS due to a combination of accumulated fuels, declining snowmelt (Westerling, 2016), and extreme weather events, such as drought, due to climatic change (Abatzoglou & Williams, 2016). Increasing fire severity is projected to continue, but its long-term effect on forest carbon sequestration remains difficult to quantify. Carbon stabilization and preservation within ecosystems must be retained and enhanced to prevent irreversible climate forcing. Specifically understanding the belowground effects of catastrophic wildfires on carbon stabilization remains challenging but is necessary to comprehend and quantify. Soil carbon stocks are affected by parameters that include vegetative inputs, topography, parent material, and microbial communities. Beyond quantifying how carbon stocks change after a fire, it remains uncertain whether soil carbon is lost or translocated and how soil carbon form alters. Here, we

combine four methods of measuring soil carbon pools to understand how belowground carbon stability shifts after a massive wildfire.

Soil organic matter (SOM) may be separated into two pools – particulate and mineral associated – where the different types possess varying residence times in the soil and distinct chemical components (Lavallee et al., 2019). These pools of carbon represent the transition away from previous paradigms of carbon stability (i.e., mean residence times) that are based on the notion of chemical recalcitrance. Particulate and mineral associated carbon highlight the relative importance of mineral-associations increasing carbon stability (Lehmann & Kleber, 2015). Particulate organic matter (POM) and mineral associated organic matter (MAOM) can be distinguished from each using their densities, where POM is considered the light fraction and MAOM the heavy fraction. POM cycles through the soil on decadal timescales whereas MAOM persists in the soil for decades to centuries (Lavallee et al., 2019). MAOM provides a pathway for carbon stability on anthropic temporal scales, so it is prudent to elucidate how disturbances, predominantly wildfire, and post-fire management affect the proportion of stable and more labile forms of carbon. Another carbon pool that falls into both POM and MAOM is soil pyrogenic carbon (PyC) which possesses a continuum of labile to resistant forms which are recalcitrant based on their chemical composition. PyC does not fit into one pool or the other because PyC recalcitrance is not solely derived from physical protection (Lavallee et al., 2019). Data suggests that approximately 50% of PyC generated from vegetative fires may persist in soils on decadal to centennial scales (Santín et al., 2016), so it is important to also quantify PyC pools after wildfire events to better understand the carbon stability of the system.

Soil carbon is derived from plant and litter input as well microbial byproducts and biomass (Cotrufo et al., 2013). WUS forests predominantly associate with ectomycorrhizal

(ECM) fungi that accumulate large pools of carbon in their mycelia (Averill & Hawkes, 2016; Hobbie, 2006). Other guilds of fungi exist in these systems such as ericoid, arbuscular, and saprotrophic fungi, which all contribute to carbon cycling (Bödeker at al., 2016). ECM fungi is dominant and can limit N availability among other fungal guilds, specifically saprotrophic fungi, referred to as the "Gadgil Effect" (Fernandez & Kennedy, 2016). Free living saprotrophic fungi are opportunistic fungi that invest their energy in decomposing SOM rather than nutrient exploration like ECM fungi, consequently increasing respiration and soil carbon emissions. The relative abundance of ECM versus saprotrophic fungi can play a significant role in the stabilization of soil carbon. Previous research has found that soil heating from fires have negative effects on ECM fungi (Peay at al., 2009), which can allow for other functional guilds (i.e., saprotrophic fungi) to occupy ECM niche space.

After wildfire events, management treatments can be applied to the landscape to promote vegetative regeneration, fuel mitigation, (Leverkus et al., 2018) or recover economic value (Thorn et al., 2018). A prevalent management practice is salvage logging - the removal of fire affected trees before they decompose, but controversy shrouds this practice due to evidence of reduced biodiversity and shifts in successional trajectories (Leverkus et al., 2018; Thorn et al., 2018). Research indicates that salvage logging after largescale natural disturbances reduces EM as well as saprotrophic species richness (Ford et al., 2018). With respect to soil carbon, evidence exists that soil carbon stocks are also lower after salvage logging (Juan-Ovejero et al., 2021; Serrano-Ortiz et al., 2011).

To enhance understanding of the dynamics of climatic change and forest management on soil carbon stability and preservation, we sampled fire-affected landscapes across the Rogue River-Siskiyou National Forest – where nearly 500,000 acres burned in the 2002 Biscuit Fire.

This region possesses diverse geology which contributes to abrupt vegetative community shifts with high biodiversity and variation in carbon pools. To understand the effect of fire on soil carbon, we collected nearly 150 samples underlain by metamorphic and ultramafic serpentine parent material in fire-affected and unburned areas to test the following hypotheses. The first being that TOC stocks will decrease along a fire intensity and management gradient, where low severity fires will have higher TOC stocks than unburned and moderate/high burn severity systems since soil carbon in low severity sites may be less likely to be combusted and lost from the system. Salvage logging will decrease soil carbon stocks through degrading soil structure post-fire. Second, MAC stocks will be higher in regions with lower fire severity and without post-fire management which possesses implications for carbon "stability" (i.e., longer soil mean residence time). And lastly, fungi composition will shift from ECM fungi dominance to saprotrophic across a fire severity and management gradient since saprotrophic fungi are opportunistic and will quickly explore abandoned niches. A high severity wildfire followed by another disturbance, such as salvage logging may further prohibit ECM reestablishment. We also address if differences in different fungal functional groups will be related to carbon stability.

Materials and Methods

Study Region

Our study region encompasses a subset of the Rogue River-Siskiyou National Forest that burned with varying degrees of severity in the 2002 Biscuit Fire in Southern Oregon (Fig. 1). This region has not subsequently burned in fires since at least 2002. We chose this region because it is an example of a mega-fire interacting with climatic change that drastically affected the landscape. This area was not only affected by varying degrees of fire intensity but post-fire management strategies (i.e., salvage logging) were subsequently applied to the landscape

allowing for the opportunity to quantify their synergistic effects on soil carbon stability and microbial composition. The region is characteristic of a Mediterranean climate – warm dry summers and cool wet winters, but droughts are becoming more frequent within this area with respect to long-term climate trends (Rincón et al., 2014). Annual total precipitation ranges from 1767.14 to 2931.63 mm whereas mean annual temperature ranges from 10.5 to 11.9 °C, over the period 1991- 2020 (PRISM, 2022). Metamorphic sites were dominated by intermixed pine pre fire and fir forests, and serpentine sites dominated by grasslands.

Fig. 1 shows the location of the study region which incorporates multiple parent materials, topographies, fire severity and post-fire management types.

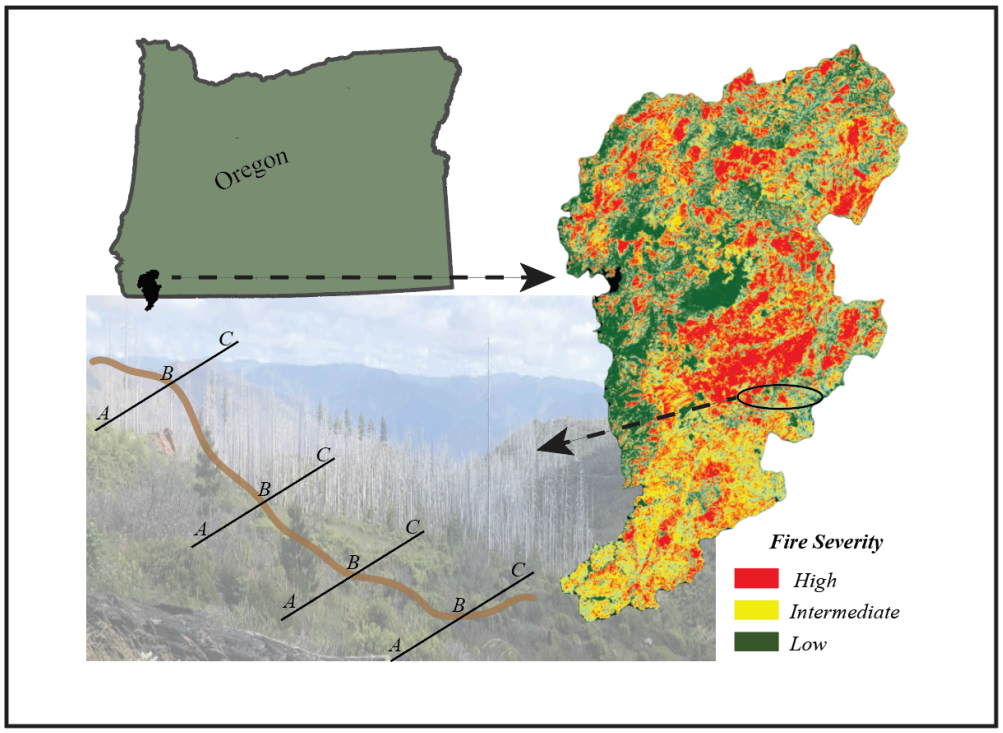

Hypothesis Testing

To test our first hypothesis, we measured total organic carbon (TOC) stocks at each site using the methods described below. Our second hypothesis was tested by quantifying different organic matter pools (i.e., MAC, POC, PyC) that have varying levels of stability. Furthermore, we linked carbon stability with fungal community composition and elemental concentrations to understand

which fungal communities correlate with higher carbon stability. Lastly, our third hypothesis was addressed through using amplicon sequencing to measure fungal community composition. We also measured soil pH, texture, and elemental composition to further understand trends observed. Our third hypothesis was tested by quantifying different organic matter pools (i.e., MAC, POC, PyC) that have varying levels of stability. Furthermore, we linked carbon stability with fungal community composition and elemental concentrations.

Soil Sampling

Soil samples were collected in July of 2020 from four forest and two grassland ecosystems that aligned with the sites' underlying parent material: metamorphic and serpentine respectively. Samples were collected from high and low fire intensity regions along with control areas in our metamorphic sites. We were unable to locate a serpentine grassland that experience low fire severity in the Biscuit Fire, so we only have a high severity and control site for our serpentine sites. Control sites were selected based on no or minimal visual burn scars. We picked our sampling sites based on Burned Area Emergency Response (BAER) maps of fire severity of the Biscuit Fire where fire severity determined using the Differenced Normalized Burn Ratio (DNBR) (BAER, n.d.) which takes into consideration pre and post fire conditions (Parsons et al., 2010). Additionally, samples were collected from sites that were and were not salvage logged after fire. Sites were only salvage logged if they were affected by a high severity fire and previously maintained forested vegetation, so our high severity metamorphic site was the only site that was salvage logged. At each site, samples were taken along a hill-slope gradient (i.e., top, middle, bottom, and valley with three replicates per topography and to a depth of 60 cm (20 cm increments) when possible (96 samples total). Valley topographies were only collected in forested sites since the serpentine sites did not possess valleys. Bulk density was collected for the

topsoil (top 20 cm) at each site and topography (n = 18), where deeper samples were not collected due to difficulty obtaining bulk density cores with field equipment. Bulk density values generally increase with depth (USDA, 2019), so carbon stock values may be underestimated for lower depths (i.e., depths 20-40 cm). Soil cores for the top 2.5 cm of the soil were collected at each site, topography, and replicates for fungal composition analysis, where the core was sterilized in between samples and put on ice in the field until they could be transferred to a -20°C freezer. The six sites and their respective dominant vegetation types are described in **Table 1**. Collected soil samples were subsequently prepared for the following analyses: organic carbon stocks, pH, soil texture, bulk density, elemental data, and fungal compositional data. To delineate the different sites more easily in the subsequent text, the following acronyms were used; MSNL (metamorphic, high severity, non-salvaged), MSL (metamorphic, high severity, salvaged), SSNL (serpentine, high severity, non-salvaged), MLNL (metamorphic, low severity, non-salvaged), MCNL (metamorphic, control, non-salvaged), SCNL (serpentine, low severity, non-salvaged).

Table 1 displays the different sites and their corresponding fire intensities, post-fire management, parent material, and dominant vegetation.

Site	Fire Intensity	Management	Parent Material	Dominant Vegetation	Average Total Depth (cm)	Coarse Fraction (%)
1: MSNL	*severe*	*non-salvaged logged*	*metamorphic*	*Douglas fir snags, Manzantia, Buckthorn, Chinquapin*	*34.6*	*54.2*
2: MSL	*severe*	*salvaged logged*	*metamorphic*	*Manzantia, Buckthorn, Chinquapin, Tanoak, Huckleberry leaved-oak*	*31.1*	*50.0*
3: SSNL	*severe*	*non-salvaged logged*	*serpentine*	*Ateraceae*	*10.0*	*38.8*
4: MLNL	*low*	*non-salvaged logged*	*metamorphic*	*Douglas fir, Incense cedar, understory shrubs*	*19.2*	*57.7*
5:MCNL	*control*	*non-salvaged logged*	*metamorphic*	*Douglas fir, Sitka spruce, fir trees*	*22.1*	*58.3*
6: SCNL	*control*	*non-salvaged logged*	*serpentine*	*Ateraceae, Posion oak*	*13.3*	*62.5*

Soil Physical and Chemical Properties: pH, Bulk Density, Texture, Elemental Composition

For soil pH and texture, samples were air-dried, passed through a two mm sieve - where coarse fraction was measured (necessary for texture modifiers), and oven-dried. Soil pH was measured for all samples using a 1:1 water to soil ratio using a Mettler Toledo soil pH meter. Samples with a pH equal to or greater than six were acid fumigated (Harris et al., 2001) and their carbon concentrations were compared to non-acid fumigated samples to determine if carbonates were present. Soil bulk density was calculated by dividing the oven-dried weight taken from our bulk density corer and divided by the volume of the corer ring. The region we collected samples from possessed substantial coarse fragments (> 2 mm), so we adjusted our bulk density values to only incorporate the "light" fraction (< 2mm). The coarse fraction (> 2mm) was measured by volume of total sample (Schoeneberger e al., 2002). We calculated the light fraction bulk density (ρFE) by dividing the oven-dried weight of the light fraction by the proportional volume of the light fraction, which is the preferred method used by the Department of Agriculture (Throop et al., 2012). We used this specific bulk density approach to reduce overestimating carbon stocks since the coarse fraction generally does not store carbon (Throop et al., 2012). We performed a Tukey HSD test on ρFE to determine differences between topography and site. Soil texture was measured using the modified pipette method (Maxwell, n.d.) where samples were mixed with 0.5% Sodium Hexametaphosphate and shaken overnight in a reciprocating shaker. After removal from the shaker, samples were agitated by hand, then supernatant to a depth of 2.5 cm was pipetted after ten seconds and put into a tin weighing dish and placed in the oven. Approximately two hours later, the supernatant was pipetted, put into a tin weighing dish, and placed in the oven. Percent clay, silt, and sand were calculated using the dry weights of the supernatants.
We used a Bruker Trace 5 portable X-ray fluorescence (pXRF) instrument to measure elemental concentration of the different soil samples. Ground and homogenized soil was added to

polyethylene sample cups with a prolene film secured over the sample cup. For major elements, the calibration Mudrock Major was used with an adjusted measuring time of three minutes (Leys et al., 2016). The Mudrock Major calibration was generated by Bruker using matrix matched calibrations.

Soil Organic Carbon: TOC, MAC, POC, PyC

Samples were air-dried, passed through a two mm sieve, oven-dried then homogenized and ground using an automated ball mill. For TOC, samples were manually encapsulated in 5 x 8 mm tin capsules (sample size approximately 30 mg) and combusted using a Costech elemental analyzer. To determine if TOC stocks were statistically different among sites, a Tukey HSD test was executed. This test was carried out on all TOC stock values not just their averages by site and topography.

A 1:1 ratio of fine fraction soil to sodium polytungstate (SPT) – which has a density of 1.85 g/cm^3 – was utilized for the mineral associated carbon (MAC) and particulate organic carbon (POC) analyses, where samples were agitated in a reciprocating shaker for two hours then centrifuged for 10 minutes at 3,000 RPM. POM was aspirated off and poured into a Büchner funnel with glass fiber filters over an Erlenmeyer vacuum flask and attached to a vacuum pump which expediated the filtering process. These steps were repeated two more times – but samples were shaken by hand rather than with shaker. Distilled de-ionized (DDI) water was added to the samples, hand shaken, centrifuged and solution aspirated off three times. POM was then collected and oven-dried at 60 °C. MAOM, was the remaining soil that was not aspirated off. After the MAOM was washed through with DDI, it was then oven-dried at °C. After the POM and MAOM came out of the oven they were subsequently ground and encapsulated (sample size approximately 30 mg) and combusted using the Flash*Smart* Elemental Analyzer. MAC and POC

stocks were calculated slightly different than TOC – both pools possess different bulk density values. Since MAC and POC were separated using a heavy liquid (i.e., SPT), bulk density values were assigned as 1.80 and 1.60 g/cm^3 respectively which correlates to approximate density cut offs for the two pools (Cotrufo et al, 2019). These bulk density values were then modified to consider each site's specific coarse fraction volume so that their adjusted bulk density would be representative of the fine earth fraction weight and volume. Since MAC and POC together comprise the entirety of the TOC stock, each pool's total stock needed to be adjusted to represent the relative proportion each carbon type makes up of the total TOC pool. Note that some discrepancies may arise between the sum of MAC and POC with total TOC stocks due to MAC and POC calculations being based on different subsamples as well as bulk density assignment.

Pyrogenic carbon (PyC) determinations were performed using a standard method for determination of charcoal content in forest soils (Kurth et al., 2006). For pyrogenic carbon analysis, approximately 0.85 g of fine-fraction soil was digested with 1M nitric acid and 30 % hydrogen peroxide for 16 hours in a digestor hot block kept at a constant temperature of 90°C. After samples were digested, they were subsequently filtered into Whatman #1 Filter Papers using DI water. The filter papers containing the samples were then dried at 60°C for 24 hours, ground, and then encapsulated (sample size approximately 30 mg) in tin capsules for determination of TOC. Encapsulate samples were combusted using the Flash*Smart* Elemental Analyzer. The concentration of PyC was adjusted by multiplying the instrument concentration value by the digested soil weight divided by pre-digested soil weight (Kurth et al., 2006).

We executed ANOVAs for the different carbon pool stocks (i.e., MAC, POC, PyC) as a function of site to determine if site had an overall significant effect on stocks. If the ANOVAs were significant (p-value < 0.05), we performed a Tukey HSD test for each carbon pool stock to

understand which sites were statistically different from one another. This test was carried out on all carbon stock values not just their averages by site and topography. We also separated carbon stocks by depth; topsoil (less than 20 cm) and greater than 20 cm to elucidate the disproportionate effects fire can have on carbon stocks. During a fire event, soil depth can dampen temperatures tenfold (W. J. Massman, 2012). To elucidate how the chemical variables influenced carbon stocks, we performed principal component analyses (PCA) separated by parent material. We excluded bulk density from our PCA because carbon stocks are derived from this value and would have possessed inflated correlation. We also performed linear regressions between the most significant principal component (PC) axes to elucidate if fire severity and management had a significant effect on them. We executed Random Forest Regressions for each carbon pool fraction (percent divided by 100), separated by parent material, because this method allows for predicting responses from heterogenous variables without overfitting the data (Ghannam & Techtmann, 2021). To elucidate if the variables that were linked with carbon fractions were fire-affected rather than an effect of underlying landscape differences, we ran Random Forest regressions on the "delta" carbon fractions ((carbon fraction – mean control carbon fraction)/(mean control carbon fraction)*100).

Fungal Community Composition and Bioinformatics Processing

Soil cores for microbial analyses were maintained at -20°C until processing for DNA extraction. Samples were hand homogenized and environmental DNA was extracted from approximately 0.25 g of soil using the DNeasy PowerSoil Pro Kit following manufacturer's protocol (Qiagen, Hilden, Germany). Fungal community composition was determined using high-throughput sequencing of the ITS2 region of fungal genomes; briefly, fungal DNA was selectively amplified with ITS1F (5'-CTTGGTCATTTAGAGGAAGTAA-3')/ITS2 (5'-

GCTGCGTTCTTCATCGATGC-3') primer pair modified with Illumina adapters and indices following the Earth Microbiome Project ITS protocol (Bokulich & Mills, 2013; Hoggard et al., 2018). Addition of a unique Nextera 8-bp barcode on the forward primer permitted multiplexing with other projects in the Illumina library. PCRs were performed on a BioRad T100 thermal cycler (BioRad, Hercules, CA, USA) in duplicate 25uL reactions, each consisting of 12.5uLGoTaq Green Master Mix (Promega, Madison, WI), 0.5uL each primer (10uM), 0.05uL bovina serum albumin (BSA), 9.95uL nuclease-free water and 1uL template DNA. Duplicate reactions were pooled and successful amplification confirmed on a 1% agarose gel. PCR products in each sample were quantified using the Quant-iT PicoGreen dsDNA Assay kit (Invitrogen, Waltham, MA, USA) and a SpectraMax M5E Microplate Reader (Molecular Devices, San Jose, CA, USA) before pooling each sample in equimolar concentrations. Pooled libraries were purified using the QIAquick PCR Purification kit (Qiagen, Hilden, Germany) and paired-end 250bp sequenced on the Illumina MiSeq platform at the University of Oregon Genomics and Cell Characterization Core Facility (Eugene, OR, USA). Raw sequence data were demultiplexed using QIIME v1.9.1 (Caporaso et al., 2010) and adapter and primer sequences were removed using cutadapt v.1.10.1 (Martin, 2011). The DADA2 pipeline (Callahan et al., 2016) was then used to quality filter, denoise and dereplicate sequences to assemble into amplicon sequence variants (ASVs) before assigning taxonomy using the UNITE database (Abarenkov et al., 2010). To account for differences in ASV counts across samples, the ASV table was normalized using a variance stabilization approach that scales per-sample reads by incorporating a Bayesian mixture model to amplicon count data using R packages 'phyloseq' and 'DEseq2' (Anders & Huber, 2010; McMurdie & Holmes, 2013). The final ASV taxonomy table

was run through the FUNGuild algorithm to assign putative functional groupings to fungi in the dataset (Nguyen et al., 2016).

To understand how fungal composition varied across fire severity, management type, topography, parent material, soil chemistry, and different soil carbon stocks a distance-based redundancy analysis (dbRDA) was performed. A distance-based redundancy analysis performs constrained ordinations on the data using non-Euclidian distances; in this case Bray-Curtis distance was utilized. dbRDAs are an appropriate tool for visualizing how samples cluster based on Bray-Curtis dissimilarly differences, in which underlying permanovas were utilized to determine if clouds of points were clustering significantly by fire intensity and if the centroids of the points of clouds were statistically different among groups. This method cannot be carried out with data that has zero values, so any soil chemistry data that were below the level of detectability was assigned a small number (1E-15). Fungal composition was also separated out by functional guild (i.e., ECM, saprotrophic) to better comprehend how the abovementioned variables influenced their grouping. The relative abundance of different functional guilds was also analyzed to see how each group teased out by parent material and fire severity. We used a Tukey HSD test to determine if fungal functional groups were statistically different among fire severities and post-fire management. We only utilized carbon stocks and soil chemical variables for the topsoil with these analyses. All statistical analyses were performed in R, version 4.1.2. (RStudio Team, 2020).

Results

Soil Physical and Chemical Properties: pH, Bulk Density, Texture, Elemental Composition

Of the samples that were acid-fumigated, only one sample possessed evidence of carbonates and was consequently removed from further analyses. The Tukey HSD test for bulk density (ρFE)

showed no significant differences (p-value > 0.05) among topographies which may be attributed to small sample size. ρFE in our SSNL site was statistically different from both the MLNL and MCNL sites. The low severity and control plots generally had lower ρFE values (Supplemental Fig. 1). It is important to quantify carbon stocks because it provides insight on ecosystem carbon cycling, but caution must be applied when interpreting results due to the large effect bulk density has on stock values (Throop et al., 2012). To elucidate how ρFE versus TOC percent were influencing the different carbon pool stocks we performed linear regressions of each stock as a function of ρFE and TOC (Supplemental Fig. 2). ρFE had a significant (p-value < 0.05) effect on MAC and POC stocks in which ρFE and MAC stocks were positively correlated and ρFE and POC stocks were negatively correlated. TOC stocks were separated out by fire severity (i.e., control, low, and high) in which ρFE had a significant (p-value < 0.05) effect on TOC stocks in low (positive correlation) and high (negative correlation) severity sites. TOC percent and POC stocks were positively significantly (p-value < 0.05) correlated. Soil texture varied dramatically across sites where the shoulder and backslope topographies possessed higher percent clays. For elemental composition, elements that possessed concentrations lower than the instruments level of detectability were not included in most analyses. Elemental concentrations that were lower than the level of detectability were replaced with very small numbers (1E-15) only in dbRDA analyses because they are more equipped to deal with sparse data (Jupke & Schäfer, 2020).

Soil Organic Carbon: TOC, MAC, POC, PyC

Prior to calculating carbon stocks, we visualized carbon percent by site incorporating the varying topographies, depths, and replicates (Fig. 2). POC percent were higher in all sites with respect to MAC and PyC. The carbon pools possessed inverse proportions of total sample weight. The integration of carbon pool fractions and their proportion of total sample weight led to the relative

carbon pool percent observed in Fig. 2C, where the POC pool is highest in the MLNL site with respect to the others. The Random Forest Regressions (Supplemental Figs. 3 and 4) separated out by parent material (i.e., metamorphic and serpentine) provide insight on the variables influencing carbon pool fractions (percent divided by 100). We had first attempted to run Random Forest regression on carbon stocks, but the regressions poorly fit our data in which regression fit improved dramatically when using carbon fractions instead. The Random Forest Regression for the metamorphic TOC fraction explained 58.38% of the variation and possessed a mean squared error (MSE) equal to 0.0006, where the variables that went into the model were based on which model had the lowest MSE value. Additionally, variables that would inflate correlation were not included, such as the total nitrogen (TN) fraction since it is inherently linked with organic matter. The different pools were not included in the separate pools' regressions. The TOC Random Forest Regression included fire severity, management, saprotroph and ECM relative abundances, Ti, Si, S, Mn, Mg, Fe, Co, and Ca concentrations. Fire severity, S, and Mn had the largest effects on TOC with respect to the other variables because if they were omitted from our Random Forest Regression the MSE would increase. S and Mn have the highest node purity which indicates that when decision tree is splitting, there is higher inter-node variance with respect to intra-node variance. The Random Forest Regression for the metamorphic MAC fraction explained 62.23% of the variation and possessed a MSE equal to 0.0002. The MAC Random Forest Regression included fire severity, management, saprotroph and ECM relative abundances, TN fraction, Ti, Si, S, Mn, Mg, Fe, Co, and Ca concentrations. The TN fraction was included in the regression because previous research has indicated that nitrogen concentrations in the soil influence MAC production (Cotrufo et al., 2013; Lavallee et al., 2019). Saprotroph relative abundance, S, Mn, and the TN fraction had the largest effects on MAC with respect to the other variables. S, Mn,

and the TN fraction had the highest node purities. The Random Forest Regression for the metamorphic PyC fraction explained 19.83% of the variation and possessed a MSE equal to 0.0004. The PyC Random Forest Regression included fire severity, saprotroph and ECM relative abundances, Ti, Si, S, Mn, Mg, and Ca concentrations. Fire severity, S, and Mn had the largest effects on PyC with respect to the other variables. S and Mn had the highest node purities. The Random Forest Regression for the metamorphic POC fraction explained 45.25% of the variation and possessed a MSE equal to 0.003. The POC Random Forest Regression included fire severity, management, saprotroph and ECM relative abundances, Ti, Si, Mn, Fe, Co, and Ca concentrations. Fire severity and Ca had the largest effects on POC with respect to the other variables. Fire severity, Ca, and Mn had the highest node purities.

As previously mentioned, we also ran Random Forest regressions on delta carbon fractions for each carbon type (Supplemental Table 1). Even though we performed these regressions on carbon fractions, we still included ρFE to see they were linked. For the delta TOC fraction, S, ECM relative abundance, and ρFE possessed higher influences on the regression with respect to the control TOC. Mn decreased in importance in the delta TOC regression with respect to the control. In the delta MAC regression, S, ECM relative abundance, Mn, Mg, Fe, Co, Ca, and management increased in importance with respect to the control, in which the importance of the nitrogen fraction decreased. For the delta PyC fraction, Ti, Mn, Mg, Ca, severity, ρFE, saprotroph and ECM relative abundance increase in importance with respect to the control. In the delta POC regression, Ti, S, ECM relative abundance, Mg, severity, management, and ρFE increased in importance with respect to the control, in which Si, Fe, Co, and Ca decreased in importance.

Management was not included in any of the Random Forest Regressions for the serpentine sites since none of them were salvage logged because they are grasslands (Supplemental Fig. 4). The Random Forest Regression for the serpentine TOC fraction explained 57.38% of the variation and possessed a mean squared error (MSE) equal to 0.0006. The TOC Random Forest Regression included fire severity, saprotroph and ECM relative abundances, Ti, Si, S, Mn, Mg, Fe, Co, and Ca concentrations. Fire severity, S, and Mn had the largest effects on TOC with respect to the other variables. S and Mn had the highest node purities. The Random Forest Regression for the serpentine MAC fraction explained 64.11% of the variation and possessed a mean squared error (MSE) equal to 0.0002. The MAC Random Forest Regression included fire severity, saprotroph and ECM relative abundances, TN fraction, Ti, Si, S, Mn, Mg, Fe, Co, and Ca concentrations. S, Mn, and the TN fraction had the largest effects on MAC with respect to the other variables and possessed the highest node purities. The Random Forest Regression for the serpentine PyC fraction explained 21.18% of the variation and possessed a MSE equal to 0.0004. The PyC Random Forest Regression included fire severity, saprotroph and ECM relative abundances, Ti, Si, S, Mn, Mg, Fe, Co, and Ca concentrations. S, Mn, Ca, and fire severity had the largest effects on PyC with respect to the other variables. S and Mn had the highest node purities. The Random Forest Regression for the serpentine POC fraction explained 40.88% of the variation and possessed a MSE equal to 0.003. The POC Random Forest Regression included fire severity, saprotroph and ECM relative abundances, Ti, Si, Mn, Fe, Co, and Ca concentrations. Fire severity and Ca had the largest effects on POC with respect to the other variables. Fire severity, Ca, and S had the highest node purities.

The Random Forest regressions for the delta carbon pools in the serpentine sites again did not include management since salvage logging did not occur in these sites. Fire severity was also

not included because serpentine sites only had absent versus high severity fire presence (Supplemental Table 2). Regressions for all control carbon pools did not fit the data, so we are unable to compare delta carbon pools. Small sample sizes generally decrease the validity of this model approach. For the delta TOC fraction, Ca, saprotroph, and ECM relative abundance were the only variables of importance. In the delta MAC regression, Ti and nitrogen fraction were the only variables of importance. For the delta POC fraction, Si, Mn, Mg, Fe, Co, and Ca were the only variables of importance. In the delta PyC regression, Ti, ρFE, saprotroph, and ECM relative abundance were the only variables of importance.

Fig. 2 a) displays carbon percent for each site, **b)** shows the percent each carbon pool makes up of the total sample weight, and **c**) is carbon percent and carbon pool sample proportion multiplied by each other to give the proportional percent C of the total sample abundance.

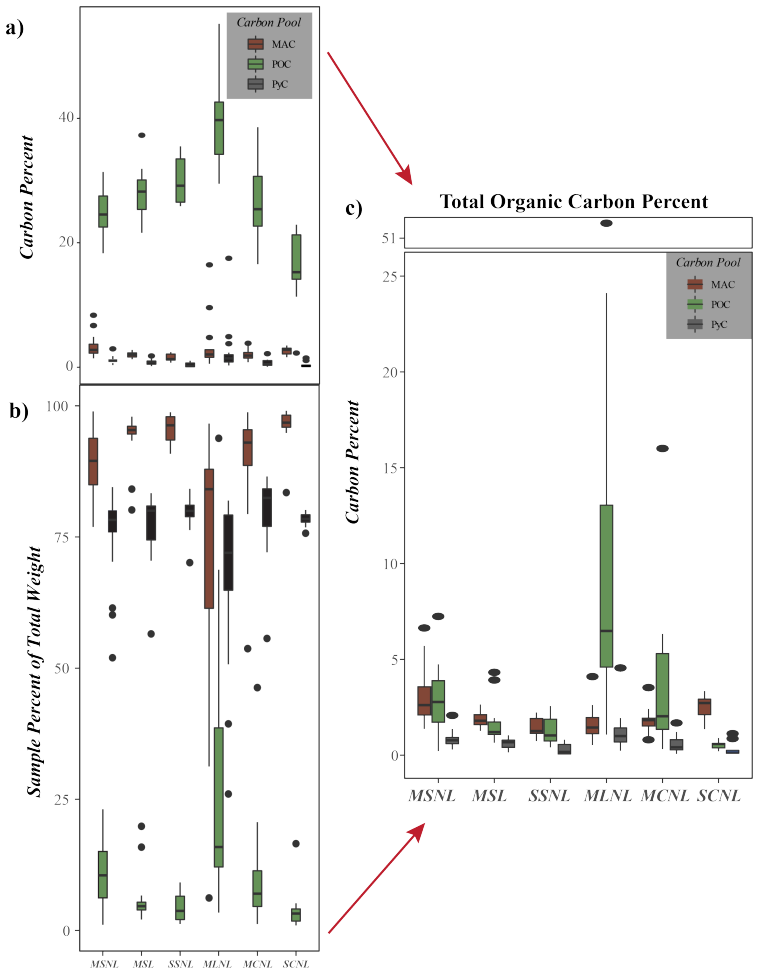

TOC stocks were calculated for each site, depth, and topography based on an area of one meter squared using an adjusted bulk density value (ρFE) to account for high course fraction volume. Since we were unable to reach a depth below 40 cm for the majority of samples, the sites that had samples below 40 cm (n = 2) were not included in carbon stock analyses. To better visualize differences in TOC stocks, valley topographies are represented in a different panel (Fig. 3). Within each site, TOC stocks for each hillslope topography were not statistically different (p-value > 0.05), so we did not separate out topography when visualizing the data. The ANOVA executed for hillslope TOC stocks as a function of site was significant (p-value < 0.05). With respect to topsoil (< 20 cm), the MSL site possessed mean TOC stocks (9.1 ± 2.4 kg/m^2) that were statistically higher than SSNL, MCNL, and SCNL (3.6 ± 1.3 kg/m^2; 5.1 ± 4.3 kg/m^2; 3.6 ± 1.9 kg/m^2;), but all other sites were not statistically different from one another. For stocks below 20 cm, the MSL site possessed mean TOC stocks (5.7 ± 2.4 kg/m^2) statistically higher than the MCNL site (2.6 ± 1.2 kg/m^2). All other sites were not statistically different. The ANOVA executed for valleys TOC stocks as a function of site was significant (p-value < 0.05). With respect to the valley topographies, the topsoil for the valley in-between the MSNL and MSL sites possessed statistically higher mean TOC stocks (13.3 ± 2.7 kg/m^2) than the MLNL and MCNL sites (3.6 ± 3.1 kg/m^2; 1 ± 0.6 kg/m^2). TOC stocks were not statistically different in depths below 20 cm. TOC mean stock values and standard deviations that were not mentioned can be observed in Supplemental Table 3.

Fig. 3 displays TOC stocks in boxplots where **a)** shows the hillslope topographies and **b)** displays the valley topography, where stocks are separated out by depth. Letters indicate which sites are statistically different, where the background color indicates topsoil or greater than 20 cm. In the histograms above the stock figures, frequency of samples is shown where (F) is footslopes, (B) backslope, (S) shoulder, and (V) valley.

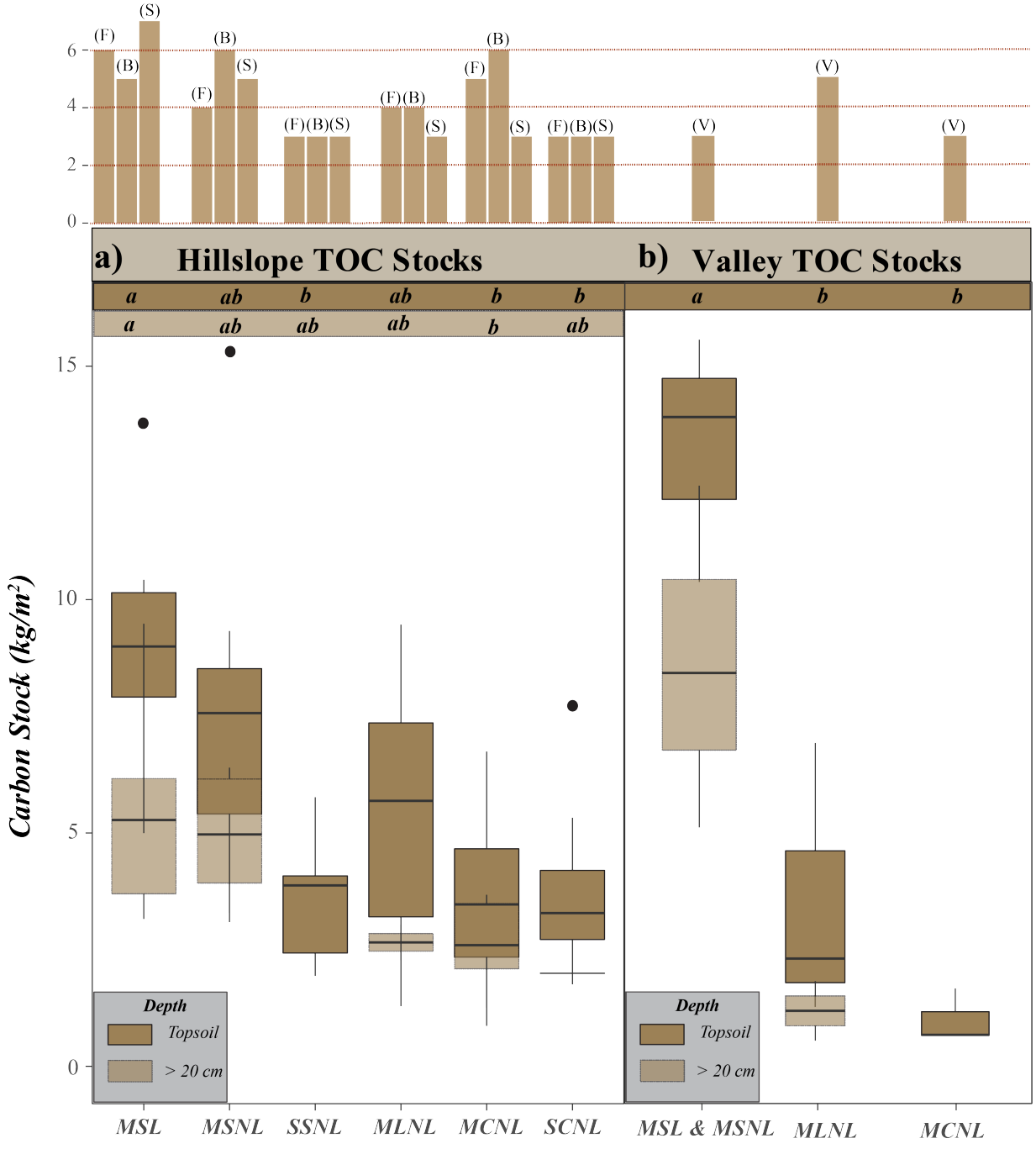

MAC and POC stocks were calculated as TOC but with adjusted bulk density as discussed in the methods and accounting for the proportion of total sample weight. With respect

to MAC stocks, there were no statistical (p-value > 0.05) differences among hillslope topographies, but in the MCNL site, footslope and backslope POC stocks were statistically (p-value > 0.05) different. Since hillslope topography generally did not have a significant effect on MAC and POC stocks, we represented stocks by site and did not separate out by hillslope topography (Fig. 4). The ANOVA executed for hillslope MAC stocks as a function of site was significant (p-value < 0.05). In the hillslope topsoil, MAC stocks were statistically higher in the MSL and MSNL sites (6 ± 1.2 kg/m^2; 5.7 ± 2.4 kg/m^2) with respect to the SSNL and MLNL sites (2.5 ± 0.9 kg/m^2; 1.9 ± 1.2 kg/m^2). The SCNL site (5.3 ± 2.9 kg/m^2) had statistically higher MAC stocks than the SSNL and MLNL sites. MAC stocks were not statistically different in depths below 20 cm in the hillslope topographies. The ANOVA executed for valley MAC stocks as a function of site was significant (p-value < 0.05). With respect to the valley topographies, the topsoil for the valley in-between the MSNL and MSL sites (15.4 ± 4.9 kg/m^2) possessed statistically higher mean MAC stocks than the MLNL and MCNL sites (1.7 ± 0.7 kg/m^2; 1.3 ± 0.5 kg/m^2). MAC stocks were not statistically different in depths below 20 cm. In all topographies (i.e., hillslope and valleys) and across both depths (i.e., topsoil and below 20 cm), POC stocks were not statistically different (p-value > 0.05) among sites. The ANOVA executed for hillslope and valley POC stocks as a function of site was not significant (p-value > 0.05). The topsoil for hillslope and valley in the MLNL site generally possessed higher POC stocks with respect to the other sites (6.1 ± 4.3 kg/m^2; 23.6 ± 25.6kg/m^2). POC stock values for other sites can be observed in Supplemental Table 3.

Fig. 4 a) shows MAC and POC stocks for each site and hillslope topography including all replicates and depths. Panel **b)** shows MAC and POC stocks for each site and valley topography including all replicates and depths. Letters show which sites are statistically different from one another. In hillslope and valley topographies, only MAC stocks showed statistical differences among sites. Note that the y-axis for panels **a)** and **b)** are not the same.

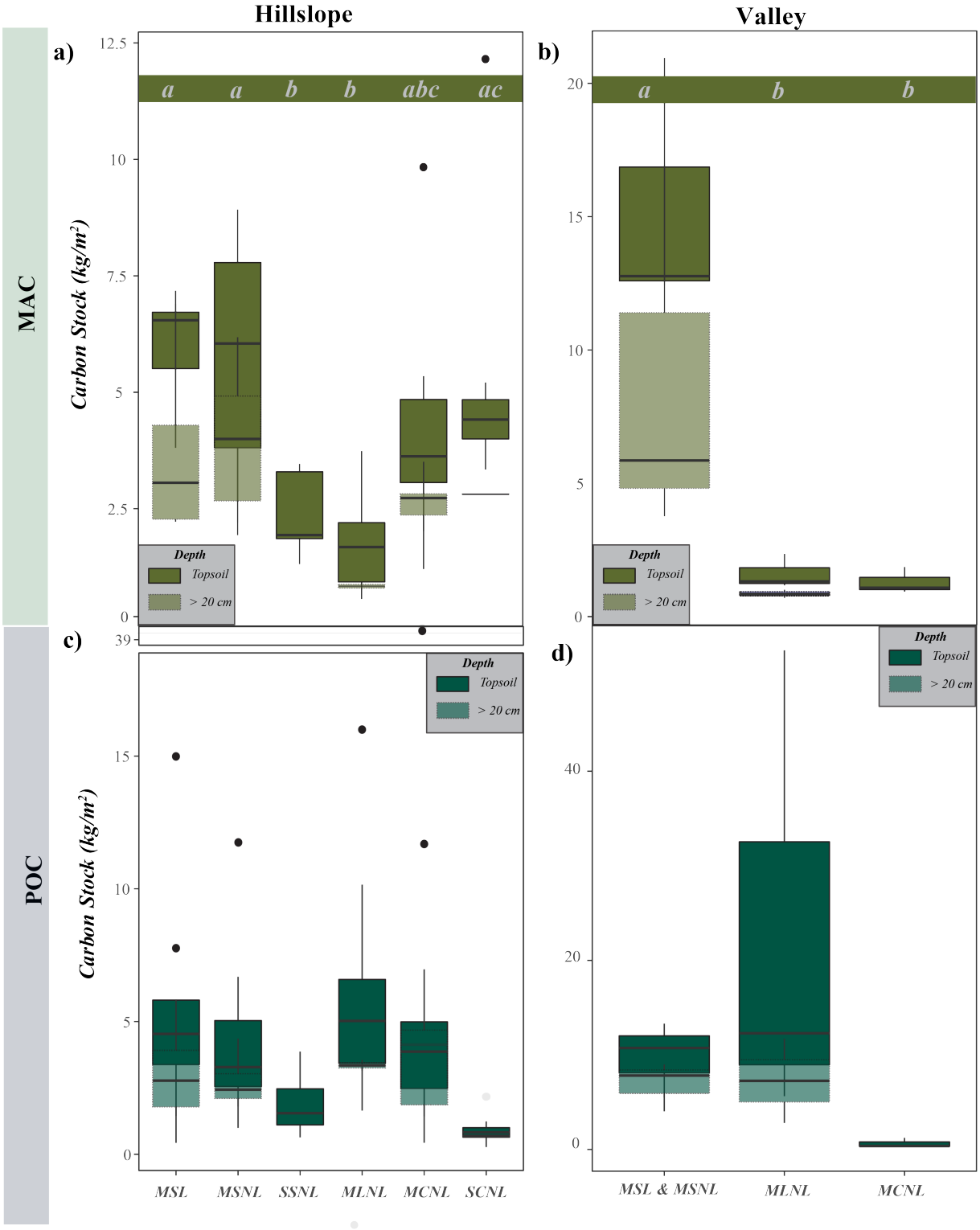

PyC stocks were calculated the same as TOC, using the same bulk density but accounting for the proportion of total sample weight. Within each site, PyC for each hillslope topography were not statistically different (p-value > 0.05), so stocks were not separated out by topography within sites (Fig. 5). The ANOVA executed for hillslope PyC stocks as a function of site was significant (p-value < 0.05). For the topsoil in hillslope topographies, PyC stocks were statistically higher in the MSL site (2.6 ± 1.4 kg/m^2) with respect to the SSNL, MLNL, MCNL, and SCNL sites (0.6 ± 0.6 kg/m^2; 1 ± 0.5 kg/m^2; 1 ± 0.6 kg/m^2; 0.6 ± 0.6 kg/m^2). In depths below 20 cm in the hillslope topographies, the MSL and MSNL sites (1.3 ± 0.6 kg/m^2; 1.3 ± 0.4 kg/m^2) possessed statistically higher PyC stocks with respect to the MCNL site (0.4 ± 0.2 kg/m^2). The ANOVA executed for valley PyC stocks as a function of site was significant (p-value < 0.05). For topsoil, the valley in between the MSL and MSNL (1.8 ± 0.2 kg/m^2) sites possessed significantly higher PyC stocks that the MCNL site (0.1 ± 0.1 kg/m^2). PyC stocks were not statistically different (p-value > 0.05) in depths below 20 cm in the valley topographies.

Our PCA (Fig. 6) for metamorphic sites explained 51.3% of the variance within those samples where MAC was strongly and positively correlated with total nitrogen (TN) stocks. The TN loadings for PC1 and PC2 positively and strongly contributed to both axes, indicating that samples within the top right corner of the PCA possess the highest TN values. The POC loading also fell within this region of the plot. Fe, Co, Mn, and Si contribute considerably to PC1. The majority of the soil chemistry variable had negative loadings associated with PC2, so the variables generally had higher concentrations at lower PC2 values. To elucidate how fire severity and post-fire management interacted with the PCA axes, we used a one-way ANOVA where management and severity only had a significant effect (p-value < 0.05) on PC2. Our PCA for the serpentine sites explained 66.7% of the variance within those samples.

Fig. 5 displays PyC carbon stocks in grams per square meter where **a)** shows the hillslope topographies and **b)** displays the valley topography. Different letters indicate whether groups are statistically significant.

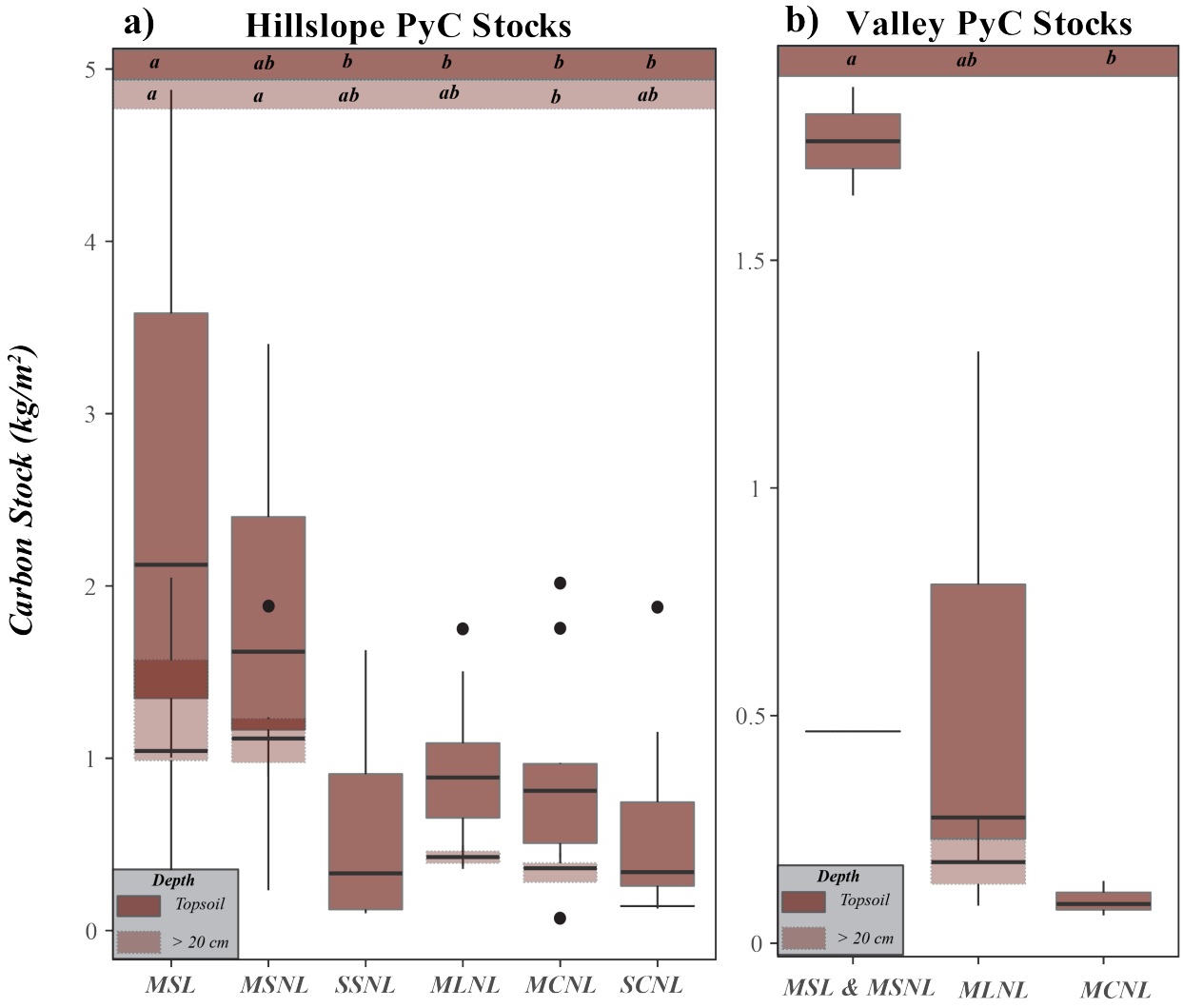

The TN loading differed in this PCA and had a zero value for PC1, where Si, Ca, Fe, Co, Mn, and Mg all had strong contributions to PC1. Only MAC stocks possessed non-zero loadings for PC1. POC and TN stocks possessed the highest positive loadings for PC2, and pH had the largest negative loading. For the serpentine PCA, fire severity (because post-fire management is not applicable in these sites) did not have a significant effect on PC1 or PC2. In our PCA for metamorphic sites, PyC stocks had larger loadings for PC2 and weaker ones for PC1. The magnitude and direction of our PyC vector may indicate that PyC stocks were not as strongly

related to soil chemistry variables such as Fe or Mn. In our PCA for serpentine sites, PyC stocks had a zero-value loading for PC1 but contributed majorly to PC2 and was strongly and positively correlated with POC and TN stocks. pXRF data can be observed in Supplemental Table 4.

Fig. 6a) is a PCA for metamorphic sites and **b)** is a PCA for serpentine sites. Samples are colored based on post-fire management and delineated by fire severity. The '*' after the PC2 equation in panel one indicates a p-value < 0.05.

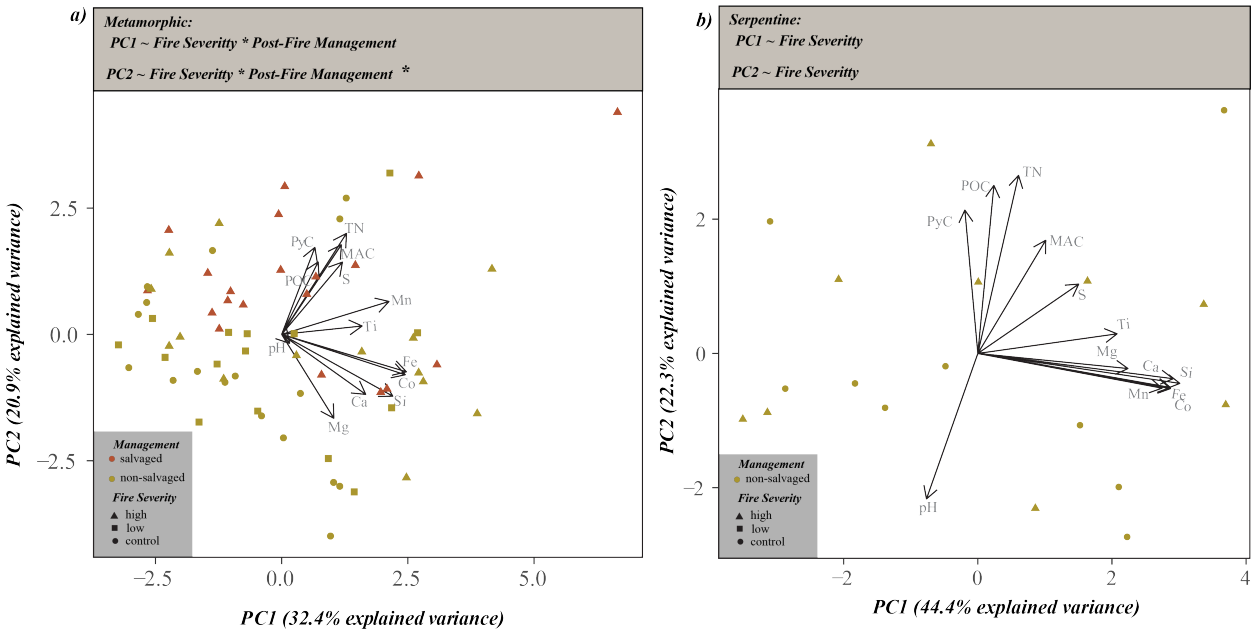

Fungal Community Composition and Bioinformatics Processing

Fungal community composition varied among parent materials where there was a higher relative abundance of ECM fungal functional groups in the metamorphic sites with respect to serpentine (Fig. 7). In the metamorphic sites, ECM fungal functional groups decreased significantly (p-value < 0.05) in relative abundance with increasing fire severity but were not statistically different between low severity and control sites. Conversely, saprotrophic fungal functional groups increased significantly (p-value < 0.05) in relative abundance with increasing fire severity but were not different between low and high severity sites. In serpentine sites, Saprotroph fungal functional groups possessed the highest relative abundance but were not statistically different

between the control and high severity site. The ECM fungal functional group increased significantly (p-value < 0.05) from control to high severity.

Fig. 7 displays the major function fungal groups delineated by parent material (i.e., metamorphic, serpentine). Relative abundance is represented on the y-axis and fire severity on the x-axis.

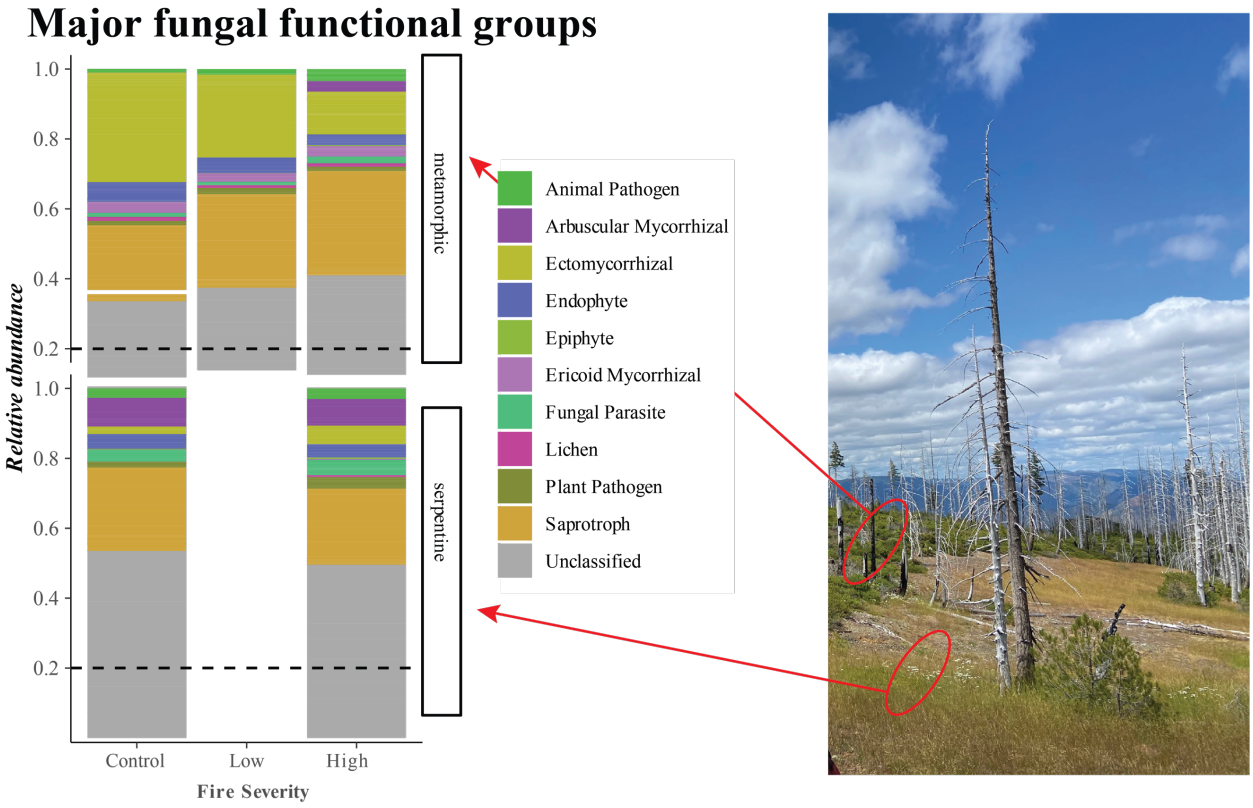

Two distance-based redundancy analyses (dbRDA) – separated by different parent materials – were performed to visualize how soil carbon pools and chemistry variables associated with fire severity and fungal composition (Fig. 8). The metamorphic dbRDA explained 32.86% of variance in fungal composition where both axes were statistically significant. MAC significantly contributed to fungal composition and was positively correlated with high fire severity samples. Ti, pH, Si, S, and Cr were the only soil chemistry variables that significantly correlated with fungal composition. ECM relative abundance was positively correlated with control and low severity samples and likely driving fungal composition within

these samples. Saprotroph relative abundance positively correlated with high severity samples but was not significant. Prior to executing the underlying permanovas for the dbRDA analyses, we ensured the data was not confounded using a beta dispersion test, which our data passed. The permanova ($R^2 = 0.13237$) for the metamorphic sites showed that fungal composition data significantly clustered by fire severity. The linear regression executed to determine if post-fire management (i.e., salvage logging) had a significant effect on the relative abundance of the dominant fungal functional groups showed that salvage logging had a significant negative effect (p-value < 0.05) on ECM relative abundance, but a significant positive effect (p-value < 0.05) on saprotrophic relative abundance. The serpentine dbRDA explained 36.4% of variance in fungal composition where only the first axis was statistically significant. MAC and POC significantly contributed to fungal composition where MAC was positively correlated with control samples and POC was positively correlated with high severity samples. No soil chemistry variables significantly affected fungal composition. ECM relative abundance was positively correlated with high severity sites but not significant. The underlying permanova ($R^2 = .27788$) for the serpentine sites passed the beta dispersion test and showed that fungal composition data significantly clustered by fire severity. For both dbRDAs, the topography variable was removed since it lowered the amount of variance explained in both models. Prior to running the two dbRDAs separate out by parent material, we included all categorical variables together with soil carbon and chemistry data which explained 99.2% of the variance in the fungal composition data.

Fig. 8 a) shows how soil carbon stocks and chemistry align with metamorphic parent material and relative abundance of ECM and saprotrophic fungi where this dbRDA explains 32.86% of variance in fungal composition for metamorphic sites. **b)** shows how soil carbon stocks and chemistry align with serpentine parent material and relative abundance of ECM and saprotrophic fungi, where this dbRDA explains 36.4% of variance in fungal composition for serpentine sites. *** indicates a p-value < 0.001; ** indicates p-value < 0.002; * indicates a p-value < 0.05.

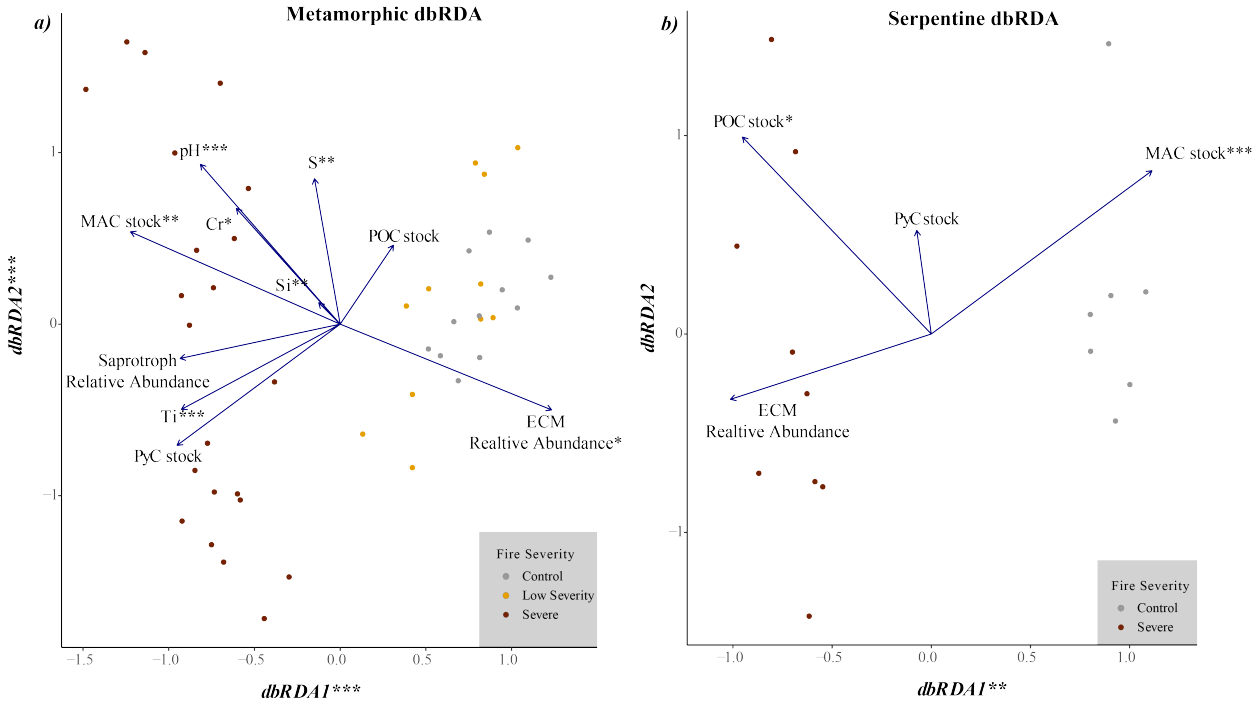

Discussion

There are numerous studies that exist researching how soil carbon stocks change after a wildfire, but these studies often do not delineate how specific carbon types (i.e., MAC, POC, PyC), in tandem with fungal community composition, shift in relation to wildfire and management. It is important to quantify how fire and post-fire management affect these individual pools because they each have varying residence times which contribute to the overall stability of the soil organic carbon pool. Here we report that soil carbon types varied with respect to fire severity and post-fire management but not in ways that we had hypothesized. Our first hypothesis that TOC stocks would decrease along an intensity gradient (fire plus management) but where low severity fires would have the highest carbon stocks was not supported by our data. Instead, we observed

that the high severity sites, including the one that was salvage logged generally possessed higher TOC stocks than the unburned and control sites. It appears that the high severity fires contributed to an organic carbon pulse post-fire. MSL had many shrubby species that may be contributing to new organic inputs in addition to a post-fire nutrient pulse. A reason why we did not see higher TOC stocks in the MSNL could be contributed to the fact that most snags where still standing, where this burnt wood possesses nutrient pools that are consequently not being integrated into the soil (Juan-Ovejero et al., 2021). Topography, specifically valleys, played a large role in carbon stocks. The observed significant trend of higher TOC stocks in the valley between the MSNL and MSL sites suggests a post-fire erosion effect (Abrahams et al., 2018). Such data indicates that even though large amounts of organic carbon are lost from an ecosystem after fire (organic matter combustion), not all of it is necessarily lost but has rather been translocated elsewhere. Lateral movement and burial of TOC to valleys could lead to increased carbon stability (Abney et al., 2017). It is important to note, when just observing the TOC percent, carbon was highest in the MLNL site. High severity fire can lead to a hydrophobic layer which can contribute to soil compaction especially in precipitation events and the addition of heavy machinery associated with salvage logging is likely driving increases in bulk density. Additional sources of bulk density compaction from fire include loss of organic matter (e.g., direct combustion, loss of roots) which can degrade aggregate stability which consequently changes soil contact surfaces and contributes to compaction (Massman et al., 2010). Caution must be applied when interpreting carbon stock results because it is uncertain if high stocks are a legacy effect of soil compaction. We did also observe decreases in TOC stocks with the highest bulk density values which is likely attributed to the serpentine sites. Our serpentine sites generally possessed shallow soils with lower aboveground vegetation diversity. These sites may have

lower aboveground inputs that shape and enhance soil structure and poor soil structure can contribute to increased bulk density values.

We had hypothesized that an intensity gradient (fire severity and post-fire management) would lead to decreased MAC stocks – inferring lower soil carbon stability. Our hypothesis was not supported by our data. It appeared that MAC stocks were driving differences in TOC among sites with respect to POC. MAC stocks were generally higher in sites that had high fire severity and were significantly higher than our low severity site. Again, we observed a potential post erosion effect where MAC stocks were highest in the high severity valley. Even though POC stocks did not vary significantly among sites in both hillslope and valley topographies, there was a general trend of higher POC stocks in Site 5 (control, non-salvaged, metamorphic). This trend could be related to the soil fungal composition where ECM fungi generally contribute to more to POC pools versus MAC (Lavallee et al., 2019). Another way that MAC is distinct from POM is that it is derived from organic matter that has either leached directly from plants or has been chemically altered by soil microorganisms which contributes to MAC being enriched in ^{13}C (Lavallee et al., 2019). Previous research found that increases in fire frequency contribute to more positive $\delta^{13}C$ values in soil organic matter (Bird, et al., 2000), so fires may be facilitating a more direct path for MAC development. In our study we observed that MAC stocks were correlated with Fe. Nutrient pulses post-fire can increase magmatism in the topsoil, where Fe and Mn are common constituents of ash (Jordanova et al., 2019). Organo-mineral clusters may be forming between MAC and Fe consequently increasing MAC stocks within the high severity sites, consequently causing MAC to become less mobile. MAC may be more likely to form these associations rather than POC due to MAC's enhanced sorption to mineral surfaces (Lavallee et al., 2019). Additionally, N increases after fire events which favors MAC development over POM

could be another reason we witnessed higher MAC stocks in the high fire severity sites (Lavallee et al., 2019). N inputs post fire can alter soil stoichiometry that matches the demand of microbes which could alter soil OM formation, where MAC is more likely to formed (Cotrufo et al., 2013; Lavallee et al., 2019). Higher N deposition decreases microbial N-limitation which can subsequently lead to increased POM decomposition (Lavallee et al., 2019). With respect to bulk density, it appeared to be driving MAC stocks but not POC stocks – which seemed to more of a function of carbon percent. Here, higher MAC stocks could have also been a legacy effect of fire increasing bulk density, so caution should again be applied when interpreting these results. Bulk density was generally higher in high severity sites which correlates with lower ECM relative abundance. ECM fungi tend to lead to the development of POC versus MAC.

Even though PyC comprised a smaller proportion of TOC stocks, it still contributes significantly to overall stability since PyC can be a highly recalcitrant pool (Lavallee et al., 2019). Our data showed that PyC stocks were greatest in our high severity hillslope sites, but there was not as strong as an erosion effect (i.e., deposition in valleys). PyC can be preferentially eroded shortly after fire events with respect to other carbon pools (Abney et al., 2017), so it is possible that PyC had been eroded and decomposed prior to our sampling. Based on the temperature at which PyC was formed, it can have different mineralization rates, specifically when PyC formed at higher temperatures (Santos et al., 2021). PyC formed at higher pyrolysis temperatures can lead to a positive priming effect consequently increasing mineralization. The larger PyC stocks in the high severity sites could exasperate organic matter decomposition in addition to the loss of ECM relative abundance and consequently lower PyC stocks.

Sulfur (S) appeared to play a major role in TOC, MAC, and PyC but not for POC in both metamorphic and serpentine parent materials. The majority of S in soil is specifically from OM,

so it is intuitive that it would be correlated with carbon (Schroth et al., 2007). S is assumed to be a stabilizing force in SOC (Kirkby et al., 2011), so smaller concentrations of S in POC could be attributed to higher lability of this pool. Organic sulfide is considered a more reactive S species that associates with labile organic pools (Schroth et al., 2007). Furthermore, S is considered somewhat sensitive to heat and volatizes at lower temperatures with respect to other elements (Hrelja at al., 2020).

Ca and Mg were included in every Random Forest regression except for the metamorphic POC regression prior and generally increased in importance in the delta carbon fraction regressions. Ca and Mg are linked to ash deposits post fire (Francos et al., 2018), so they may be contributing to increased OM formation after wildfire events. Ti, Si, and Co were included in all the Random Forest regressions, but Ti was the only variable that increased in relative importance in the delta carbon fraction regressions. These elements are likely derived from the underlying parent material where fire may be further releasing Ti from rock/ minerals. These variables may simply be correlated with stocks as a byproduct of fire rather than a mechanism of increasing carbon stocks. As mentioned previously, there are caveats using Random Forest regressions with small sample sizes in that there will be increased output variability. It would be prudent to add more samples to this study in the future to validate our regression results which would enable us to quantify with more certainty which variables are driving soil carbon stability, and which are a byproduct of a small sample size.

Our final hypothesis was predominantly supported. ECM fungal functional groups decreased significantly along a severity gradient (i.e., fire severity plus management) in the metamorphic sites while saprotrophic fungal functional groups increased significantly with severity. Our data supports the “Gadgil Effect” (Fernandez & Kennedy, 2016), where increasing

disturbance allowed for a transition in fungal functional groups. Decreases in ECM relative abundance with an increasing severity gradient, provides an opening for opportunistic fungi, like saprotrophs, to establish. Fire frequency is likely to increase in this region, consequently reinforcing changes in dominant fungal functional guilds which can consequently lead to a tipping point of more decomposition versus sequestration. We also observed a different trend occurring in our serpentine sites, where ECM fungal functional groups increased in relative abundance with increasing fire severity. When executing our underlying statistics for our dbRDA analyses, the beta dispersion for our clouds of data was not tightly clustered which can indicate increased microbial diversity. The serpentine sites are characterized by fewer vegetative species and minimal woody vegetation; so, fire plus lower aboveground biodiversity may have allowed ECM fungi to inhabit unoccupied niche spaces more easily.

As aforementioned regarding the metamorphic sites, ECM relative abundance was positively associated with low severity and control sites' fungal composition, in which POC stocks share a similar trend. POC and ECM fungi being correlated is consistent with previous research supporting that ECM fungi generally contribute more to POC production (Lavallee et al., 2019). The significant chemical variables were generally more positively correlated with fungal communities associated with the high severity site. The increased niche availability because of fire severity's negative influence on ECM relative abundance plus post-fire nutrient pulses – specifically nitrogen – could have facilitated saprotroph establishment. In our serpentine sites, we observed POC stocks significantly contributing to fungal community composition specifically in the severe sites where there was a higher relative abundance of ECM fungi functional groups. This supports previous research that ECM fungi enhance the production of the POC pool. MAC stocks were significantly contributing to fungal community composition in the

control sites which may be attributed to less competition for N resources due to the lower relative abundance of ECM fungi.

Conclusion

Soil carbon pools can persist on decadal to millennia temporal scales where changes may not be apparent on anthropic scales. These samples were collected only 20 years after the Biscuit Fire, so it is possible that we will be unable to truly realize the effects of this fire on soil carbon stability for another few decades. We were able to elucidate multiple environmental and biotic variables that are likely influencing not just total carbon stocks but individual carbon pools (i.e., MAC, POC, PyC). The dominant driver of increased carbon stocks in TOC and MAC pools appeared to be bulk density in the metamorphic sites rather than actual carbon percent. The alleged increases in stocks may just be a legacy effect of fire severity and superimposed management. As time moves forward and increased aboveground vegetation inputs influence the soil system, we may observe a shift in bulk density (lower values). With respect to POC stocks, carbon percent over bulk density seemed to be driving stocks where we observed high POC stocks even with low bulk density values, so these may be more accurate carbon stock representations. We also observed the potential for increases in importance with organo-mineral complexes in MAC and PyC specifically in fire affected sites which has implications for enhanced carbon stability. This study also provided insight on the importance of different fungal functional guilds on the establishment of different carbon pools, in which ECM relative abundance was associated with higher POM production and saprotroph with MAC. Over the next century, it would be prudent to continuously measure soil carbon pools and fungal community composition within the Biscuit Fire burn scar to delineate the long-term effects of severe wildfire and post-fire management. Through understanding how soil carbon sequestration and stability

changed in this system, we may be able to discern how other megafires have been influencing their soil environment.

CHAPTER IV

ELUCIDATING ECOSYSTEM PRODUCTIVITY AND TERRESTRIAL DEVELOPMENT IN THE PACIFIC NORTHWEST

Contributions

This chapter in coauthored by Jamie L. Wright, Natalie J. Kozlowski, Dan G. Gavin, and Lucas C.R. Silva. I was responsible for data collection and sample analyses where Natalie J. Kozlowski was also a part of sample acquisition and pollen analyses. I am responsible for data analyses and writing the manuscript, where coauthors have contributed to the review process.

Introduction

In the Puget Lowland of the Pacific Northwest (USA) ecosystems have shifted dynamically throughout the Holocene reflecting the changing climate. The vegetation and fire history of this region has mirrored these changes in climate (Walsh et al., 2015; Whitlock, 1992). Several previous studies have demonstrated that over the middle Holocene (ca. 8000 to 4000 cal yr BP), the Puget Lowland forest composition transitioned from early successional (i.e., *Pseudotsuga menziesii*, *Alnus rubra*) to late successional species (i.e., Cupressaceae, *Tsuga heterophylla*) which remain today (Crausbay et al., 2017b; Gavin & Brubaker, 2013; Tsukada et al., 1981). Higher fire frequency in the early Holocene is also widely reconstructed across this region (Walsh et al 2015). The early Holocene was characterized by greater summer drought associated with increased summer insolation and an intensified Pacific Subtropical High pressure system, which diminished in intensity into the late Holocene (Nelson et al., 2011; Thompson et al., 1993). In the dry rain-shadowed areas of the Puget Lowland and Willamette Valley, a land-use regime involving cultural and sustenance use of fire may have enhanced oak prairie extent through the early Holocene (Leopold and Boyd 1999); though a widely observed increase in fire

in the late Holocene may also reflect similar land-use (Leopold & Boyd, 1999; Walsh et al., 2018). The encroachment of Euro-colonization in the late 1800s led to rapid transformation of the landscape through logging and agriculture (Constantine *et al.*, 2016).

The Puget Lowland provides a unique opportunity to study the transection of post glacial landforms, long records of human influence, fire, and climatic change with ecosystem development and change. Glacial landforms resulted in numerous deep kettle lakes in the Puget Lowland. Although the general pattern of vegetation change in the Puget Lowlands has been well described, no studies have yet taken advantage of a more complete ecosystem reconstruction using multiple proxies that record vegetation, fire, erosion, leaching, mass sediment influx events from disturbances, and aquatic productivity. In lakes where carbonate precipitation is minimal, organic matter (OM), biogenic silica (BSi), and detrital clastic inputs comprise the entirety of sediment. Their proportions in lake sediment serve as a first-order proxy of ecosystem change over time (Liu et al., 2013). Further characterizing these components (e.g., organic geochemistry and elemental analyses) provide a better understanding how ecosystems have been responding to climatic change and disturbance (Davies et al, 2015).

Sediment organic matter (OM) is derived from terrestrial and aquatic inputs but disentangling the two can be difficult. A combination of geochemical and productivity processes contributes to terrestrial and aquatic organic carbon (OC) often possessing overlapping carbon isotopic signatures. However, in some cases respired organic matter is reused by aquatic productivity which further depletes ^{13}C from that of terrestrial matter (Meyers and Lallier-Vergès, 1999). In addition, aquatic organic matter possesses lower atomic C:N ratios with respect to terrestrial OM (Meyers and Teranes, 2001). The overall OC accumulation rates of the lake, coupled with percent BSi, provides further insight on lake productivity and the overall

ecosystem ability to sequester carbon (Brown, 2015). BSi is a direct indicator of lake productivity since it is derived from diatom production and preserves well at low pH. BSi is strongly affected by both nutrient availability and climate (Brown, 2015).

Clastic material in sediment is derived from the bedrock and soil, consequently linking sediment geochemistry to the terrestrial ecosystem (Davies et al., 2015). Clastic materials' geochemistry possesses specific markers that reflect processes and events that develop over millennia. For instance, magnetic susceptibility of bulk sediment and weathering indices derived from elemental analyses such as x-ray diffraction can reveal erosion events and the progressive weathering of soils, respectively (Price and Velbel, 2003). Ti concentration is especially informative because it is only a terrigenous input (Arnaud *et al.*, 2012) and can be used to normalize Si concentrations and therefore reflect BSi (Brown, 2015).Clastic geochemistry additionally provides insight on the lacustrine environment, such as oxygenation levels inferred from Mn:Fe (Melles *et al.*, 2014).

To elucidate how ecosystems have responded to long-term climatic change and shifting disturbance regimes, we retrieved a sediment core from Shadow Lake – a small, deep lake within the Puget Lowland. Here, we used a multiproxy approach of biological and geochemical indicators to first detangle how the surrounding terrestrial ecosystem responded to the intersection of climate and disturbance, and second, to quantify lake productivity along the same axis. We first hypothesized that lake productivity would be high in the early Holocene due to warmer summer temperatures and significantly more fire than present and consequently increased erosional nutrient input (Shelley D Crausbay *et al.*, 2017; Cwynar, 2019). Second, cooler summers, a reduction of fire and development of old growth forests in the mid Holocene would result in lower erosional input, more weathered soils, and lower aquatic productivity.

Lastly, in the late Holocene we hypothesized that lake productivity increased as a combined effect of increased cultural fire use and climatic variability, and that soil weather increased progressively through the late Holocene.

Materials and Methods

Study Site

Shadow Lake (122.09 °W, 47.41 °N) has a surface area of 20 ha and watershed area of 209 ha, with a maximum depth of approximately 13.5 m (Figure 1). Shadow Lake has no inflowing or outflowing streams. The western shore of Shadow Lake is a peat fen which blocks the outlet of the lake. Mean annual precipitation is 1730 mm whereas mean annual temperature is 10.7 °C, over the period 1991- 2020 (PRISM, 2022). Shadow Lake possesses a mesotrophic (moderately productive) trophic state. Monitoring of the last thirty years showed that dissolved oxygen levels decrease rapidly four meters below the surface and are usually anoxic below 10 meters. The watershed is composed of Vashon Till parent material formed following the retreat of the Vashon Lobe of the Cordilleran Ice Sheet ca. 16,000 yr BP (Porter and Swanson, 1998). The vegetation surrounding Shadow Lake is currently dominated by *Tsuga heterophylla*, *Pseudotsuga menziesii*, *Thuja plicata*, and *Alnus rubra*.

Sediment Sampling

A sediment core was collected during September 2019 at the deepest part of the lake using a 5-cm diameter Livingstone piston corer. A surface core was collected prior to subsurface sediment depths using a clear tube fitted with a piston. We collected sediment in approximately one-meter drive lengths. Each time a sediment interval was retrieved, the sediment was extruded from the core barrel into a PVC case lined with plastic wrap. We collected two adjacent cores for the uppermost sediment intervals to ensure we obtained overlapping depths for samples not acquired

between the surface core and the Livingstone cores. The sediment cores were split lengthwise and stored in their PVC cases at 4°C. The surface core was subsampled at 0.5 cm intervals. A continuous sequence of the working halves of the cores were subsampled into bags at 1 cm increments. Magnetic susceptibility measurements were used to correlate the surface core and the Livingstone core drives.

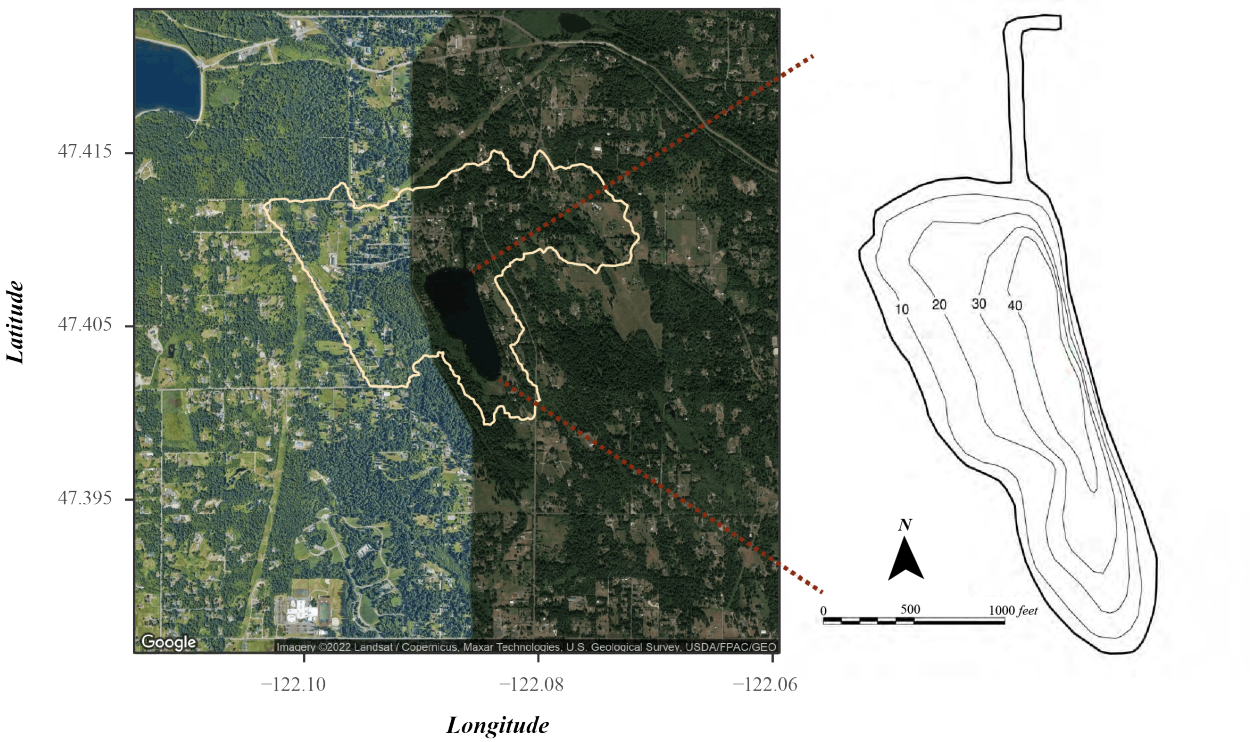

Figure 1 Shadow Lake on the top left with its watershed colored in yellow. The image on the top right is the bathymetry map where depths are in units of feet. The bathymetry map is adjusted from Constantine et al., (2016).

Sediment Chronology

An age-depth model was constructed using 11 radiocarbon dates and the Mazama tephra. Eight samples were macrofossils (plant or wood), two were pollen fractions, and one was from bulk sediment (> 150 µm). Macrofossil samples were pretreated using warm 10% HCl, repeated warm 10 % KOH, and a final warm 10% HCl. The pollen and bulk sediment fractions were analyzed at depths that did not yield macrofossils. Pollen fractions of ca. 3 cm^3 of sediment were isolated

using KOH, HCl, and HF following traditional pollen preparation methods (Bennett and Willis, 2001). The sample was then treated three times with a weak 1% bleach and sieving to isolate the 10-150 μm fraction. Samples were oven-dried at 60 °C overnight. Samples were dated at the Woods Hole Oceanographic Institution's National Ocean Sciences Accelerator Mass Spectrometry Facility. An age-depth model was fitted with a monotonic spline using a modified version of the CLAM program (Blaauw, 2010; Schwörer et al., 2017).

Sediment Organic Matter

We obtained percent mass of carbon (C) and nitrogen (N), and their respective isotopic ratios ($\delta^{13}C$; $\delta^{15}N$) on 116 samples. Samples were acid-rinsed with 0.5 N HCl to remove carbonates. Sediment pH was increased after acid-rinsing by decanting off HCl, adding DDI water, centrifuging and repeating the process three times. Samples were oven-dried and ground, homogenized, and subsamples incapsulated in 5x8 mm tin cups. Measurements were made via dry combustion gas chromatography coupled with continuous-flow isotopic-ratio mass spectrometry (GC-IRMS 20-20/ANCA-NT; Europa) at the Davis Stable Isotope Facility at the University of California. The reported mean absolute accuracy of reference materials was ±0.05‰ for both $\delta^{13}C$ and $\delta^{15}N$. The atomic ratio was calculated for C:N and is referred to as C:N in the subsequent text.

Bulk density of 60 samples were calculated by oven-drying one cm^3 of sediment. For C and N measurements at depths lacking a bulk density estimate, we used a linear interpolation of bulk density values. Carbon mass accumulation rate (C_{MAR}) was calculated as the product of percent C divided by 100, bulk density, and sedimentation rate determined from the age-depth model. To elucidate how organic variables changed over time, linear regressions were utilized where the data was separated into three-time intervals that corresponded to the early (10,700 –

7,400 cal yr BP), mid (7,400-2,900 cal yr BP), and late (2,900 cal yr BP – present) Holocene. These delineations were assigned based on pronounced shifts in the geochemical data.

Sediment Geochemistry: Charcoal, Magnetic Susceptibility, and Elemental Composition

We measured magnetic susceptibility and charcoal concentration contiguously down-core at 1 cm intervals on 1 cm^3 subsamples. Magnetic susceptibility was measured using the Sapphire Instruments cup meter and reported as emu/ cm^3. Samples were then soaked overnight in 10% sodium hexametaphosphate and then wet-sieved at 250 and 125 μm. The 125-250 μm fraction was then treated with a weak hydrogen peroxide (3%) overnight. Samples then received a final wet-sieved at 125 μm. Charcoal was counted using a stereoscope in a Bogorov counting tray. Charcoal accumulation rate was calculated as the product of the charcoal concentration and the sedimentation rate. Prior to measuring charcoal concentration, samples' magnetic susceptibility was measured first – which provides insight localized erosion events - since it is a nondestructive process.

We used a Bruker Trace 5 portable X-ray fluorescence (pXRF) instrument to measure elemental concentration at 1-cm intervals. Dried, ground, and homogenized sediment (~1 to 2 g) was added to polyethylene sample cups with a prolene film secured over the sample cup. For major elements, the calibration Mudrock Major was used with an adjusted measuring time of three minutes (Leys et al., 2016). The calibration procedure provides concentration (ppm) estimates for most elements heavier than Fluorine. We calculated the Si:Ti ratio as a proxy of BSi (Brown, 2015). Mn:Fe ratios reflect redox conditions at the sediment-water interface (Davies et al., 2015; Unkel et al., 2008). The Chemical Index of Weathering (CIW; [100 x $Al_2O_3/(Al_2O_3 + CaO + Na_2O)$]) was determined and used as another proxy of ecosystem development (Price and Velbel, 2003). The CIW was calculated by adjusting Ca and Al from ppm to molarity and

then to their oxides using their molar ratio. We did not include NaO since Na values were lower than the level of detectability, and therefore we assumed Na concentration was negligible.

To better understand if lake productivity was driven more by climate versus fire (i.e., nutrient pulses) we executed cross correlations between charcoal concentration with magnetic susceptibility as well as Si:Ti. We examined lags of ± 10 cm to incorporate times of charcoal counts lagging or leading magnetic susceptibility and Si:Ti. We used depth rather than ages from our age-depth model to preserve variability of our raw data. In order to avoid millennial scale trends imparted by changing sedimentation rates, we used charcoal concentrations and performed analyses separately for each of the three time periods. To elucidate how the different sediment properties related to each other, a PCA was applied to the data removing variables that were derived from each other. pXRF data that was predominantly lower than the level of detectability was also removed. We also utilized the three time periods (late, mid, and early Holocene) to visualize how the samples arranged in "space" and time.

Results

Sediment Chronology

We collected a total of 581 cm of sediment, in which the first 38 cm comprised the surface core. Our coring was halted before reaching glacial silts and clay due to a stiff sediment layer. The sediment core possessed predominantly uniform color and texture except for the tephra layer at depth 377 cm (~ 7 cm thickness) from Mount Mazama. Radiocarbon dates and calibrations can be observed in Figure 2, where the age-depth table can be observed in Supplemental Table 1.

Sediment Organic Matter

Percent TOC varied between 15 and 20% downcore with no pattern except for two excursions to 30% and the core base (10,700 cal yr BP) and at 500 cm (9550 cal yr BP) (Supplemental Figure

1). Percent carbon and C_{MAR} were positively correlated (Supplemental Figure 2), in which we performed a Tukey HSD test to determine if carbon precents were statistically different throughout the Holocene, in which they were not (p-value > 0.05).

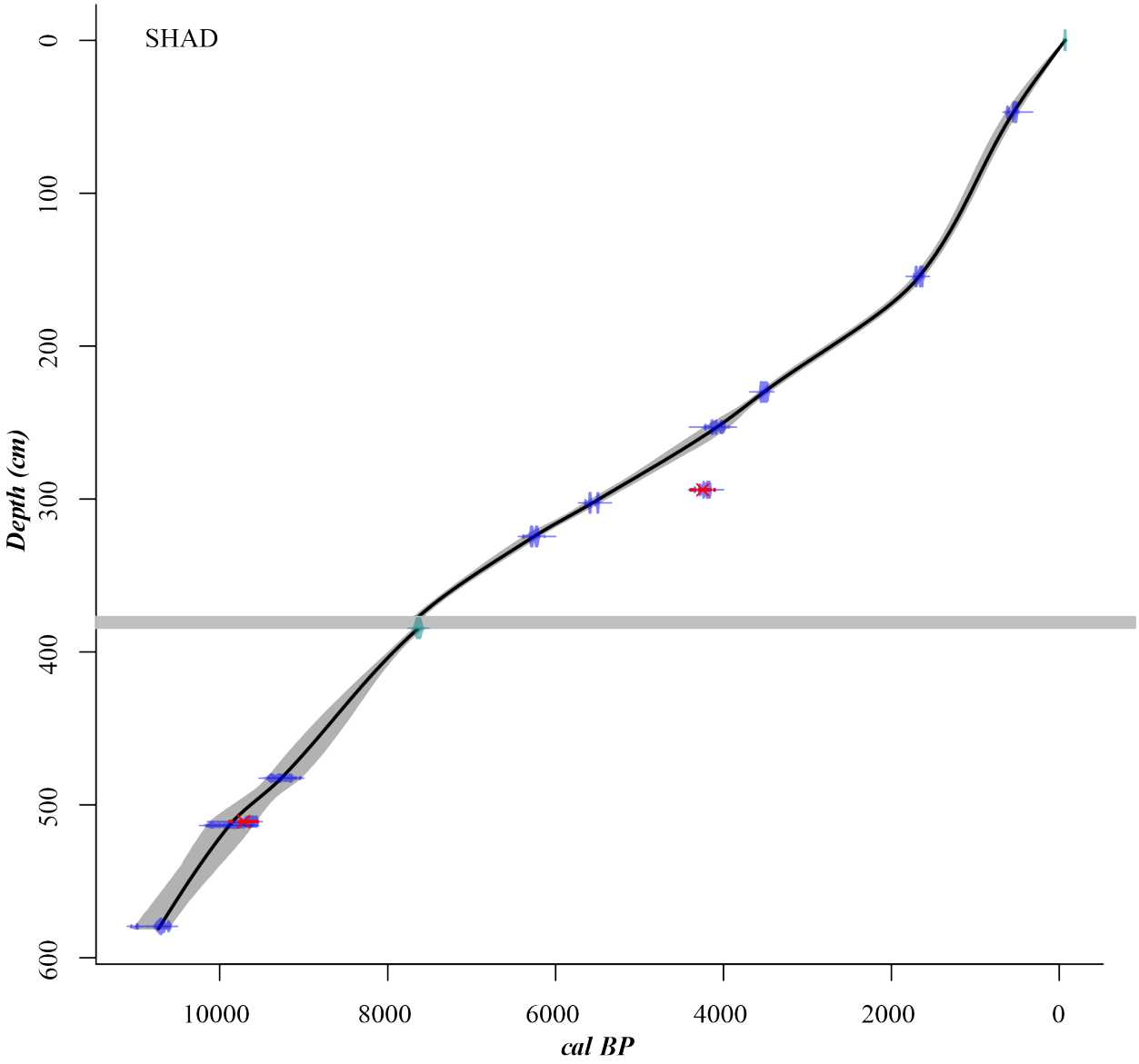

Figure 2 displays the age depth model fitted with a spline adjusted for the Mount Mazama eruption. Where depth in cm is represented on the y-axis and calendar year on the x-axis.

Carbon mass accumulation rates (C_{MAR}) were highest at the bottom of the core (132.1 – 181.3 mg cm^{-2} yr^{-1}) but dropped throughout the early Holocene (20.5 – 95.6 mg cm^{-2} yr^{-1}) to levels

similar to the mid Holocene (Figure 3). C_{MAR} ranged between 14.6 and 48.3 mg cm^{-2} yr^{-1} in the mid Holocene, where C_{MAR} increased dramatically in the late Holocene (32.8 – 153.6 mg cm^{-2} yr^{-1}). It is important to note that C_{MAR} values are being driven by sedimentation rates. C:N values were similar throughout the entire Holocene (13-16), but dropped to its lowest values (12.2) in our depth closet to the surface, likely due to pollution.

Carbon stable isotopes ($\delta^{13}C$) followed an inverse trend to C_{MAR}. $\delta^{13}C$ reached its lowest values in the early Holocene (-33.0 ‰) and then increased throughout the mid Holocene (-26.7 – -30.3‰). $\delta^{13}C$ values became more negative in the late Holocene (-29.2 – -31.2‰). Nitrogen stable isotopes ($\delta^{15}N$) were the lowest at the bottom of the core (-0.3 – 0.0‰) and increased from 0.2 to 1.6 ‰ in the early Holocene. $\delta^{15}N$ were generally lower throughout the mid Holocene (0.2 – 1.2‰). In the late Holocene, $\delta^{15}N$ was consistently higher (0.7 – 4.3‰) than the previous periods. In the uppermost two samples (ca. the last 100 yrs), $\delta^{15}N$ reached its highest value (5.0‰).

To understand how terrestrial and aquatic organic matter varied throughout the Holocene, we examined correlations among organic variables. Analyses were divided among three time periods (early, mid, and late Holocene) to account for changing relationships over time. $\delta^{13}C$ and C:N were positively correlated throughout the Holocene but they only covaried significantly (p-value < 0.05) during the late Holocene even when the C:N outlier was removed (Figure 4). The relationship between $\delta^{13}C$ and $\delta^{15}N$ varied throughout the Holocene where they were significantly negatively correlated ($p < 0.05$) during the mid Holocene and significantly positively correlated ($p < 0.05$) during the early Holocene. C_{MAR} and C:N shared a significant (p-value < 0.05) relationship in the mid Holocene where they were positively correlated. C_{MAR} and

$\delta^{13}C$ were negatively correlated throughout the Holocene and did not possess any significant ($p < 0.05$) relationships.

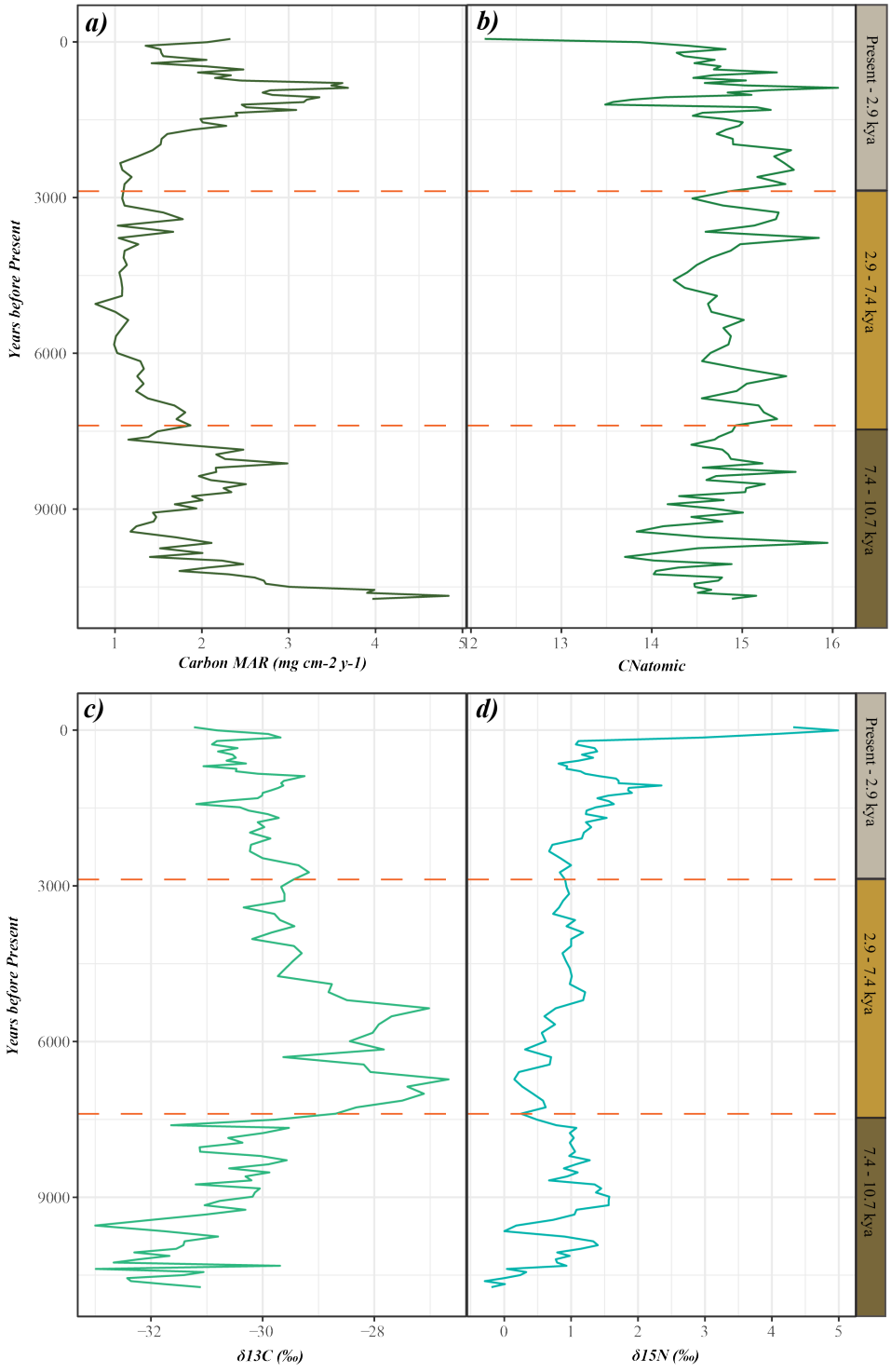

Figure 3 a) C_{MAR}, **b)** C:N **c)** $\delta^{13}C$ and **d)** $\delta^{15}N$ over time where they horizontal dotted lines represent the different time intervals corresponding to the late, mid, and early Holocene.

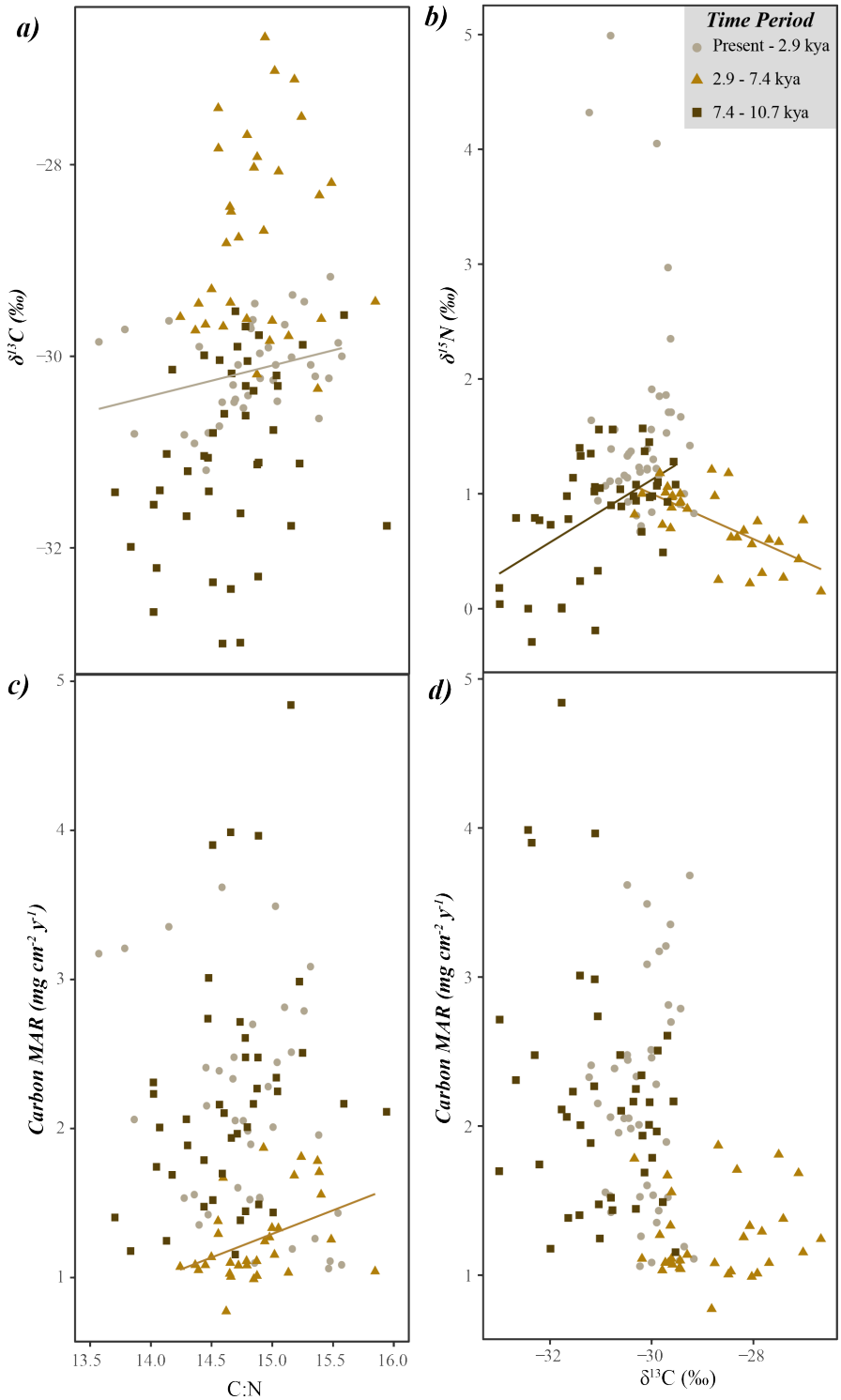

Figure 4 a) displays $\delta^{13}C$ versus C:N **b)** $\delta^{15}N$ versus $\delta^{13}C$ **c)** C_{MAR} versus C:N and **d)** $\delta^{13}C$ versus C:N where the differently colored points and shapes correspond to different time intervals. Linear regression lines per plot are only represented when the regression was significant. The surface sample was an outlier in C:N, likely the result of human impacts, and removed from this analysis.

Sediment Geochemistry: Charcoal, Elemental Composition, and Magnetic Susceptibility

Charcoal accumulation rate (CHAR) in the early Holocene ranged from 0.1 to 2.67 counts cm^{-2} yr^{-1} (Figure 5). CHAR was slightly lower in the mid Holocene (0 – 1.95 counts cm^{-2} yr^{-1}). In the late Holocene CHAR increased dramatically and reached its highest values (0.07 – 12.4 counts cm^{-2} yr^{-1}). Mean CHAR was statistically greater ($p < 0.05$) in the late Holocene compared to the mid and early Holocene, but not statistically different between the mid and early Holocene. Magnetic susceptibility (proxy for local erosion) possessed high variability and was peaky throughout the entire Holocene. Si:Ti (proxy for BSi) was highest in the early Holocene (0.1 – 496.5) but decreased throughout the mid Holocene (60.5 – 167.0). Si:Ti increased again in the late Holocene (50.7 – 206.6). Si:Ti was statistically different ($p < 0.05$) between the early, mid, and late Holocene. The chemical index of weathering (CIW) ranged from 4 to 63 in the early Holocene and increased throughout the mid Holocene (10 – 68). CIW in the late Holocene possessed similar ranges (9 – 68) to the mid Holocene. CIW was statistically different ($p < 0.05$) between the early, mid, and late Holocene. Throughout the entire Holocene, sporadic peaks were observed in the Mn:Fe ratio, with more frequent peaks in the early and late Holocene. The Mn:Fe ratio was only statistically different ($p < 0.05$) between the mid and early Holocene.

We performed cross correlations to determine if charcoal possessed leading or lagging effects on magnetic susceptibility and Si:Ti. Magnetic susceptibility and Si:Ti were highly correlated with charcoal counts during the early and late Holocene (Figure 6). Magnetic susceptibility was negatively correlated with charcoal counts in the late Holocene but positively correlated in the mid and early Holocene. Negative correlations in the late Holocene indicate an above average value of charcoal counts is likely to lag (i.e., positive x-value) behind a below average value of local erosion by approximately 5 cm (~65 years). And vice versa.

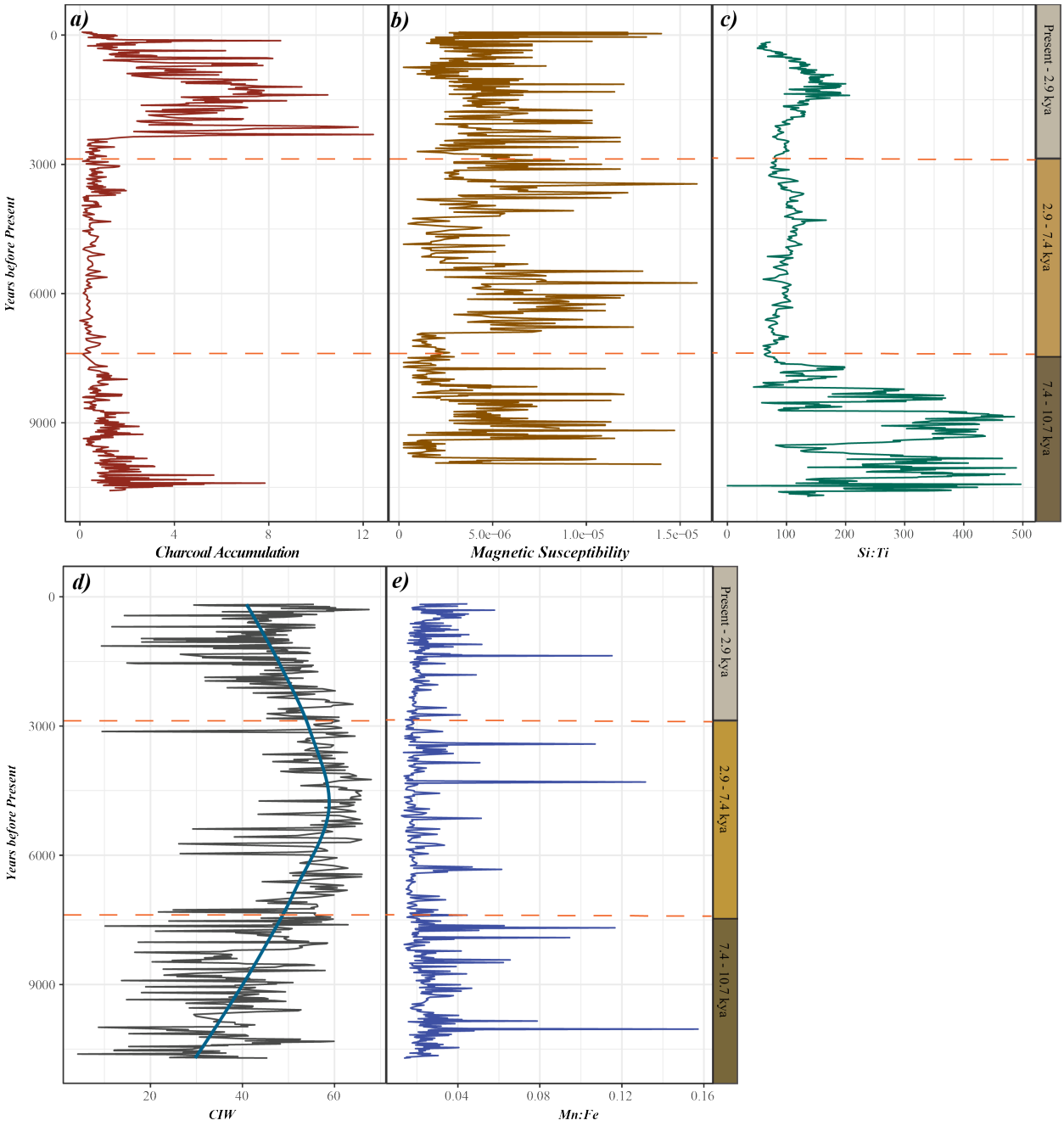

Figure 5 a) Charcoal concentration, **b)** magnetic susceptibility, **c)** Si:Ti a proxy for BSi, **d)** Chemical Index of Weathering (CIW) fitted with "geom_smooth" function, and **e)** Mn:Fe versus time. Dotted lines delineate the early, middle, and late Holocene time periods.

Positive correlations (i.e., mid and early Holocene) indicate an above average value of charcoal counts is likely to lead (i.e., negative x-value) to an above average value of local erosion about 3 cm later (~ 40 years). And vice versa. Charcoal counts and Si:Ti were positively correlated

throughout the entire Holocene, indicating that an above average value of charcoal counts are leading to an above average value of Si:Ti. In the late Holocene, Si:Ti and charcoal counts are extremely correlated and we cannot necessarily discern leading or lagging effects. This trend was visualized in Figure 5 where charcoal accumulation and Si:Ti increased drastically in the late Holocene. In the early Holocene, we observed that charcoal counts were leading Si:Ti values by 5 cm (~85 years).

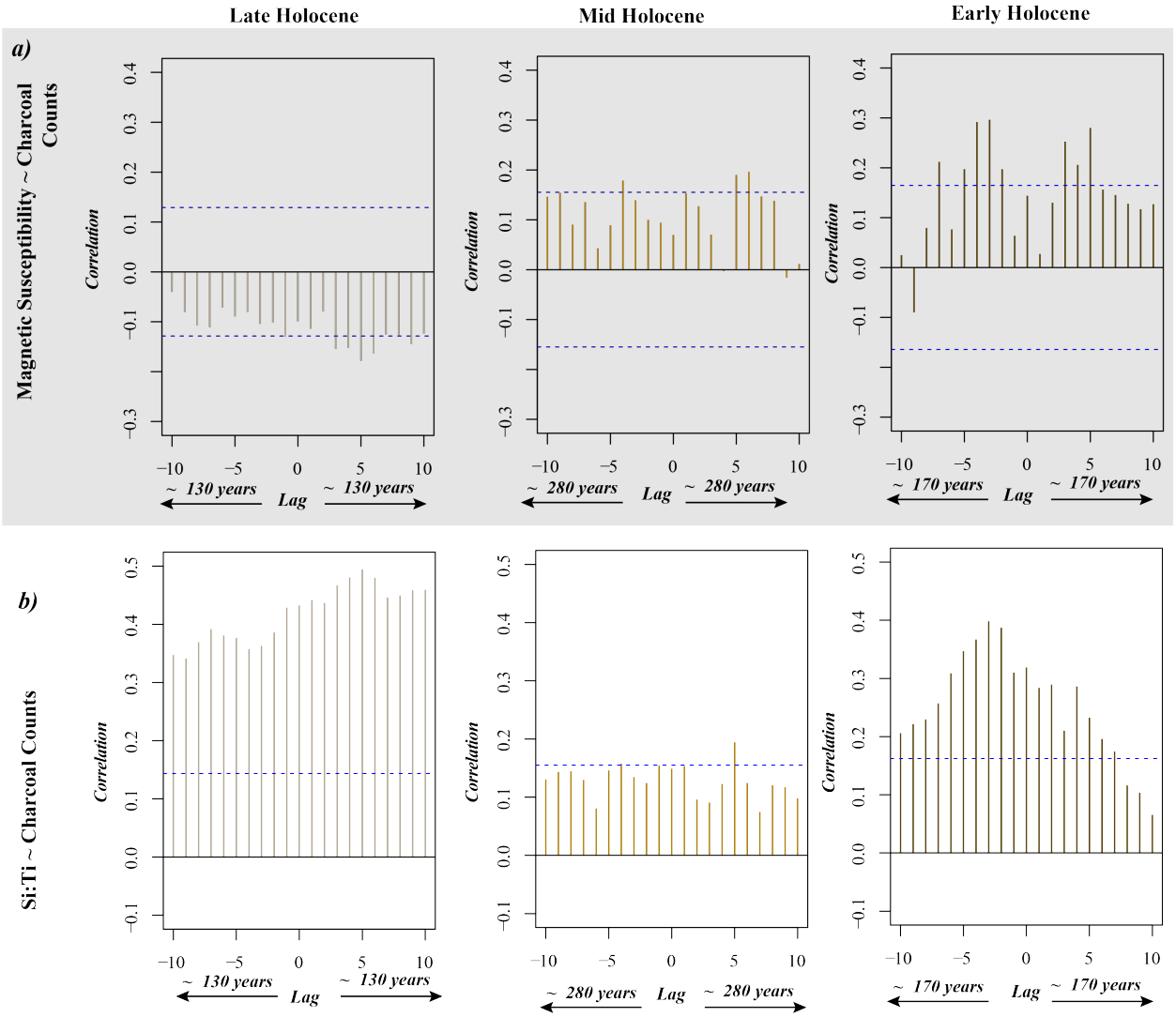

Figure 6 a) The cross-correlation between charcoal counts and magnetic susceptibility. Panel **b)** displays the cross correlation between charcoal counts and Si:Ti throughout the Holocene. Depth leads and lags have been converted to approximate years by taking the inverse of the average sedimentation rate per time period. In the late, mid, and early Holocene, one cm is equivalent to 13, 28, and 17 years.

The first two axes of the principal components analysis (PCA) explained 62.2% of the variance observed in the combined organic geochemistry and pXRF-derived data (Figure 6). Many of the inorganic (clastic-derived) variables were strongly correlated with each other, specifically Ti, Co, Al, Fe, P, Mn, Ca, and S and they contributed to PC1 negatively. Thus, higher concentrations of the aforementioned elemental concentrations were highest in the lower left section of the PCA. Charcoal, $\delta^{13}C$, $\delta^{15}N$ and C_{MAR} all had zero value loadings for PC1. Mg positively and strongly contributed to PC2. Many variables related to organic matter inputs, such as Si:Ti, $\delta^{15}N$ and $C_{MAR,}$ negatively contributed to PC2. To determine if time periods had a significant effect on PC1 or PC2 we performed an ANOVA, where time period had a significant effect on PC1 and PC2 (p-value < 0.05).

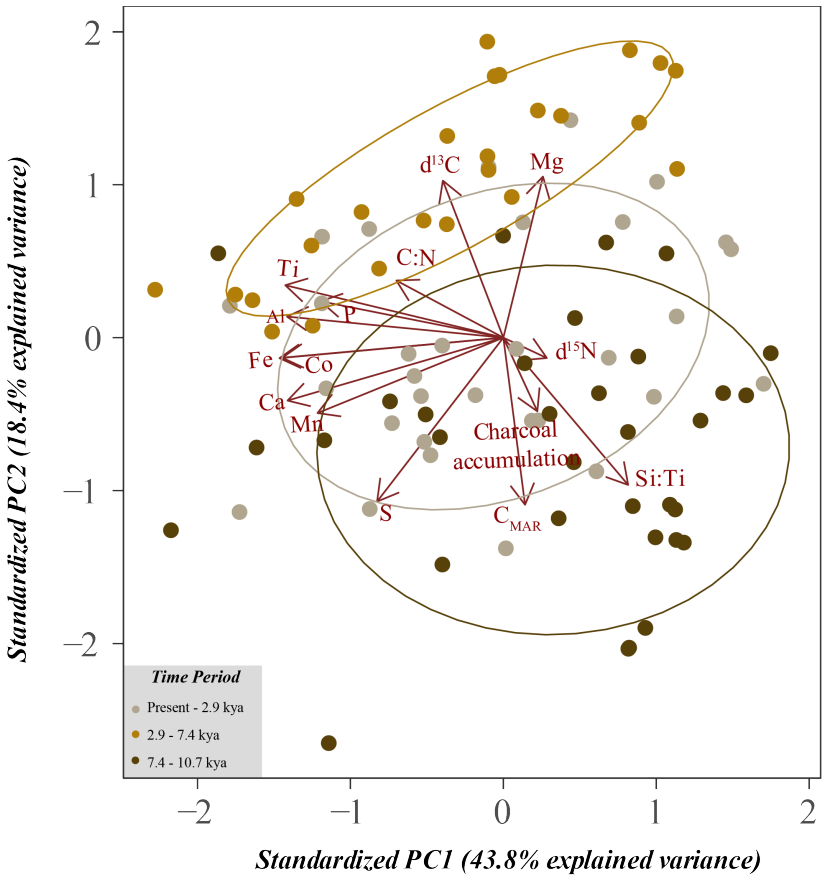

Figure 7 displays a PCA where PCA1 and PCA2 explain 43.8% and 18.4% of the variance in the data. The data points are colored to represent the different time intervals.

Discussion

Early Holocene (Present – 2,900 cal yr BP)

During the early Holocene, the climate was drier and warmer than modern conditions in the Puget Lowland where *Pseudotsuga*, *Alnus rubra*, and *Pteridium* dominated the pollen records (Whitlock, 1992). At this time, increased aridity and drought conditions resulted in regionally higher fire frequency that supported fire adapted vegetation such as *Pseudotsuga* and *Alnus rubra*. Our first hypothesis that lake productivity would be high in the early Holocene was supported by high Si:Ti as a proxy for BSi. High charcoal accumulation and subsequent erosion events appeared to be a driving force in increased productivity in the early Holocene since Si:Ti and magnetic susceptibility were positively correlated with charcoal counts. Given the maritime summer climate of the Puget Lowland, moderate increases in temperature could greatly influence lake productivity. High lake productivity in the early Holocene (reflected by our Si:Ti data) is likely a combined effect of erosional inputs from fire and a warmer climate.

Interpreting $\delta^{13}C$ in response to ecosystem productivity is complicated by multiple processes acting upon bulk organic $\delta^{13}C$ (Meyers and Teranes, 2001). High aquatic productivity can lead to enriched $\delta^{13}C$ values (i.e., more positive) due to Rayleigh distillation, which occurs when dissolved CO^2 is diminished resulting in an enrichment of dissolved $^{13}CO_2$. In addition, carbonate sources ($\delta^{13}C \sim 1‰$) may be more important during periods of high productivity (Talbot, 2001). However, these processes do not appear to be a dominant process in the early Holocene, because even though Si:Ti is high, $\delta^{13}C$ values remain highly negative (-33‰), below that expected from C_3 photosynthesis of atmospheric carbon sources, which is typically -28‰. The continued low $\delta^{13}C$ values throughout the early Holocene may be attributed to increased CO_2 sourced from sediment respiration, since sediment organic matter possesses more negative

$\delta^{13}C$ values with respect to the $\delta^{13}C$ of air (Meyers and Teranes, 2001). The adjacent peat fen may have also been supplying dissolved inorganic carbon (DIC) (Wallin et al., 2010), and may have been increased importance as a source of dissolved CO_2 (relative to atmospheric sources) during periods of high productivity.

Other geochemical proxies support the interpretation of higher early Holocene aquatic productivity. During the early Holocene, increased fire and drought would have resulted in the adjacent vegetation to Shadow Lake to have lower stature forest (i.e., early successional species) and thus increased wind at the water surface leading to increased water-column mixing (Klaus et al., 2021). Windier conditions, and potentially lower lake water levels, would lead to higher likelihood of oxygenation events at the sediment-water interface and subsequently increased sediment respiration and DIC inputs, consistent with our $d^{13}C$ record. This is supported by the Mn:Fe ratio for the early Holocene which shows evidence of oxygenation through sporadic peaks consistent with oxic conditions in the sediment (Burn and Palmer, 2014; Melles *et al.*, 2014). However, when productivity increases in tandem with decomposition, Mn can be mobilized and lower the Mn:Fe ratio which could explain the generally low values between peaks (Unkel et al., 2008).

The positive relationship between $\delta^{13}C$ and $\delta^{15}N$ during this period could be associated with increased lake productivity, where $\delta^{15}N$ becomes enriched in ^{15}N as a byproduct of nitrogen cycling from photosynthesis – since ^{14}N is preferentially used (Talbot, 2001). C_{MAR} was generally higher in the early Holocene with respect to the mid Holocene which could be a result of aquatic productivity being higher than the rate of decomposition. Our data also shows that the early Holocene was characterized by high terrigenous ecosystem development based on CIW

which corroborates that progressive soil weathering was occurring under the early successional forest (Arnaud *et al.*, 2012).

Mid Holocene (2,900 – 7,400 cal yr BP)

Approximately 6000 cal yr BP, the climate shifted away from longer summer drought to wetter and cooler climate attributed to decreasing summer insolation (Whitlock, 1992; Whitlock and Knox, 2002). Our data supports this trend with low charcoal accumulation rates in the mid Holocene. During this time, late successional dense forests of *Thuja*, *Tsuga heterophylla*, and *Picea sitchensis* became more abundant due to lower fire frequency and shifting climate (Gavin and Brubaker, 2013; Shelley D Crausbay *et al.*, 2017). Our second hypothesis that aquatic productivity would be lower and soil weathering would increase during the mid Holocene was supported by our data – where Si:Ti and C_{MAR} reached their lowest ranges throughout the Holocene and CIW increased from the early Holocene. The more positive $\delta^{13}C$ values could indicate less sediment or peat derived DIC entering the photic zone. The $\delta^{13}C$ and $\delta^{15}N$ negative relationship during the mid Holocene could be the result of higher terrestrial POC inputs causing both higher $d^{13}C$ (-28‰) and lower $d^{15}N$ (0.5‰). The overall lower $\delta^{15}N$ may be a result of lower aquatic nutrient cycling in general (Talbot, 2001). However, C:N only slightly increased, though if terrestrial productivity was relatively high during this period, we would have observed a larger change in C:N. Whether diagenetic effects or other processes maintained the low C:N cannot be deduced from our data.

The Mn:Fe record is generally lower during the mid Holocene suggesting less frequent oxygenation events (Melles *et al.*, 2014). Transitions from early to late successional species correspond to the development of taller forests which can reduce wind speed at the lake and decrease mixing/ increase stratification – which contributes to lower aquatic productivity (Klaus,

Karlsson and Seekell, 2021). A wetter climate may have increased the lake level and raised the mixing zone above the sediment surface and lowered the pH, thus lowering Mn:Fe (Burn and Palmer, 2014).

Our hypothesis of increased soil weathering following the early Holocene was supported by CIW which increased to its highest values (ca. 60) during the mid Holocene. Increases in CIW during this period could be attributed to a wetter climate that promoted soil weathering and the development of a late successional forest contributing to a thick organic horizon where enhanced terrestrial decomposition may be occurring as well as increased acidic leaching (Brantley et al., 2011).

Late Holocene (7,400 – 10,700 cal yr BP)

The late Holocene is characterized by a continued wet and cool climate where the vegetation in the Puget Lowland reflects that of the mid Holocene but with increased Cupressaceae and persistent *Alnus rubra*. Our final hypothesis of increased late Holocene productivity was supported by the Si:Ti record and its correlation with the charcoal record. The abrupt increase in fire at 1800 cal. yr BP inferred from the charcoal accumulation rate is not matched by increased magnetic susceptibility (only moderate cross-correlation, Figure 6), thus the fires were likely not local high severity events (Millspaugh and Whitlock, 1995). However, the increase in fire is matched by a similarly abrupt increase in productivity (Si:Ti), with Si:Ti peaking a few cm (ca. x years) following the peak in charcoal. There is also more N cycling (slightly higher ^{15}N) and increased sedimentation rate and C_{MAR} through this fire period, though not as abrupt a change. If fires were indeed not local to the erosional watershed, then fires were not likely affecting nutrient availability. The increased productivity we observed could be attributed to the higher El Niño–

Southern Oscillation (ENSO) variability. ENSO events could have increased bioturbating in the lake which would have increased water mixing and reduced stratification.

The abrupt increased fire at 1800 cal yr BP is consistent with other records in the Pacific Northwest (Prichard et al., 2009; Walsh et al., 2015), though few other study has found such an abrupt increase in fire in the late Holocene. The abrupt change in fire at 1800 cal yr BP could be a result of cultural use of fire or climate. During the late Holocene, the Coast Salish transitioned from a mobile to sedentism lifestyle where fire was a common method to maintain open savannas for dietary as well as cultural purposes (Ames, 2003; Walsh *et al.*, 2015). In southern British Columbia, a similarly abrupt increase in charcoal inputs into montane meadow and lakes was found at 2400 cal yr BP and attributed to cultural fire use (Hallett et al., 2003; Lepofsky et al., 2005). In addition, climate variability increased in the late Holocene, attributed to ENSO events which could have been a contributing factor for increased fire frequency (Walsh *et al.*, 2015).

Decreased CIW, suggesting less-weathered soils around the lake, is in contradiction to progressive development of weathered soils during the Holocene. However, despite the evidence for increased fire during the late Holocene, pollen evidence suggests the development of old-growth forest structures including forests dominated by large Pseudotsuga. These large trees, when wind-thrown and creating root tip-ups, rejuvenate soils by mixing regolith into surface horizons (Phillips and Marion, 2005).

However, recent centuries of anthropic climate forcing have been contributing to increased drought and fire frequency (Halofsky et al., 2020). As aforementioned, humans have been modifying the Puget Lowlands long before Euro settlement. This region experienced a transition in human influence from indigenous groups to Euro settlement beginning in the late

1800s, however it was not until the beginning of the twentieth century that the land adjacent to Shadow Lake was logged and developed (Constantine *et al.*, 2016). This transition is most apparent in our $\delta^{15}N$ record which increased drastically, a likely indicator of human pollution and increase *Alnus rubra* presence. We observed an increase in C_{MAR} during the late Holocene which could be a reflecting of nutrient pulses with increasing fire frequency. However, $\delta^{13}C$ data was not as negative with respect to the early Holocene. This trend could be indicative that the adjacent bog was unable to maintain a DIC supply to the lake that matched productivity demands. Therefore, with increasing productivity and increased nutrients into the lake (i.e., pollution, fire, development), Shadow Lake may be decreasing in its ability to be a carbon sink. Overall, we observed that the time periods clustered together more frequently with periods that were more similar than more dissimilar. Therefore, the sediment's biogeochemical records appropriately reflect the changes in climate and disturbance regimes. The current landscape is a relic of the previous periods' influence where it is slowly transitioning into a new forest that is interacting with rapid anthropic climatic change and novel disturbance regimes.

Conclusion

Throughout the Holocene, ecosystems with the Puget Lowland have experienced drastic changes in climate that in turn influence disturbance regimes. In the early Holocene, this region experienced high fire frequency and aquatic productivity. Mirroring climate, the mid Holocene experienced fewer fires, lower aquatic productivity, and increased soil weathering. The late Holocene experienced a dramatic increase in fire not previously recorded in other studies attributed to human presence and climate variability. As time moved forward, climate and disturbance have only become more complex due to human influence. Here, we were able to report how an ecosystem responded to changes through generating biogeochemical records. This

region will only become more impacted by climate change, potential for increased fire, and human influence. Through understanding how this ecosystem responded in the past, we can make inferences regarding how this system – and those similar to it – will respond to rapid and dramatic anthropic climatic change and disturbances in the coming decades.

CHAPTER V

CONCLUSION

The Holocene has significantly influenced changes in vegetative communities that have consequently altered terrestrial carbon pools. However, these changes have been occurring over a millennia scale where anthropic influences are exacerbating the effects of climatic change. Modern ecosystems may respond to intensified change in novel ways that have not been previously experienced – however – understanding paleo ecosystems in tandem with modern ecosystems provides insight on the trajectory of future systems. Given the current climate crisis, it is prudent to understand how carbon stability and sequestration will respond to future climate change and disturbance regimes. My dissertation aimed to understand the intersection of ecosystem function with shifting climate and disturbance regimes using multiproxy analyses across spatiotemporal scales.

Chapter II investigated shifts between different vegetative types to garner insight on how regional climate influenced woody vegetation. Our data showed a widespread trend of woody vegetation expansion throughout the Amazon–Cerrado region since at least ~1,600 years prior to modern deforestation. However, woody encroachment did not appear to be a direct reflection of wetter conditions but rather biophysical and biogeochemical mechanisms that may have contributed to positive feedbacks between tree cover and precipitation. Such interactions may have negatively influenced fire disturbance while consequently promoting nutrient accumulation. Future directions for this research encompass integrating plant, soil, and atmospheric data to quantify human influence on ecosystem–climate feedbacks.

Chapter III focused on a modern temporal scale to quantify the effects of a catastrophic fire, fueled by anthropic climatic change and management, on soil carbon stability and fungal

composition. Where our data displayed shifts in carbon type data that did not support our hypotheses. However, soil pools are slow moving and to fully quantify the effects of novel climate and fire systems on the landscape, longer temporal scales our necessary. However, microbial communities' function on a much shorter temporal scale with respect to soil carbon and nutrient pools. In which we observed marked shifts in fungal composition with an increasing severity gradient. Prospective research would be to put in place a long-term sampling scheme that would shine light on the legacy effect of anthropic climatic change and novel disturbance regimes.

Chapter IV aimed to quantify the biogeochemical shifts within an ecosystem throughout the Holocene to enhance predictive capabilities for forthcoming systems. Through generating a detailed biogeochemical record, we were able to observe that ecosystems are significantly influenced by climate and human influence. The late Holocene showed marked changes in lake biogeochemistry that were not consistent with previous climatic trends. Future work would entail further quantification of the mean residence time of carbon in this ecosystem to elucidate if lakes in this region are losing their ability to be carbon sinks.

APPENDIX A

SUPPLEMENTAL MATERIAL FOR CHAPTER II

Supplemental Figures

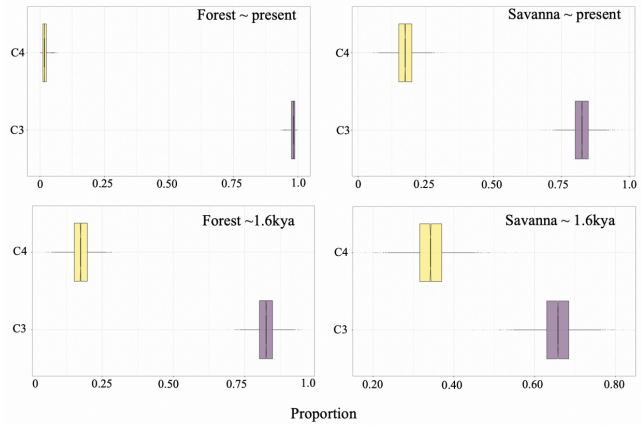

	C3	C4
Forest: 0 - 10 cm	0.98 ± 0.01	0.02 ± 0.01
Savanna: 0 - 10 cm	0.84 ± .045	0.16 ± .045
Forest: 70 - 80 cm	0.825 ± 0.035	0.175 ± 0.035
Savanna: 70 - 80 cm	0.66 ± 0.042	0.34 ± 0.042

Supplemental Figure 1 a) boxplots from simmr model displaying how the proportions of C3 and C4 contributions change through time. Present time is represented by a depth of 0-10 cm whereas 1.6kya is represented by a depth of 70-80 cm. b) provides C3 and C4 estimates with standard deviations for each depth and ecosystem.

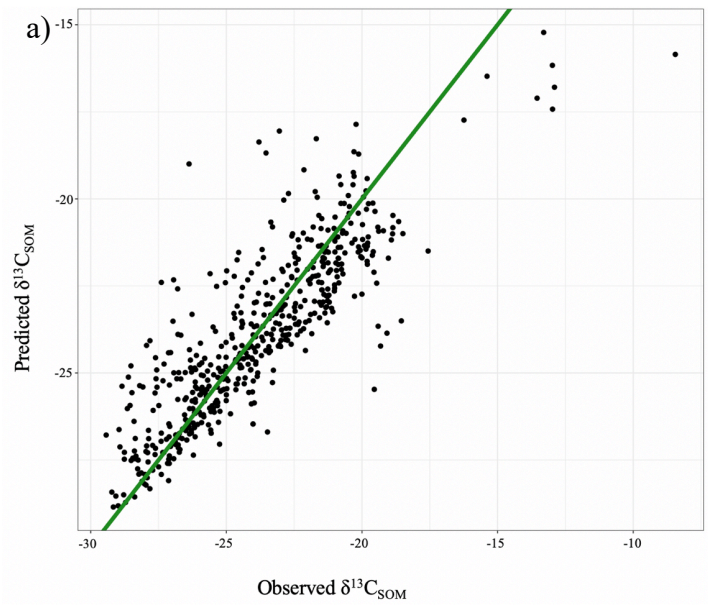

b)

	δ13CSOM		
Predictors	*Estimates*	*CI*	*p*
(Intercept)	-29.06	-33.37 – -24.76	**<0.001**
Depth_cm	-0.03	-0.04 – -0.03	**<0.001**
savanna	2.62	1.31 – 3.92	**<0.001**
transition	5.69	3.76 – 7.62	**<0.001**
Histosol	4.91	-0.79 – 10.61	0.099
Inceptisol	4.05	-0.61 – 8.70	0.096
Oxisol	2.04	-2.24 – 6.33	0.355
Plinthite soil	0.95	-3.32 – 5.23	0.665
Ultisol	1.90	-2.48 – 6.27	0.400
Depth_cm:subsetsavanna	0.01	0.01 – 0.02	**<0.001**
Depth_cm:subsettransition	0.06	0.04 – 0.08	**<0.001**
Random Effects			
σ2	2.60		
Observations	543		
Marginal R2 / Conditional R2	0.325 / 0.713		

c)

Analysis of Deviance Table (Type II Wald chi-square tests)

	Chi-squared	*Df*	*p*
Depth_cm	257.123637	1	**< 0.001**
subset	12.094805	2	**0.002**
US.soil.order	9.238971	5	0.100
Depth_cm:subset	62.486083	2	**< 0.001**

Supplemental Figure 2 a) displays the relationship between observed and predicted values from the mixed-effect model. The green line represents a one-to-one slope, which represents when observed and predicted values for a sample are equal. The mixed-effect model's results are shown in b) which displays estimate values, confidence intervals, and p-values for the fixed-effects and the variance is displayed for the random-effect.

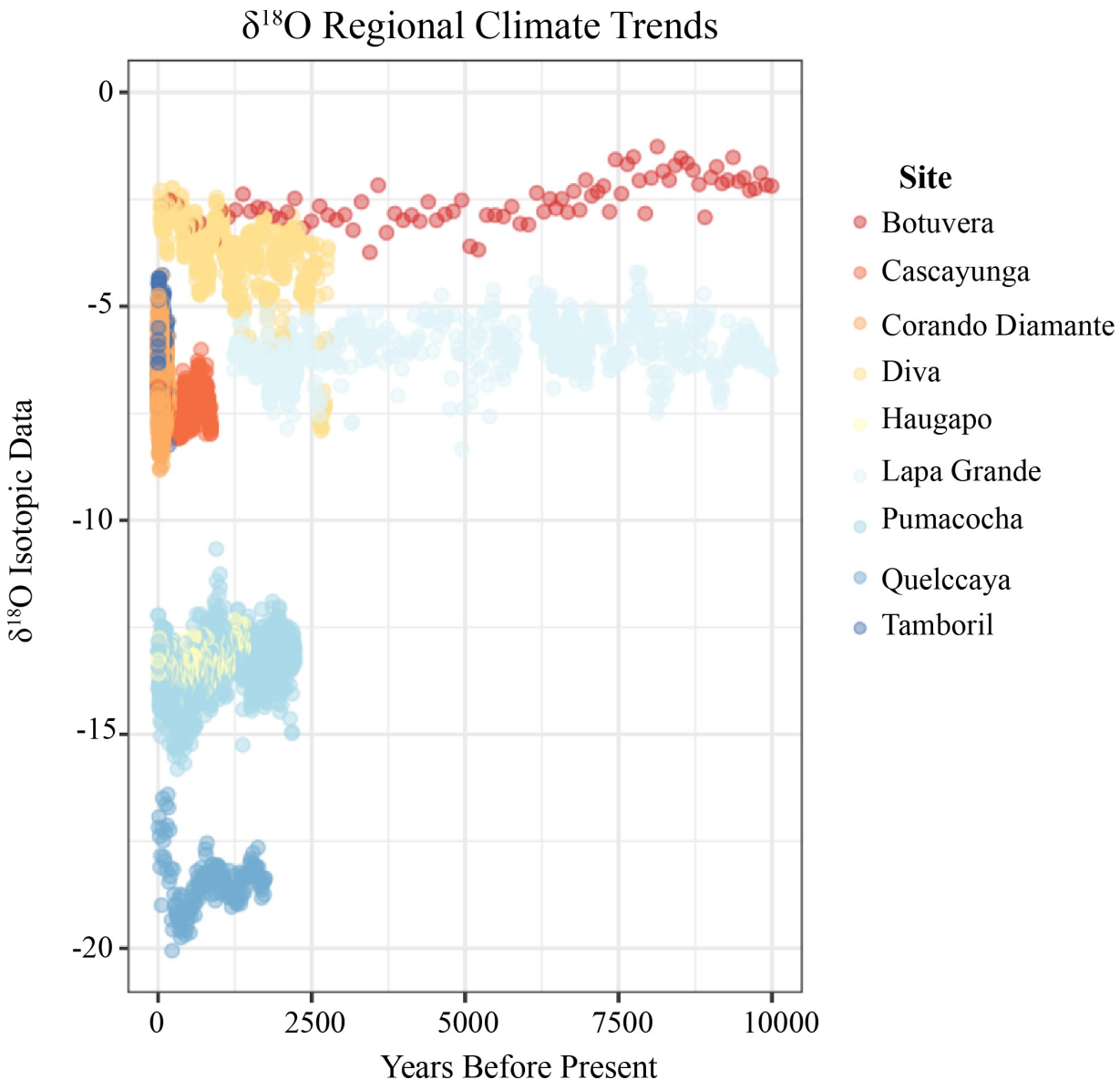

Supplemental Figure 3 Speleothem carbonate oxygen stable isotope ratios measured throughout the Amazon region (the locations of cave sites are shown in Figure 1). At any given site, departures from the mean towards more negative oxygen isotope ratios are interpreted as increases in monsoon intensity (Wortham et al. 2017). Overall, a consistent trend towards wetter conditions is observed for most of the Holocene until about 200 years ago. For the local hydroclimate manifestation of regional changes in monsoon see speleothem strontium isotope ratios, which serve as a proxy for changes in soil moisture and rock dissolution (Figure 5c).

Supplemental Tables

Supplemental Table 1 Study sites, ecosystems, and soil types. *Radiocarbon dated sites in age-depth model.

Site ID	Sample size	Ecosystem	State	Latitude	Longitude	Soil Type
1	10	Evergreen forest	Mato Grosso	13°25'S	53°18'W	Oxisol
2	10	Savanna	Mato Grosso	13°28'S	53°21'W	Oxisol
3*	15	Evergreen forest	Mato Grosso	13°05'S	53°21'W	Oxisol
4*	15	Evergreen forest	Mato Grosso	12°58'S	52°55'W	Oxisol
5*	15	Evergreen forest	Mato Grosso	13°18'S	53°24'W	Oxisol
6*	15	Evergreen forest	Mato Grosso	10°57'S	52°10'W	Histosol
7*	10	Savanna	Mato Grosso	10°47'S	51°49'W	Ultisol
8	15	Evergreen forest	Mato Grosso	13°04'S	52°22'W	Oxisol
9*	10	Savanna	Mato Grosso	14°46'S	52°21'W	Oxisol
10	10	Savanna	Mato Grosso	12°49'S	51°46'W	Oxisol
11	10	Savanna	Mato Grosso	12°50'S	51°45'W	Oxisol
12*	10	Savanna	Mato Grosso	12°48'S	55°58'W	Oxisol
13	10	Evergreen forest	Mato Grosso	11°24'S	55°19'W	Oxisol
14*	10	Savanna	Mato Grosso	13°08'S	52°15'W	Oxisol
15	10	Deciduous forest	Mato Grosso	14°49'S	52°21'W	Oxisol
16*	10	Evergreen forest	Mato Grosso	09°50'S	50°27'W	Ultisol
17*	10	Savanna	Mato Grosso	10°23'S	50°38'W	Ultisol
18*	15	Evergreen forest	Mato Grosso	12°48'S	51°51'W	Oxisol
19*	15	Evergreen forest	Mato Grosso	12°45'S	51°52'W	Oxisol w/ plinthic horizon
20	10	Savanna	Tocantins	11° 9'S	49°40'W	Oxisol w/ plinthic horizon
21	15	Evergreen forest	Tocantins	11° 9'S	49°40'W	Oxisol w/ plinthic horizon
22	10	Evergreen forest	Tocantins	11° 9'S	49°40'W	Oxisol w/ plinthic horizon
23*	10	Savanna-evergreen forest transition	Tocantins	11° 9'S	49°40'W	Oxisol w/ plinthic horizon
24	10	Savanna	Tocantins	12°39'S	49°59'W	Ultisol
25	15	Evergreen forest	Tocantins	12°39'S	49°59'W	Oxisol w/ plinthic horizon
26	10	Evergreen forest	Tocantins	12°39'S	49°59'W	Oxisol w/ plinthic horizon
27*	10	Savanna-evergreen forest transition	Tocantins	12°39'S	49°59'W	Ultisol
28	10	Savanna	Tocantins	11°21'S	46°53'W	Inceptisol
29	10	Deciduous forest	Tocantins	11°21'S	46°53'W	Inceptisol
30	10	Deciduous forest	Tocantins	11°21'S	46°53'W	Inceptisol
31*	10	Savanna-decidious forest transition	Tocantins	11°21'S	46°53'W	Inceptisol
32	10	Savanna	Tocantins	12°53'S	12°53'S	Oxisol w/ plinthic horizon
33	10	Evergreen forest	Tocantins	12°53'S	12°53'S	Entisol
34	10	Evergreen forest	Tocantins	12°53'S	12°53'S	Entisol
35*	10	Savanna-evergreen forest transition	Tocantins	12°53'S	12°53'S	Entisol
36	10	Savanna-riparian forest transition	Tocantins	11°58'S	48°14'W	Oxisol w/ plinthic horizon
37	10	Savanna-riparian forest transition	Tocantins	11°58'S	48°14'W	Oxisol w/ plinthic horizon
38	10	Savanna	Tocantins	11°58'S	48°14'W	Oxisol w/ plinthic horizon
39	10	Savanna	Tocantins	11°58'S	48°14'W	Oxisol w/ plinthic horizon
40	10	Riparian forest	Tocantins	11°58'S	48°14'W	Oxisol w/ plinthic horizon
41	10	Riparian forest	Tocantins	11°58'S	48°14'W	Oxisol w/ plinthic horizon
42	10	Riparian forest	Tocantins	11°58'S	48°14'W	Oxisol w/ plinthic horizon
43	10	Riparian forest	Tocantins	11°58'S	48°14'W	Oxisol w/ plinthic horizon
44	50	Savanna	Federal District	15°56'S	47°56'W	Oxisol
45	50	Riparian forest	Federal District	15°56'S	47°56'W	Oxisol
46*	10	Transition	Federal District	15°56'S	47°56'W	Oxisol
47	50	Savanna	Federal District	15°56'S	47°56'W	Oxisol
48	50	Riparian forest	Federal District	15°56'S	47°56'W	Oxisol
49*	10	Transition	Federal District	15°56'S	47°56'W	Oxisol
50	50	Savanna	Federal District	15°36'S	47°42 W	Oxisol
51*	50	Xeromorphic forest	Federal District	15°36'S	47°42 W	Oxisol
52	10	Transition	Federal District	15°36'S	47°42 W	Oxisol
53	50	Savanna	Federal District	15°33'S	47°51'W	Oxisol
54*	30	Deciduous forest	Federal District	15°33'S	47°51'W	Oxisol
55	10	Transition	Federal District	15°33'S	47°51'W	Oxisol
56	10	Deciduous forest	Pará	4°4'S	55°27'W	Ultisol
57	20	Deciduous forest	Minas Gerais	16°19'S	46°59'W	Inceptisol
58	10	Savanna	Tocatins	10°14.7'S	48°16.2 'W	Oxisol
59	10	Savanna	Tocatins	10°54.3'S	48°21.2' W	Oxisol
60	11	Savanna	Tocatins	11°59.5'S	47°33.2' W	Ultisol
61	5	Evergreen forest	Tocatins	7°6.3'S	48°13.5' W	Oxisol
62	5	Evergreen forest	Tocatins	8°41.2'S	48°44.7' W	Oxisol w/ plinthic horizon
63	5	Evergreen forest	Tocatins	9°32.9'S	48°29.5' W	Entisol
64	5	Xeromorphic forest	Tocatins	10°14.5'S	48°16.5' W	Oxisol
65	6	Evergreen forest	Tocatins	10°14.494'S	48°16.484 'W	Oxisol
66	6	Evergreen forest	Tocatins	10°14.49'S	48°16.505 'W	Oxisol
67	7	Evergreen forest	Tocatins	10°29.776'S	48°21.202 'W	Oxisol
68	8	Evergreen forest	Tocatins	10°29.76'S	48°21.16' W	Oxisol
69	8	Evergreen forest	Tocatins	10°29.79'S	48°21.155'W	Oxisol
70	9	Evergreen forest	Tocatins	11°59.278'S	47°33.492'W	Ultisol
71	11	Evergreen forest	Tocatins	11°59.292'S	47°33.474'W	Ultisol
72	9	Evergreen forest	Tocatins	11°59.336'S	47°33.487'W	Ultisol
73	8	Riparian forest	Tocatins	12°25.2'S	47°11.9'W	Oxisol w/ plinthic horizon
74*	8	Savanna	Tocatins	12°25.3'S	47°11.8'W	Oxisol w/ plinthic horizon
75*	7	Xeromorphic forest	Tocatins	12°47.43'S	47°2.99'W	Oxisol w/ plinthic horizon
76*	8	Savanna	Tocatins	12°47.4'S	47°2.98'W	Oxisol w/ plinthic horizon
77	8	Evergreen forest	Tocatins	12°56.77'S	46°55.24'W	Entisol
78*	8	Savanna	Tocatins	12°58.39'S	46°54.13'W	Entisol
79	8	Gallery forest	Goiás	13°6.05'S	46°44.96'W	Entisol

Supplemental Table 2 (Part 1) Soil organic matter carbon isotopes and leaf area index raw data

Source	Topsoil δ13C (per mil)	Ground LAI (m2/m2)	MODIS LAI (m2/m2)
This study	-26.79	NA	1.63
This study	-27.39	NA	1.44
This study	-26.94	NA	1.43
This study	-24.26	1.97	1.50
This study	-19.23	0.73	1.47
This study	-22.71	NA	1.47
This study	-29.38	NA	1.69
This study	-29.89	NA	2.10
This study	-29.44	NA	1.99
This study	-28.91	NA	1.52
This study	-28.79	NA	1.52
This study	-28.57	NA	1.52
This study	-29.22	NA	1.65
This study	-29.16	NA	1.65
This study	-28.99	NA	1.65
This study	-28.37	NA	1.55
This study	-27.94	NA	1.51
This study	-28.51	NA	1.51
This study	-20.99	NA	1.92
This study	-24.21	2.68	1.73
This study	-18.28	0.42	1.92
This study	-26.12	NA	4.93
This study	-28.84	NA	5.22
This study	-28.02	NA	5.18
This study	-23.53	NA	1.43
This study	-28.09	NA	2.10
This study	-28.54	NA	4.73
This study	-27.72	NA	1.60
This study	-27.32	NA	2.23
This study	-26.62	NA	0.88
This study	-26.82	3.42	1.44
This study	-21.97	0.75	1.44
This study	-27.25	NA	5.00
This study	-28.07	NA	1.36
This study	-26.28	NA	1.14
This study	-27.12	NA	1.59
This study	-28.76	NA	1.50
This study	-27.40	NA	1.69
This study	-27.13	NA	1.51
This study	-25.58	NA	1.71
This study	-21.61	NA	1.28
This study	-27.13	NA	1.57
This study	-29.19	NA	2.79
This study	-25.83	NA	2.51
This study	-28.55	NA	4.82
This study	-27.86	NA	1.66
This study	-28.31	1.53	1.67
This study	-27.85	NA	1.67
This study	-19.68	NA	1.32
This study	-22.16	NA	1.91
This study	-26.84	1.8	1.51
This study	-24.10	NA	1.46
This study	-26.34	NA	2.07
This study	-24.36	NA	2.10
This study	-26.09	NA	1.17
This study	-26.37	NA	1.64
This study	-28.17	NA	5.09
This study	-24.64	3.1	1.53
This study	-18.65	0.52	1.53
This study	-19.55	NA	1.55
This study	-26.98	NA	1.57
This study	-22.75	NA	1.43
This study	-26.52	NA	1.47
This study	-27.02	NA	2.17
This study	-26.55	NA	2.17
This study	-21.72	NA	1.52
This study	-26.10	NA	1.37
This study	-23.99	NA	1.24
This study	-27.46	NA	1.24
This study	-23.16	NA	1.61
This study	-27.57	NA	1.61
This study	-28.17	NA	1.77
This study	-27.45	NA	1.65
This study	-19.40	NA	1.57
This study	-27.94	NA	1.28
Ladd et al Jecol 2009, 97, 964–971	-26.57	0.65	1.34
Ladd et al Jecol 2009, 97, 964–971	-24.67	0.44	1.12
Ladd et al Jecol 2009, 97, 964–971	-26.20	1.34	1.09
Ladd et al Jecol 2009, 97, 964–971	-26.10	1.13	2.76
Ladd et al Jecol 2009, 97, 964–971	-27.00	1.96	3.29
Ladd et al Jecol 2009, 97, 964–971	-27.33	1.08	3.14
Ladd et al Jecol 2009, 97, 964–971	-26.17	1.95	3.63

Supplemental Table 2 (Part 2)

Source	Topsoil δ13C (per mil)	Ground LAI (m2/m2)	MODIS LAI (m2/m2)
Ladd et al Jecol 2009, 97, 964–971	-26.27	1.93	3.21
Ladd et al Jecol 2009, 97, 964–971	-26.63	1.8	3.26
Ladd et al Jecol 2009, 97, 964–971	-26.67	2.93	3.39
Ladd et al Jecol 2009, 97, 964–971	-25.40	0.72	0.79
Ladd et al Jecol 2009, 97, 964–971	-24.70	1.34	2.94
Ladd et al Jecol 2009, 97, 964–971	-25.33	0.66	2.95
Ladd et al Jecol 2009, 97, 964–971	-26.07	2.11	3.01
Ladd et al Jecol 2009, 97, 964–971	-25.23	0.85	3.62
Ladd et al Jecol 2009, 97, 964–971	-25.83	1.52	0.77
Ladd et al Jecol 2009, 97, 964–971	-26.20	0.95	0.94
Ladd et al Jecol 2009, 97, 964–971	-25.93	0.75	0.94
Ladd et al Jecol 2009, 97, 964–971	-25.33	0.69	1.02
Ladd et al Jecol 2009, 97, 964–971	-27.23	1.23	1.75
Ladd et al Jecol 2009, 97, 964–971	-26.40	0.99	1.64
Ladd et al Jecol 2009, 97, 964–971	-27.23	2	0.58
Ladd et al Jecol 2009, 97, 964–971	-26.20	1.21	0.60
Ladd et al Jecol 2009, 97, 964–971	-25.90	1.72	0.80
Ladd et al Jecol 2009, 97, 964–971	-25.57	1.61	0.80
Ladd et al Jecol 2009, 97, 964–971	-25.93	1.82	1.06
Ladd et al Jecol 2009, 97, 964–971	-25.97	1.94	1.05
Ladd et al Jecol 2009, 97, 964–971	-26.93	0.91	0.77
Ladd et al Jecol 2009, 97, 964–971	-25.93	2.24	1.89
Ladd et al Jecol 2009, 97, 964–971	-25.73	0.75	0.87
Ladd et al Jecol 2009, 97, 964–971	-26.50	1.94	.
Ladd et al Jecol 2009, 97, 964–971	-27.57	2.21	2.47
Ladd et al Jecol 2009, 97, 964–971	-26.63	1.19	1.16
Ladd et al Jecol 2009, 97, 964–971	-27.37	2.6	2.67
Ladd et al Jecol 2009, 97, 964–971	-27.67	2.22	1.53
Ladd et al Jecol 2009, 97, 964–971	-27.67	2.02	1.11
Ladd et al Jecol 2009, 97, 964–971	-28.47	2.58	1.11
Ladd et al Jecol 2009, 97, 964–971	-27.80	3.45	1.11
Ladd et al Jecol 2009, 97, 964–971	-28.73	3.73	1.11
Ladd et al Jecol 2009, 97, 964–971	-26.14	2.02	1.57
Ladd et al Jecol 2009, 97, 964–971	-26.60	2.9	1.57
Ladd et al Jecol 2009, 97, 964–971	-28.47	2.23	1.57
Ladd et al Jecol 2014, 102, 1606–1611	-28.52	4.36	2.87
Ladd et al Jecol 2014, 102, 1606–1611	-28.32	4.66	1.83
Ladd et al Jecol 2014, 102, 1606–1611	-27.79	4.6	2.87
Williams etal 2002 Ecosystems, 5, 692-704	-30.01	5.84	3.15
Williams etal 2002 Ecosystems, 5, 692-704	-30.34	6.07	3.11
Williams etal 2002 Ecosystems, 5, 692-704	-30.19	5.96	2.78
Williams etal 2002 Ecosystems, 5, 692-704	-30.31	6.56	3.13
Williams etal 2002 Ecosystems, 5, 692-704	-29.69	7	2.65
Williams etal 2002 Ecosystems, 5, 692-704	-30.60	6.48	2.65
Williams etal 2002 Ecosystems, 5, 692-704	-29.28	5.24	1.91
Williams etal 2002 Ecosystems, 5, 692-704	-30.02	5.81	1.91
Williams etal 2002 Ecosystems, 5, 692-704	-30.03	6.06	3.53
Williams etal 2002 Ecosystems, 5, 692-704	-30.84	6.91	2.84
Williams etal 2002 Ecosystems, 5, 692-704	-30.83	6.73	2.69
Williams etal 2002 Ecosystems, 5, 692-704	-31.14	6.2	3.79
Williams etal 2002 Ecosystems, 5, 692-704	-30.04	6.48	2.79
Ladd et al. 2013 Global Ecology and Biogeography, 22, 461-469.	-26.17	3.26	3.39
Ladd et al. 2013 Global Ecology and Biogeography, 22, 461-469.	-26.15	3.59	3.59
Ladd et al. 2013 Global Ecology and Biogeography, 22, 461-469.	-25.73	3.31	3.46
Ladd et al. 2013 Global Ecology and Biogeography, 22, 461-469.	-25.96	4.4	3.57
Ladd et al. 2013 Global Ecology and Biogeography, 22, 461-469.	-25.05	4.92	3.59
Ladd et al. 2013 Global Ecology and Biogeography, 22, 461-469.	-24.95	5.05	3.59
Ladd et al. 2013 Global Ecology and Biogeography, 22, 461-469.	-24.05	4.72	3.12
Ladd et al. 2013 Global Ecology and Biogeography, 22, 461-469.	-25.00	4.82	3.84
Ladd et al. 2013 Global Ecology and Biogeography, 22, 461-469.	-22.81	1.71	0.94
Ladd et al. 2013 Global Ecology and Biogeography, 22, 461-469.	-20.91	1.62	0.94
Ladd et al. 2013 Global Ecology and Biogeography, 22, 461-469.	-23.66	2.44	0.96
Ladd et al. 2013 Global Ecology and Biogeography, 22, 461-469.	-23.76	2.4	0.96
Ladd et al. 2013 Global Ecology and Biogeography, 22, 461-469.	-24.10	2.35	0.97
Ladd et al. 2013 Global Ecology and Biogeography, 22, 461-469.	-23.88	2.36	0.97
Ladd et al. 2013 Global Ecology and Biogeography, 22, 461-469.	-24.98	2.21	0.83
Ladd et al. 2013 Global Ecology and Biogeography, 22, 461-469.	-26.98	2.09	1.03
Ladd et al. 2013 Global Ecology and Biogeography, 22, 461-469.	-28.92	6.17	3.19
Ladd et al. 2013 Global Ecology and Biogeography, 22, 461-469.	-27.83	5.98	3.59
Ladd et al. 2013 Global Ecology and Biogeography, 22, 461-469.	-27.46	5.4	2.74
Ladd et al. 2013 Global Ecology and Biogeography, 22, 461-469.	-27.44	6.49	4.12
Ladd et al. 2013 Global Ecology and Biogeography, 22, 461-469.	-27.77	6.41	4.12
Ladd et al. 2013 Global Ecology and Biogeography, 22, 461-469.	-28.58	6.07	4.12
Ladd et al Jecol 2014, 102, 1606–1611	-26.76	3.02	1.97
Ladd et al Jecol 2014, 102, 1606–1611	-26.56	3.47	1.79
Ladd et al Jecol 2014, 102, 1606–1611	-26.11	3.82	1.89
Ladd et al Jecol 2014, 102, 1606–1611	-27.26	3.19	1.99
Ladd et al Jecol 2014, 102, 1606–1611	-27.10	4.13	1.85
Ladd et al Jecol 2014, 102, 1606–1611	-26.82	2.87	2.09
Ladd et al Jecol 2014, 102, 1606–1611	-27.13	4.17	1.96
Ladd et al Jecol 2014, 102, 1606–1611	-26.82	3.84	2.02
Ladd et al Jecol 2014, 102, 1606–1611	-27.34	4.77	2.00

Supplemental Table 3 Ecosystem means

	δ13C Ecosystem means and standard deviations					
	n = 46		n = 26		n = 10	
Depth from soil surface (cm)	Forest Mean	Forest SD	Savanna Mean	Savanna SD	Transition Mean	Transition SD
-10	-27.669	1.439244	-25.083	3.09559	-22.435	2.242299
-20	-26.97616	1.7327499	-23.14403	3.1833917	-21.28679	0.7221882
-30	-26.35602	1.857883	-23.10899	3.372263	-22.03131	2.489459
-40	-25.78669	2.4501014	-21.64502	3.0457955	-20.26767	0.1996956
-50	-25.48755	2.731869	-22.07987	3.442516	-23.3721	3.352556
-60	-23.83645	3.2274818	-21.29086	3.0013381	-20.89891	0.7505945
-70	-24.67536	3.027599	-21.8794	3.025015	-23.21428	3.365414
-80	-23.04611	3.29103	-21.57912	2.831803	-23.30363	2.903167
-90	-24.18811	2.981668	-21.47505	2.286381	-24.50509	3.040226
-100	-22.53297	3.045217	-20.81802	2.380188	-23.0423	2.201508
-110	-21.78624	4.502964	-22.48373	1.861262	NA	NA
-120	-22.66909	1.651885	-22.42465	1.5839438	NA	NA
-130	-21.86386	3.1635812	-22.49417	1.2933013	NA	NA
-140	-22.53963	1.6703772	-22.65707	1.4854634	NA	NA
-150	-22.81907	1.642099	-23.04661	1.4608606	NA	NA
-180	-22.16924	1.7074575	-22.71836	1.6494073	NA	NA
-200	-21.9323	1.527857	-23.04884	1.6410579	NA	NA

Supplemental Table 4 Carbon isotopes to leaf area index conversion

Latitude	Longitude	topsoil d13C	d13C at 80 cm	LAI topsoil	LAI at 80 c	LAI Change
-10.24461	-48.27078	-26.79324488	-20.82942804	2.99034983	-5.5293885	8.51973834
-10.90576	-48.35378	-27.39412531	-19.9404702	3.84875044	-6.7993283	10.6480787
-11.99114	-47.55305	-26.94191059	-19.77910514	3.20272941	-7.0298498	10.2325792
-15.6	-47.7	-24.25527066	-22.09354647	-0.6353276	-3.723505	3.08817741
-15.5991	-47.6991	-19.23347107	-19.01436285	-7.809327	-8.1223388	0.31301174
-15.59955	-47.69955	-22.70905816	-21.25077929	-2.8442026	-4.9274582	2.08325553
-7.10479	-48.22565	-29.37996646	-24.61407418	6.68566637	-0.1227512	6.80841754
-10.49626	-48.35347	-29.22031394	-27.08422769	6.45759134	3.40603956	3.05155179
-10.49604	-48.35262	-29.16445654	-27.63579857	6.37779506	4.19399796	2.1837971
-10.49645	-48.35259	-28.98566842	-26.53431337	6.12238346	2.62044767	3.50193579
-11.98796	-47.5582	-28.37085725	-25.77753725	5.24408179	1.53933893	3.70474286
-11.9882	-47.5579	-27.93691197	-25.68697996	4.62415996	1.40997137	3.21418859
-11.98894	-47.55811	-28.5088909	-25.14554398	5.44127271	0.6364914	4.80478131
-15.54955	-47.84955	-20.98969854	-25.3564776	-5.3004307	0.93782514	-6.2382558
-15.55	-47.85	-24.21396676	-23.12195174	-0.6943332	-2.2543547	1.56002146
-15.5491	-47.8491	-18.27986524	-18.68362161	-9.1716211	-8.5948263	-0.5767948
-12.81	-51.85	-26.12353362	-21.36257753	2.03361946	-4.7677464	6.80136584
-12.76	-51.88	-28.83808288	-23.84103658	5.91154697	-1.2270906	7.13863757
-11.48	-51.52	-28.01872233	-21.745403	4.7410319	-4.2208529	8.96188476
-13.14	-52.25	-23.53452584	-18.85950251	-1.6649631	-8.3435678	6.67860476
-13.43	-53.31	-28.08944583	-21.30082821	4.84206547	-4.8559597	9.69802517
-13.48	-53.353	-28.54473671	-25.84363273	5.49248101	1.63376104	3.85871997
-13.1	-53.352	-27.71691428	-25.08662606	4.30987754	0.55232294	3.7575546
-13.31	-53.41	-27.32191703	-24.04170765	3.74559576	-0.9404176	4.6860134
-14.78	-52.35	-26.62106292	-23.64569858	2.7443756	-1.5061449	4.25052049
-15.933122	-47.878508	-26.82030156	-21.88491242	3.02900223	-4.0215537	7.05055591
-15.933122	-47.8776071	-21.96601186	-19.77867917	-3.9056973	-7.0304583	3.12476099
-10.96	-52.17	-27.24545262	-19.81011491	3.63636089	-6.9855501	10.621911
-10.8	-51.82	-28.06779223	-23.91660115	4.81113176	-1.1191412	5.93027297
-11.96333	-48.23013	-26.28176537	-22.789	2.25966481	-2.73	4.98966481
-11.99807	-48.25917	-27.11715571	-25.33352977	3.45307959	0.90504253	2.54803706
-11.98273	-48.23983	-28.76370425	-27.92278626	5.80529179	4.60398037	1.20131141
-11.99185	-48.2465	-27.39548859	-26.23331541	3.85069799	2.19045059	1.6602474
-11.98898	-48.23995	-27.12694177	-26.53777912	3.46705967	2.62539874	0.84166093
-11.98717	-48.24085	-25.57698456	-24.19586341	1.25283509	-0.7201951	1.97303021
-11.97108	-48.23742	-21.61130396	-23.33810018	-4.4124229	-1.9455712	-2.4668517
-11.99172	-48.2506	-27.12927085	-25.44509642	3.47038693	1.06442346	2.40596347
-9.84	-50.46	-29.19133921	-23.70579157	6.41619887	-1.4202978	7.83649663
-10.4	-50.64	-25.82707023	-20.9133434	1.61010033	-5.4095094	7.01960976
-11.41	-55.33	-28.54579084	-26.22058993	5.49398691	2.17227133	3.32171559
-12.4213	-47.19715	-27.85607159	-26.23848859	4.5086737	2.19784084	2.31083286
-12.79057	-47.04976	-28.30881048	-22.00083932	5.15544354	-3.8559438	9.01138737
-12.79011	-47.04969	-27.85187022	-26.17117251	4.50267174	2.10167501	2.40099673
-12.97313	-46.90214	-19.67975691	-22.29419665	-7.1717758	-3.4368619	-3.7349139
-13.097	-46.75083	-22.16496597	-21.24627252	-3.6214772	-4.9338964	1.31241921
-13.70691	-47.23608	-26.83969883	-26.07110013	3.05671261	1.95871447	1.09799814
-13.7097	-47.23706	-24.0950808	-21.11202805	-0.8641703	-5.1256742	4.26150393
-12.82	-51.77	-26.33621062	-23.34939566	2.33744374	-1.9294348	4.26687851
-12.83	-51.77	-24.36474698	-21.15371643	-0.4789329	-5.0661194	4.5871865
-12.8	-55.98	-26.09137197	-21.46815821	1.98767424	-4.6169168	6.60459109
-16.33	-46.98	-26.3730791	-12.90279139	2.390113	-16.853155	19.2432682
-13.1	-52.38	-28.17498447	-24.55715465	4.96426353	-0.2040648	5.16832831
-15.95485	-47.888622	-24.64481323	-18.192925	-0.0788382	-9.2958214	9.21698319
-15.95485	-47.8877211	-18.65203797	-15.13677247	-8.6399458	-13.661754	5.02180786
-11.33788	-49.28043	-19.54565102	-27.05347256	-7.3633557	3.36210366	-10.725459
-11.15725	-49.67742	-26.91650254	-26.02473068	3.1664322	1.8924724	1.2739598
-11.15682	-49.67747	-26.98362596	-26.57600822	3.2623228	2.68001174	0.58231106
-11.2485	-49.45132	-22.75304992	-22.60706177	-2.7813573	-2.9899118	0.2085545
-12.52298	-49.9106	-26.52484334	-25.90564476	2.60691906	1.72234966	0.8845694
-12.66583	-49.9945	-27.01607649	-26.88520394	3.3086807	3.12171991	0.18696079
-12.6654	-49.99483	-26.55246452	-26.49759401	2.64637789	2.56799144	0.07838644
-12.62288	-49.97302	-21.72375347	-17.56219507	-4.2517808	-10.196864	5.94508343
-11.46357	-46.88225	-26.10282604	-23.421268	2.0040372	-1.82676	3.8307972
-11.36442	-46.89143	-23.98507412	-27.35004629	-1.0213227	3.78578041	-4.8071031
-11.41582	-46.88278	-23.15725388	-26.13177594	-2.203923	2.0453942	-4.2493172

APPENDIX B

SUPPLEMENTAL MATERIAL FOR CHAPTER III

Supplemental Figures

Supplemental Fig. 1 displays the light fraction bulk density separated by site.

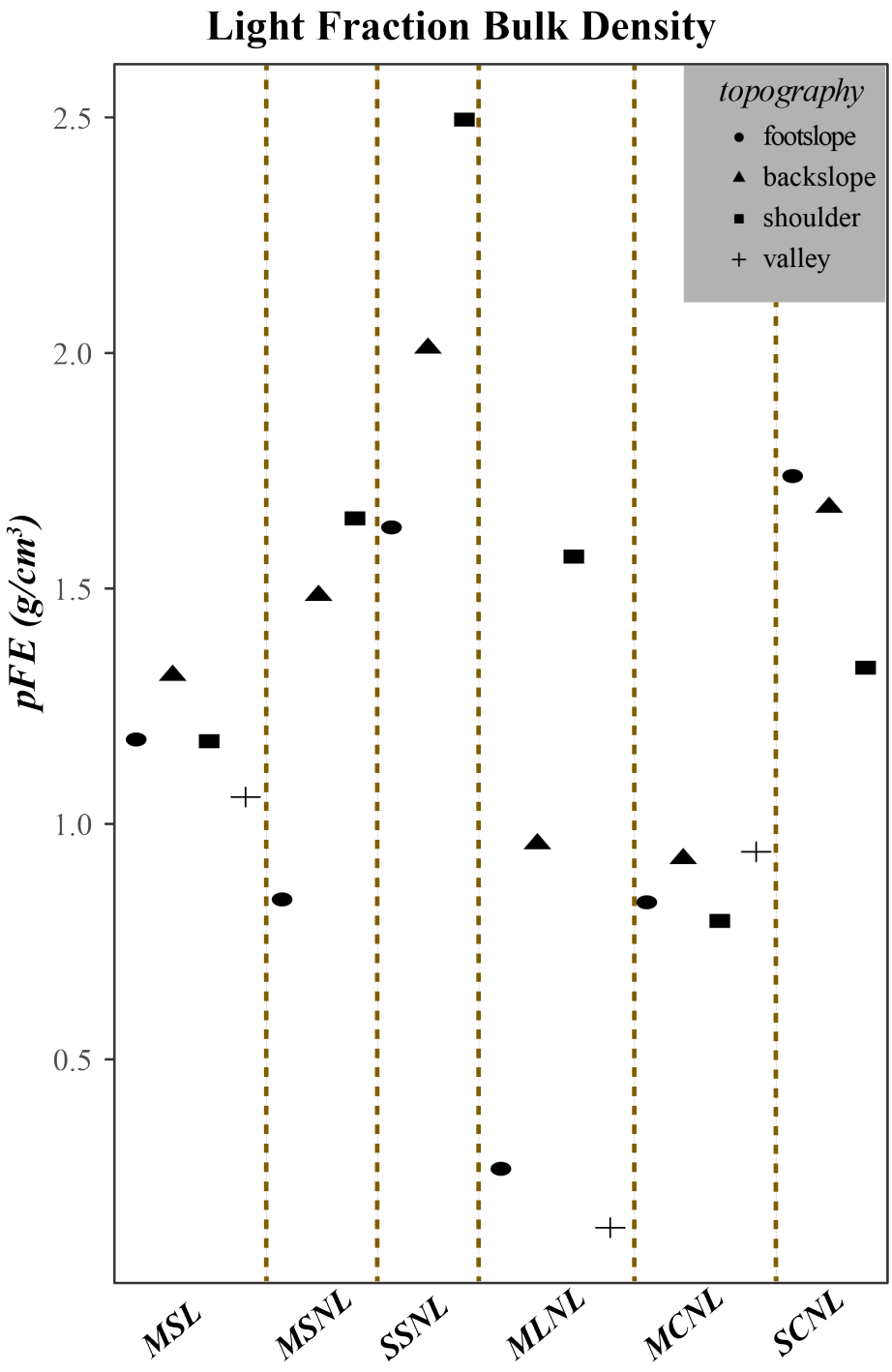

Supplemental Fig. 2 a-d left panel displays the relationship between light fraction bulk density and carbon stocks and **a-c** right panel displays carbon stocks vs TOC percent. a) MAC, b) POC, c) PyC, d) TOC.

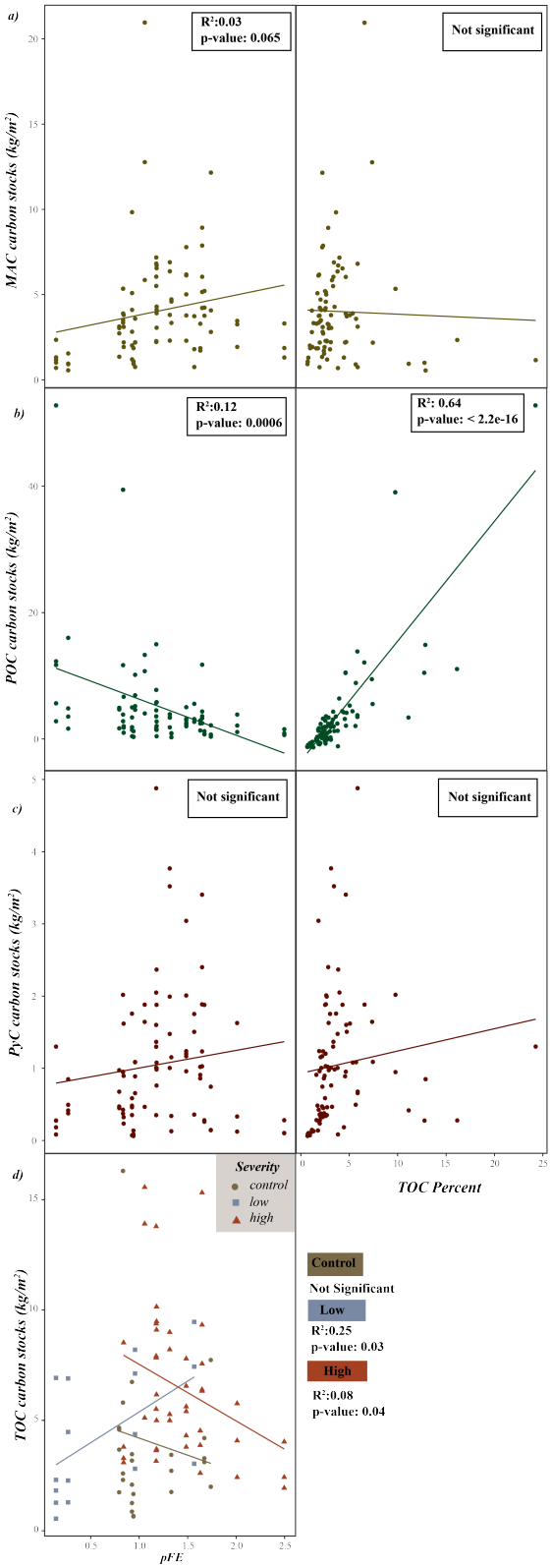

Supplemental Fig. 3 a-d show the output of the Random Forest regressions for the metamorphic parent material sites.

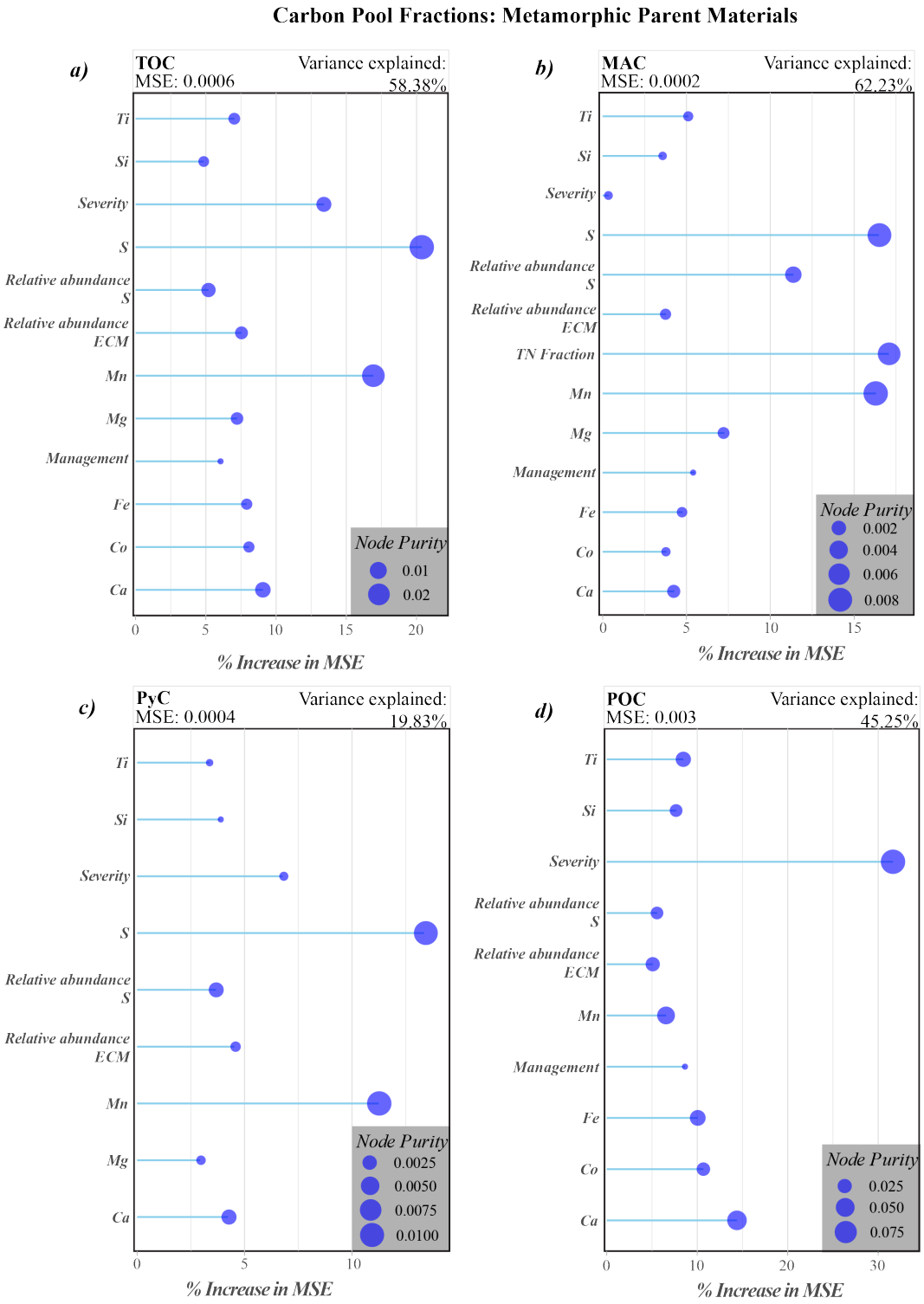

Supplemental Fig. 4 a-d show the output of the Random Forest regressions for the serpentine parent material sites.

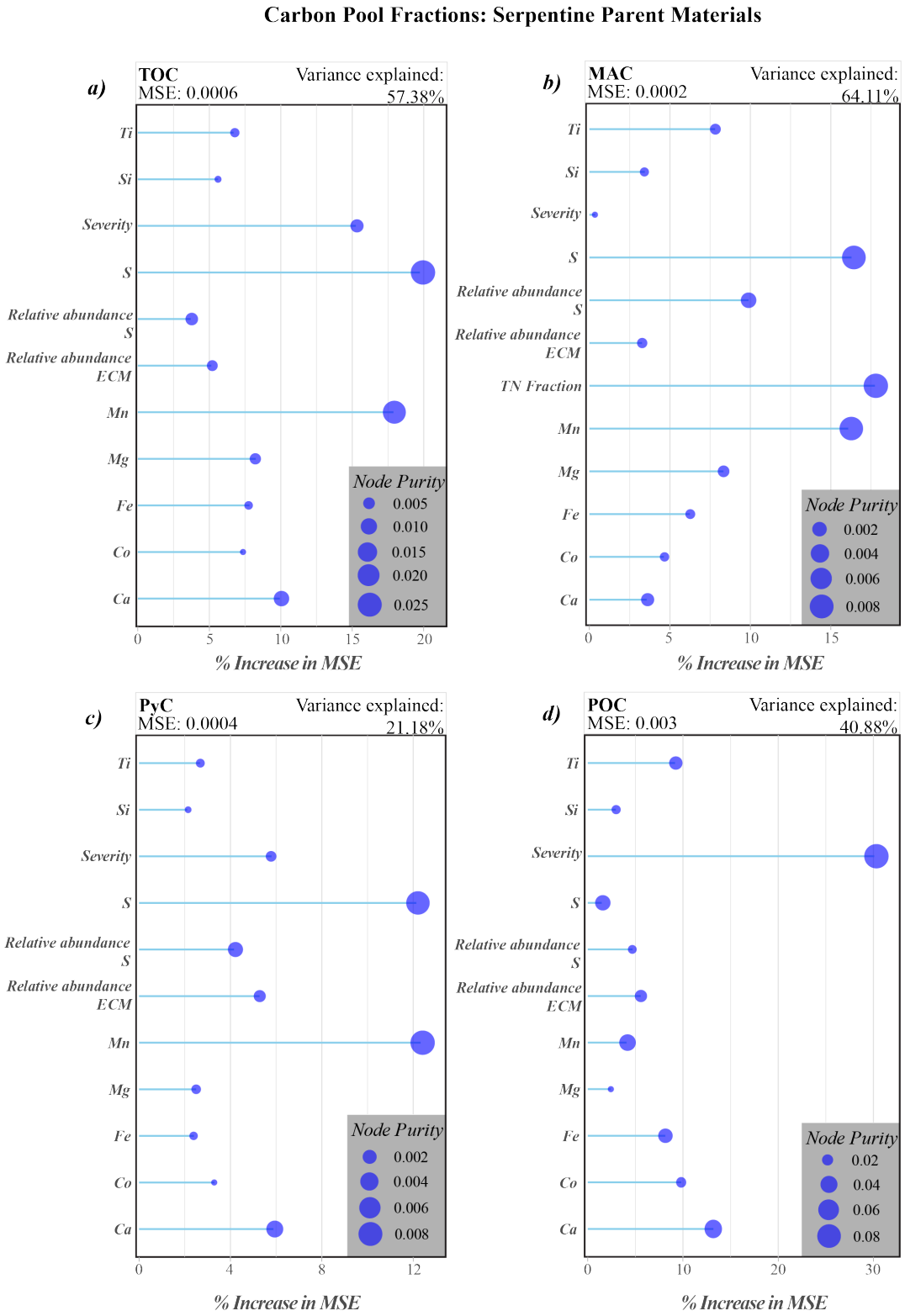

Supplemental Tables

Supplemental Table 1 shows the results of Random Forest regressions for delta carbon fractions as a function of measured variables compared with control samples in metamorphic sites.

(metamorphic)		Ti	Si	S	Relab S	Relab ECM	Nitrogen Fraction	Mn	Mg	Fe	Co	Ca	Severity	Manage-ment	pFE	MSE	% var
	control	5.29	6.72	0.35	2.73	1.45	NA	2.27	NA	10.26	8.97	8.19	NA	NA	6.38	381.3	26.2
POC	delta	6.84	0.64	4.05	1.95	10.81	NA	1.86	4.25	2.082	4.55	6.64	22.66	11.32	13.16	449.4	46.7
	control	2.09	1.95	6.21	8.21	5.61	17.07	10.06	NA	NA	NA	NA	NA	NA	1.79	1008.0	45.8
MAC	delta	2.54	1.54	14.25	15.02	4.02	13.43	13.51	7.43	3.13	2.73	2.62	2.62	5.68	1.89	6094.9	60.9
	control	1.21	4.02	11.57	5.67	NA	NA	6.94	NA	2.72	4.11	NA	NA	NA	1.19	6507.8	2.8
PyC	delta	2.25	1.64	11.92	9.34	9.58	NA	9.47	1.68	2.17	2.11	2.82	4.47	NA	5.10	109984.5	20.0
	control	5.22	4.87	10.24	5.72	2.88	NA	14.42	1.24	4.18	5.03	4.09	NA	NA	6.74	2514.3	62.2
TOC	delta	3.31	1.36	15.44	7.49	10.17	NA	11.48	3.97	4.77	4.36	7.07	7.54	3.31	13.20	7533.0	50.9

Supplemental Table 2 shows the results of Random Forest regressions for delta carbon fractions as a function of measured variables compared with control samples in serpentine sites.

(serpentine)		Ti	Si	S	Relab S	Relab ECM	Nitrogen Fraction	Mn	Mg	Fe	Co	Ca	pFE	MSE	% var
	control	NA	NA	NA	NA	NA	NA	NA	NA	NA	NA	NA	NA	NA	NA
POC	delta	NA	6.48	NA	NA	NA	NA	6.41	5.63	6.73	6.75	5.08	NA	350.6626	35.0
	control	NA	NA	NA	NA	NA	NA	NA	NA	NA	NA	NA	NA	NA	NA
MAC	delta	13.24	NA	NA	NA	NA	16.92	NA	NA	NA	NA	NA	NA	178.5502	58.3
	control	NA	NA	NA	NA	NA	NA	NA	NA	NA	NA	NA	NA	NA	NA
PyC	delta	5.21	NA	NA	11.33	8.76	NA	NA	NA	NA	NA	NA	8.15	4229.8	48.1
	control	NA	NA	NA	NA	NA	NA	NA	NA	NA	NA	NA	NA	NA	NA
TOC	delta	NA	NA	NA	13.20	11.86	NA	NA	NA	NA	NA	1.21	NA	716.6	47.6

Supplemental Table 3 a-b Display stock averages and standard deviations for each pool and site. NA values indicate where samples were not collected

a)

Site	TOC stocks (kg/m^2) *topsoil*	TOC stocks (kg/m^2) > *20 cm*	MAC stocks (kg/m^2) *topsoil*	MAC stocks (kg/m^2) > *20 cm*	POC stocks (kg/m^2) *topsoil*	POC stocks (kg/m^2) > *20 cm*	PyC stocks (kg/m^2) *topsoil*	PyC stocks (kg/m^2) > *20 cm*
MSL	(9.1 ± 2.4)	(5.7 ± 2.4)	(6 ± 1.2)	(3.8 ± 1.9)	(5.2 ± 4.2)	(3.4 ± 2.2)	(2.6 ± 1.4)	(1.3 ± 0.6)
MSNL	(7.6 ± 3.6)	(5 ± 1.4)	(5.7 ± 2.4)	(4 ± 1.7)	(4.4 ± 3.3)	(2.8 ± 1)	(1.8 ± 1.2)	(1.3 ± 0.4)
SSNL	(3.6 ± 1.3)	NA	(2.5 ± 0.9)	NA	(1.9 ± 1.1)	NA	(0.6 ± 0.6)	NA
MLNL	(5.4 ± 2.9)	(2.7 ± 0.6)	(1.9 ± 1.2)	(0.9 ± 0.2)	(6.1 ± 4.3)	(3.4 ± 0.3)	(1 ± 0.5)	(0.5 ± 0.1)
MCNL	(5.1 ± 4.3)	(2.6 ± 1.2)	(4.2 ± 2.4)	(2.7 ± 0.6)	(7.8 ± 11.5)	(3.6 ± 2.6)	(1 ± 0.6)	(0.4 ± 0.2)
SCNL	(3.6 ± 1.9)	NA	(5.3 ± 2.9)	NA	(1 ± 0.6)	NA	(0.6 ± 0.6)	NA

b)

Site	TOC stocks (kg/m^2) *topsoil*	TOC stocks (kg/m^2) > *20 cm*	MAC stocks (kg/m^2) *topsoil*	MAC stocks (kg/m^2) > *20 cm*	POC stocks (kg/m^2) *topsoil*	POC stocks (kg/m^2) > *20 cm*	PyC stocks (kg/m^2) *topsoil*	PyC stocks (kg/m^2) > *20 cm*
MSL & MSNL	(13.3 ± 2.7)	(8.7 ± 3.7)	(15.4 ± 4.9)	(8.9 ± 7.1)	(9.9 ± 4)	(7 ± 2.6)	(1.8 ± 0.2)	(0.5 ± NA)
MLNL	(3.6 ± 3.1)	(1.2 ± 1)	(1.7 ± 0.7)	(0.9 ± 0.3)	(23.6 ± 25.6)	(7.3 ± 6.3)	(0.6 ± 0.7)	(0.2 ± 0.2)
MCNL	(1 ± 0.6)	NA	(1.3 ± 0.5)	NA	(0.7 ± 0.6)	NA	(0.1 ± 0.1)	NA

Supplemental Table 4 displays XRF results, where data are represented as percentages.

Site	Mg	Al	Si	P	S	K	Ca	Ti	V	Cr	Mn	Fe	Co	Ba
site 1 bototm B 20-30	1.0298	5.039	9.487	0.0904	0.0279	0.559	0.5745	1.483	< LOD	< LOD	0.2468	7.2444	0.0032	< LOD
site 1 bottom A 0-20	0.8601	1.9091	4.8638	0.0359	0.0228	0.1971	0.2684	0.7042	< LOD	< LOD	0.1456	3.2113	0.0015	< LOD
site 1 bottom A 20-35	0.954	5.5407	11.3315	0.1023	0.0326	0.6696	0.5768	1.6325	0.0049	< LOD	0.2901	8.0899	0.0036	< LOD
site 1 bottom B 0-20	0.8865	1.126	2.7962	0.0253	0.0248	0.0735	0.1737	0.4469	< LOD	< LOD	0.0707	2.2363	0.0011	< LOD
site 1 bottom C 0-20	0.8877	< LOD	0.276	< LOD	0.0281	< LOD	0.026	0.0281	< LOD	0.0026	0.0145	0.1891	0.0002	< LOD
site 1 bottom C 20-30	0.8243	< LOD	1.0312	< LOD	0.0259	< LOD	0.1099	0.2355	< LOD	< LOD	0.0543	1.3428	0.0006	< LOD
site 1 middle A 0-20	0.8882	2.9377	6.8451	0.0717	0.0245	0.3862	0.1403	0.9768	< LOD	< LOD	0.1508	4.4951	0.0021	< LOD
site 1 middle A 20-35	0.9268	< LOD	1.0123	0.0049	0.0259	< LOD	0.0423	0.0836	< LOD	0.0011	0.0176	0.4491	0.0002	< LOD
site 1 middle B 0-20	0.8716	1.3652	3.3846	0.0331	0.0243	0.1513	0.1649	0.5888	< LOD	< LOD	0.1957	2.7896	0.0012	< LOD
site 1 middle C 0-20	0.8196	5.2771	12.1496	0.1152	0.0356	0.784	0.4293	1.5259	0.0035	0.0009	0.4132	6.503	0.0029	< LOD
site 1 middle C 20-30	0.8623	1.3211	3.8323	0.0351	0.0234	0.1703	0.1462	0.4659	< LOD	< LOD	0.156	1.9838	0.001	< LOD
site 1 top A 0-20	0.8331	1.7601	4.0034	0.0279	0.0294	0.0651	0.1462	0.6695	< LOD	< LOD	0.1038	2.6769	0.0013	< LOD
site 1 top A 20-30	0.8378	1.565	3.6024	0.0232	0.0232	0.0672	0.1311	0.6459	< LOD	< LOD	0.075	2.6959	0.0013	< LOD
site 1 top A 30-40	0.876	3.8245	7.0994	0.0601	0.0265	0.3199	0.185	1.3001	0.0065	< LOD	0.1462	6.1088	0.0028	< LOD
site 1 top B 0-20	0.9278	0.8354	2.3446	0.0133	0.0242	0.0412	0.1469	0.3424	< LOD	< LOD	0.0421	1.7171	0.0008	< LOD
site 1 top B 20-40	0.9371	3.3845	6.3474	0.0653	0.0313	0.3893	0.3898	1.0991	< LOD	0.0034	0.2356	5.0453	0.0023	< LOD
site 1 top C 0-20	0.89	3.4327	6.1493	0.0508	0.0293	0.3209	0.2592	0.9635	< LOD	< LOD	0.0937	4.2626	0.002	< LOD
site 1 top C 20-30	0.8346	5.5061	9.718	0.0875	0.0341	0.5255	0.2534	1.3764	0.0105	0.004	0.2162	7.928	0.0036	< LOD
site 1 valley A 0-20	1.801	2.6526	6.4288	0.0645	0.0424	0.2471	0.7865	0.7681	0.0093	0.0374	0.2044	5.8684	0.0027	< LOD
site 1 valley A 20-35	1.2014	0.3145	2.2377	0.0161	0.0322	0.0385	0.3292	0.3837	< LOD	0.0134	0.0928	3.1924	0.0014	< LOD
site 1 valley B 0-20	1.621	2.2974	6.1667	0.1353	0.0646	0.2638	1.057	0.8644	0.0186	0.0623	0.7788	11.0761	0.0046	< LOD
site 1 valley B 20-30	0.9728	< LOD	0.4586	< LOD	0.0321	< LOD	0.0497	0.023	< LOD	0.0029	0.0242	0.2926	0.0001	< LOD
site 1 valley C 0-20	1.7219	2.0277	5.834	0.0842	0.0498	0.1499	0.7757	0.5702	0.0092	0.0612	0.2577	5.178	0.0024	< LOD
site 1 valley C 20-40	1.3267	0.4959	2.4421	0.022	0.0306	< LOD	0.268	0.2017	< LOD	0.0159	0.0568	1.8265	0.0009	< LOD
site 1 valley C 40-50	1.5994	1.4885	4.5554	0.04	0.0326	0.1106	0.6146	0.5318	0.008	0.0459	0.1256	4.9639	0.0023	< LOD
site 2 bottom A 0-20	1.3584	3.8762	9.8859	0.1276	0.032	0.4508	0.7451	1.1973	0.0069	0.0079	0.2935	6.9161	0.0031	< LOD
site 2 bottom B 0-20	1.395	< LOD	1.8486	< LOD	0.0287	< LOD	0.226	0.0968	< LOD	0.021	0.0309	1.108	0.0006	< LOD
site 2 bottom B 20-30	2.1597	1.3078	5.588	0.0214	0.0217	0.0968	0.7668	0.3418	0.002	0.0567	0.0849	4.012	0.0018	< LOD
site 2 bottom C 0-20	2.0379	0.3313	3.2952	0.0106	0.0245	< LOD	0.6083	0.1898	< LOD	0.056	0.0583	2.9623	0.0014	< LOD
site 2 bottom C 20-35	4.0346	2.3942	9.0741	0.0372	0.0289	0.097	1.6419	0.4752	0.0191	0.1758	0.2022	8.471	0.0037	0.0433
site 2 middle A 0-20	1.0245	< LOD	0.543	< LOD	0.0263	< LOD	0.0819	0.0216	< LOD	0.0064	0.011	0.3115	0.0002	< LOD
site 2 middle A 20-30	1.4205	< LOD	1.8242	< LOD	0.0267	< LOD	0.3394	0.0939	< LOD	0.0253	0.0419	1.3973	0.0007	< LOD
site 2 middle B 0-20	3.4964	1.1499	5.6552	0.0242	0.0295	< LOD	1.0929	0.2333	0.012	0.2011	0.1815	9.859	0.0043	0.0531
site 2 middle B 20-35	1.0746	< LOD	0.3964	< LOD	0.0295	< LOD	0.0695	0.0145	< LOD	0.0098	0.0112	0.4145	0.0002	< LOD
site 2 middle C 0-20	4.7413	1.8263	7.1655	0.0446	0.0236	< LOD	1.6121	0.2485	0.0162	0.2337	0.1919	12.1211	0.0052	0.0596
site 2 middle C 20-40	2.6395	0.4852	3.5745	0.0244	0.0191	< LOD	0.7264	0.1363	0.0032	0.094	0.1122	5.5967	0.0025	< LOD
site 2 top A 0-20	2.3927	2.797	9.4295	0.0812	0.0272	0.2605	1.8518	0.7161	0.0141	0.0613	0.538	6.979	0.003	< LOD
site 2 top B 0-20	2.7118	1.9389	4.958	0.0572	0.0235	< LOD	1.1467	0.3466	0.0131	0.2136	0.1347	11.8666	0.005	< LOD
site 2 top B 20-35	1.058	< LOD	0.5476	< LOD	0.0268	< LOD	0.0791	0.0142	< LOD	0.0073	0.0087	0.4512	0.0002	< LOD
site 2 top C 0-20	1.3002	< LOD	1.0491	< LOD	0.0274	< LOD	0.1821	0.0424	< LOD	0.0329	0.0358	1.6863	0.0008	< LOD
site 2 top C 20-35	2.6749	0.4569	3.6058	0.0216	0.03	< LOD	0.6309	0.1561	0.006	0.1689	0.1821	9.1539	0.0039	< LOD
site 3 bottom A 0-10	5.6863	2.1647	8.6278	0.0556	0.0244	< LOD	1.6224	0.446	0.0161	0.1673	0.4608	11.0828	0.0047	0.0602
site 3 bottom B 0-10	4.4907	0.8467	5.9085	0.0364	0.0293	< LOD	1.1048	0.2621	0.0031	0.0994	0.3025	7.3312	0.0031	< LOD
site 3 bottom C 0-10	2.001	< LOD	1.9654	0.0111	0.0291	< LOD	0.2624	0.074	< LOD	0.0208	0.0806	1.5868	0.0008	< LOD
site 3 middle A 0-10	1.6547	< LOD	0.9008	< LOD	0.028	< LOD	0.078	0.0106	< LOD	0.0092	0.0153	0.5558	0.0003	< LOD
site 3 middle B 0-10	7.129	1.0896	8.5121	0.035	0.0408	< LOD	1.3725	0.2275	0.0123	0.1561	0.2444	9.415	0.0041	0.0651
site 3 middle C 0-10	3.4326	< LOD	3.618	0.0183	0.0313	< LOD	0.4027	0.1049	< LOD	0.0616	0.1075	3.6801	0.0017	< LOD
site 3 top A 0-10	7.8699	0.468	7.4343	0.0203	0.0341	< LOD	1.0072	0.0417	0.0038	0.0723	0.1395	5.8112	0.0027	0.0895
site 3 top B 0-10	1.0683	< LOD	0.3351	< LOD	0.026	< LOD	0.0468	0.0061	< LOD	0.0063	0.0121	0.2148	0.0002	< LOD
site 3 top C 0-10	4.65	0.0734	4.5547	0.0159	0.0351	< LOD	0.653	0.0897	< LOD	0.071	0.1005	3.8707	0.0018	< LOD
site 4 bottom A 0-20	1.3472	1.8291	4.9109	0.0497	0.0391	< LOD	1.4782	0.2601	0.0048	0.0028	0.3114	3.0151	0.0013	< LOD
site 4 bottom B 0-15	1.9214	1.3741	4.5964	0.0292	0.0226	< LOD	1.4682	0.2324	0.0108	0.0192	0.1533	3.6609	0.0017	< LOD
site 4 bottom B 15-30	0.972	< LOD	0.2391	< LOD	0.0313	< LOD	0.0301	0.0066	< LOD	0.0015	0.0043	0.0715	< LOD	< LOD
site 4 bottom C 0-20	1.0306	< LOD	0.4448	< LOD	0.0289	< LOD	0.066	0.0134	< LOD	0.002	0.0055	0.1573	0.0001	< LOD
site 4 middle A 0-15	1.2873	2.3301	4.1946	0.0394	0.0228	< LOD	1.0228	0.2318	0.0058	0.0017	0.089	2.7575	0.0013	< LOD
site 4 middle A 15-20	1.0929	0.6474	1.904	0.0153	0.0244	< LOD	0.484	0.1187	< LOD	0.0016	0.0566	1.3822	0.0007	< LOD
site 4 middle B 0-10	0.9838	< LOD	0.9905	< LOD	0.0278	< LOD	0.2467	0.0546	< LOD	0.003	0.0363	0.6958	0.0004	< LOD
site 4 middle C 0-10	1.404	1.9801	3.143	0.0268	0.0272	< LOD	0.9421	0.1439	0.002	0.0059	0.1416	1.9883	0.001	< LOD
site 4 top A 0-20	1.3542	2.2266	5.2715	< LOD	0.016	< LOD	1.0994	0.1903	0.006	0.0062	0.0655	2.9235	0.0013	< LOD
site 4 top A 20-30	2.1881	4.2421	9.2365	0.0158	0.0257	< LOD	2.0005	0.3168	0.0186	0.0178	0.1301	5.2867	0.0024	0.0249
site 4 top B 0-10	1.3555	2.1635	4.864	0.011	0.0221	< LOD	1.0394	0.1545	0.0036	0.0044	0.0726	2.7074	0.0013	< LOD
site 4 top C 0-10	2.2822	5.8435	9.2762	0.0825	0.023	0.071	2.4688	0.419	0.0181	0.017	0.3272	5.6282	0.0024	< LOD
site 4 valley A 0-20	2.7348	2.7599	10.1659	0.0735	0.0132	0.0706	2.4771	0.4174	0.0141	0.0213	0.3489	4.7325	0.0021	0.0341
site 4 valley A 20-30	1.7311	0.8202	4.4401	0.0276	0.0186	< LOD	0.978	0.1594	< LOD	0.007	0.1282	1.8125	0.0009	< LOD
site 4 valley B 0-20	1.1556	0.176	3.2597	0.0797	0.0792	< LOD	1.7244	0.1749	< LOD	0.0023	0.8111	1.9668	0.0008	< LOD
site 4 valley B 20-30	1.2926	0.3946	3.5304	0.0523	0.0307	< LOD	0.9231	0.1555	< LOD	0.0044	0.208	1.7431	0.0009	< LOD
site 4 valley C 0-10	1.5392	1.7576	7.8195	0.0993	0.0756	0.1356	2.441	0.3398	0.0096	0.0112	0.7024	3.9384	0.0016	0.0511
site 5 bottom A 0-15	0.9407	< LOD	0.8475	< LOD	0.0254	< LOD	0.1204	0.0228	< LOD	0.0021	0.0123	0.2955	0.0002	< LOD
site 5 bottom B 20-30	1.3687	1.2409	3.4869	0.0082	0.0249	< LOD	0.6627	0.123	< LOD	0.0055	0.0847	1.7174	0.0009	< LOD
site 5 bottom B 0-30	1.5542	1.9779	5.5218	0.0273	0.044	< LOD	1.2589	0.1736	0.0034	0.0063	0.324	2.5191	0.0011	< LOD
site 5 bottom C 0-15	1.7843	0.8143	3.2726	0.0093	0.0211	< LOD	0.6122	0.0997	< LOD	0.0171	0.087	1.8642	0.0009	< LOD
site 5 bottom C 15-30	2.1007	1.054	4.0256	0.0104	0.0231	< LOD	0.8245	0.1307	0.0017	0.0255	0.1429	2.3071	0.0011	< LOD
site 5 middle A 0-20	1.6177	< LOD	1.59	0.0082	0.0281	< LOD	0.2648	0.0462	< LOD	0.0139	0.0863	1.1547	0.0006	< LOD
site 5 middle A 20-30	5.3058	1.4977	8.58	0.062	0.0243	< LOD	1.126	0.1964	0.011	0.0628	0.1527	5.4475	0.0025	0.0561
site 5 middle B 0-20	3.2975	0.2249	3.8608	0.0155	0.0252	< LOD	0.5676	0.0839	< LOD	0.022	0.1007	2.3922	0.0012	< LOD
site 5 middle B 20-30	7.0184	1.6293	7.5574	0.0189	0.02	< LOD	1.4149	0.1421	0.0106	0.0935	0.1427	5.3755	0.0025	0.052
site 5 middle C 0-15	1.1385	< LOD	0.6921	< LOD	0.0261	< LOD	0.1097	0.0152	< LOD	0.0042	0.0132	0.3096	0.0001	< LOD
site 5 middle C 15-20	1.8972	< LOD	2.4671	0.0084	0.0266	< LOD	0.413	0.0515	< LOD	0.0165	0.0845	1.4504	0.0007	< LOD
site 5 top A 0-20	2.0034	6.7409	11.2454	0.0181	0.0155	< LOD	2.7108	0.4315	0.0252	0.0092	0.0917	6.439	0.0029	< LOD
site 5 top A 20-40	1.4446	3.8932	6.7456	0.0134	0.0185	< LOD	1.4539	0.2622	0.0126	0.0036	0.0545	3.8478	0.0018	< LOD
site 5 top A 40-50	1.3548	3.7399	6.6562	0.0151	0.0199	< LOD	1.3938	0.2595	0.0087	0.0015	0.0489	3.8315	0.0018	< LOD
site 5 top B 0-20	1.29	< LOD	0.5906	< LOD	0.029	< LOD	0.0446	0.0084	< LOD	0.0034	0.014	0.2806	0.0002	< LOD
site 5 top C 0-10	3.0563	0.5319	4.7837	0.0208	0.0262	< LOD	1.4602	0.1522	0.0065	0.0358	0.373	3.4745	0.0015	< LOD
site 5 valley A 0-10	1.0209	< LOD	1.187	< LOD	0.0263	< LOD	0.2336	0.0409	< LOD	0.002	0.0173	0.6656	0.0003	< LOD
site 5 valley B 0-10	2.431	6.7961	10.2507	0.0209	0.0244	0.1164	1.6681	0.3696	0.023	0.0235	0.1275	6.3395	0.0029	0.0336
site 5 valley C 0-10	1.9533	4.8269	7.7963	0.0277	0.0238	0.0496	1.2944	0.2727	0.0139	0.0142	0.1094	4.5104	0.0021	< LOD
site 6 bottm A 0-20	1.7443	0.5786	6.2005	< LOD	0.0367	< LOD	0.5687	0.0699	0.0091	0.4557	0.3446	13.3386	0.0057	0.0848
site 6 bottom A 20-30	1.1556	< LOD	2.8476	< LOD	0.0324	< LOD	0.1851	0.0389	0.0019	0.1459	0.119	5.3856	0.0024	< LOD
site 6 bottom B 0-20	3.3576	0.5863	7.1737	< LOD	0.0395	< LOD	0.8822	0.0822	0.0108	0.4214	0.4517	13.3201	0.0057	0.0841
site 6 bottom C 0-10	3.3676	0.5226	6.7948	< LOD	0.0282	< LOD	1.0553	0.0867	0.0061	0.4474	0.4957	11.8889	0.0051	0.045
site 6 middle A 0-10	1.2988	< LOD	0.9275	< LOD	0.0274	< LOD	0.0888	0.0127	< LOD	0.0368	0.0522	1.0372	0.0006	< LOD
site 6 middle B 0-10	1.4161	< LOD	2.0615	< LOD	0.0274	< LOD	0.2854	0.0356	< LOD	0.1137	0.1177	3.6312	0.0017	< LOD
site 6 middle C 0-10	0.9771	< LOD	0.1929	< LOD	0.0307	< LOD	0.022	0.0028	< LOD	0.0049	0.006	0.142	0.0001	< LOD
site 6 top A 0-10	2.9205	0.2175	5.7554	< LOD	0.0335	< LOD	0.8857	0.0804	0.0073	0.4636	0.3947	10.5683	0.0044	0.0248
site 6 top B 0-10	2.3605	< LOD	3.7359	0.0078	0.0305	< LOD	0.4475	0.0526	0.003	0.23	0.227	6.5845	0.0029	< LOD
site 6 top C 0-10	3.2827	0.6207	7.6402	< LOD	0.0332	< LOD	0.8508	0.0614	0.0134	0.4569	0.4457	13.9484	0.006	0.1251

APPENDIX C

SUPPLEMENTAL MATERIAL FOR CHAPTER IV

Supplemental Figures

Supplemental Figure 1 displays a) C:N b) TOC percent and c) TN percent.

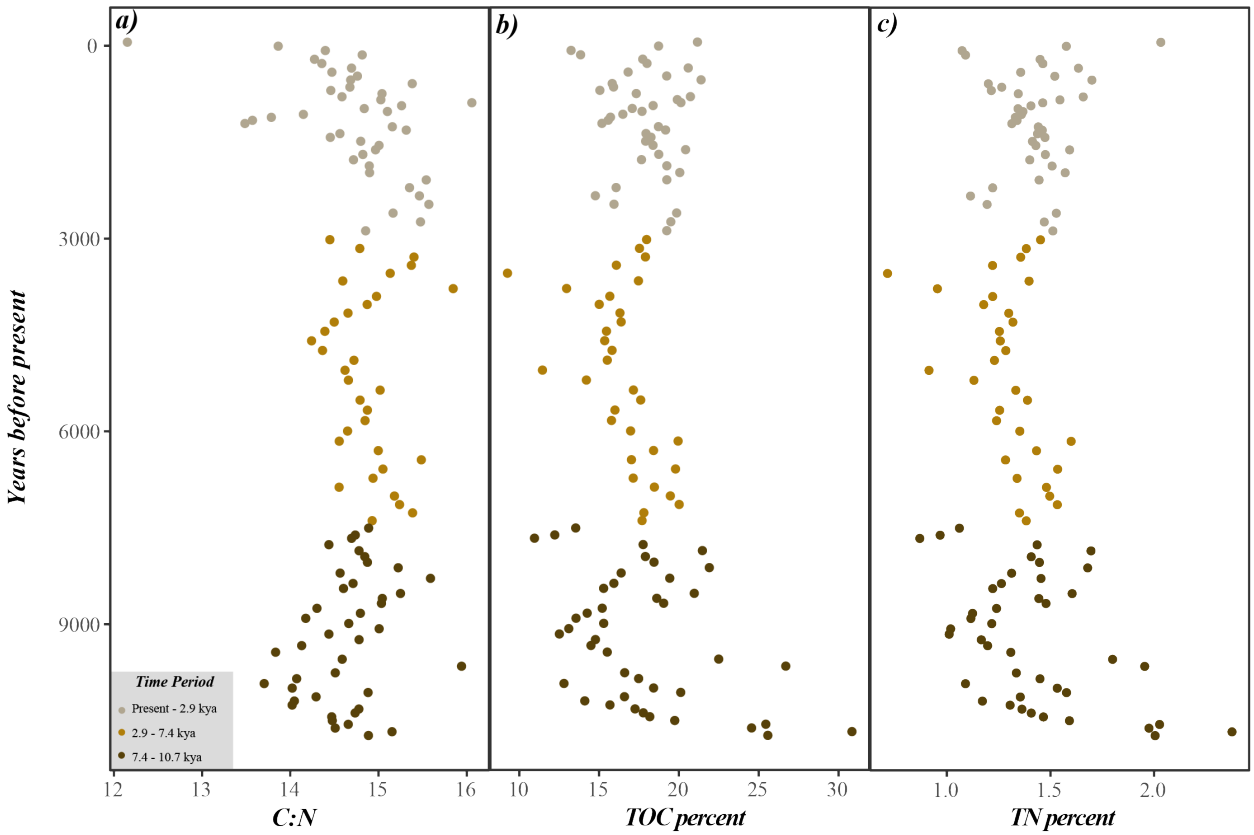

Supplemental Figure 2 displays the relationship between percent carbon and C_{MAR} throughout the Holocene.

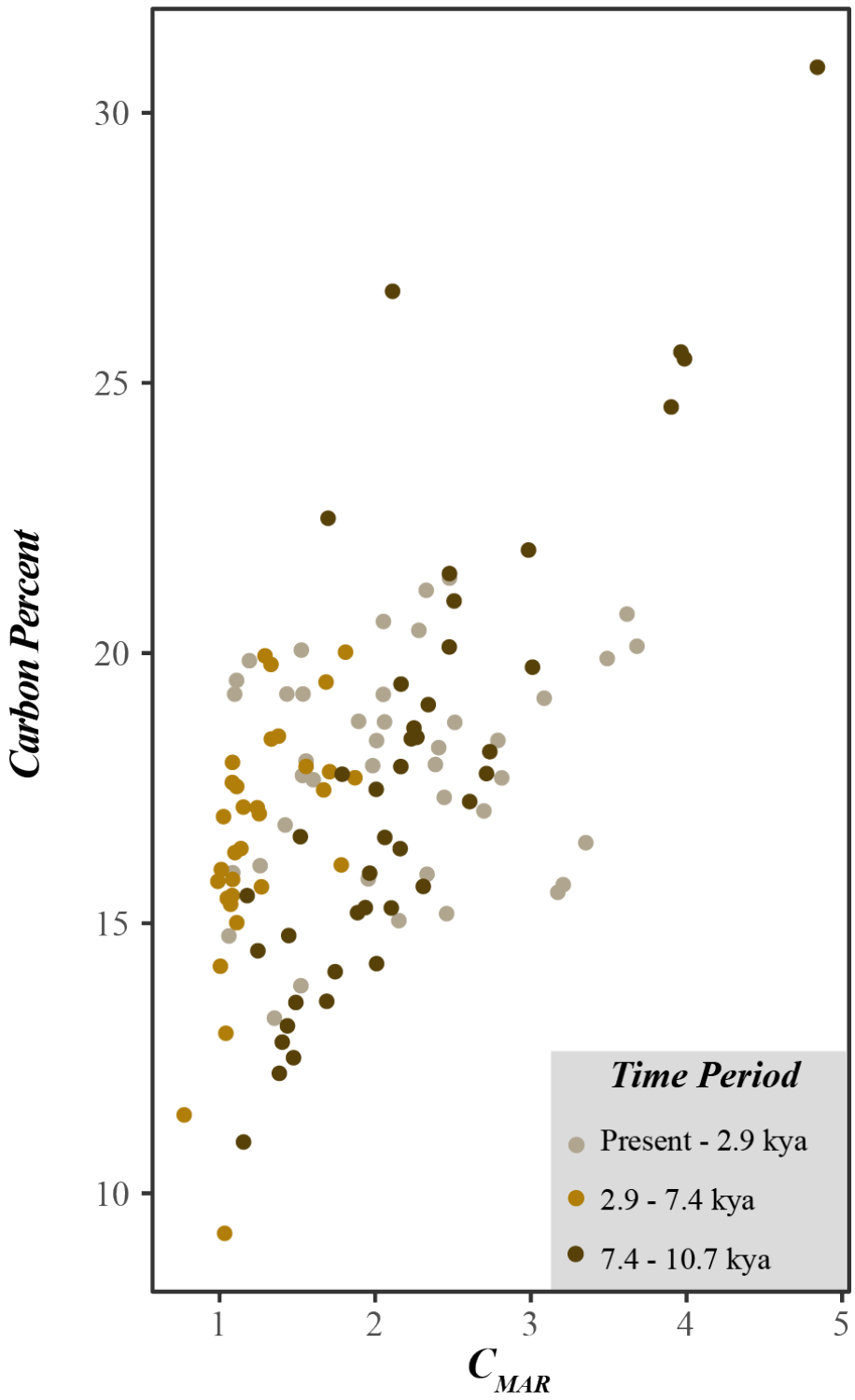

Supplemental Figure 3 displays the relationship between (a) Si:Ti and C_{MAR} and (b) $\delta^{13}C$ throughout the Holocene. The linear regression between Si:Ti to $\delta^{13}C$ is significant.

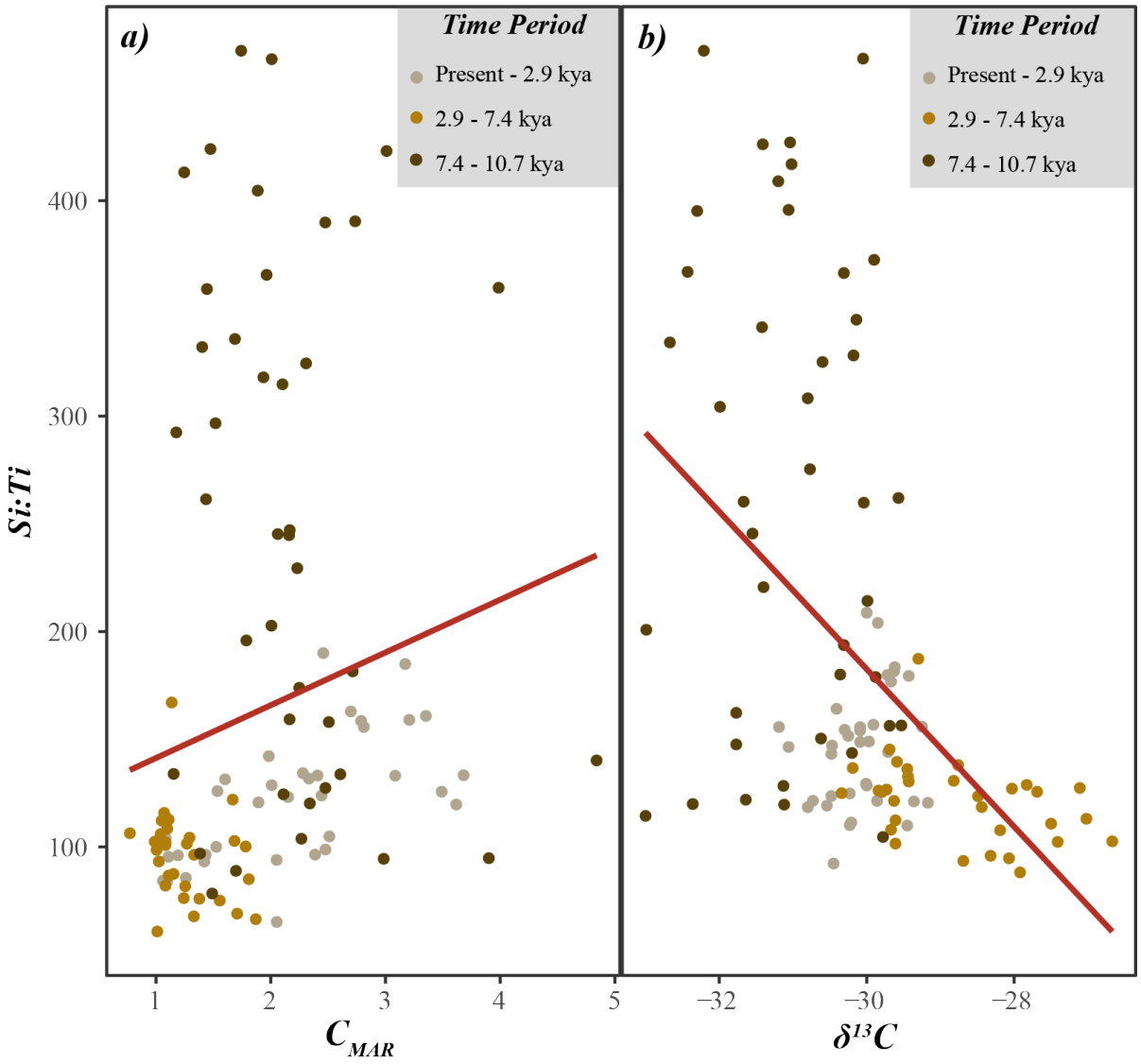

Supplemental Tables

Supplemental Table 1 includes the sediment depths that were submitted for radiocarbon dating. * Indicates outlier ages that were not included in the age-depth model. D-AMS=Direct AMS, Bothell WA; OS=NOSAMS, Woods Hole Oceanographic Institute, Woods Hole, MA

Lab ID	Depth (cm)	Material dated	Radiocarbon Age (^{14}C yr BP)	Calibrated Age (cal yr BP)
OS-170039	47	Deciduous leaf	510 ± 45	550 (630-500)
D-AMS-41112	154-155	Needle fragments	1788 ± 22	1680 (1730-1620)
OS-166895	230-231	pollen fraction	3300 ± 20	3530 (3480-3580)
D-AMS-42760	251-254	conifer needle fragments	3733 ± 38	4010 (4140-3900)
OS-170036	294-295	western redcedar needle	3830 ± 25 *	5310 (5400-5230)
D-AMS41113	302-303	Cone bracts, seed wings, needle	4846 ± 28	5560 (5640-5490)
D-AMS-42761	324-325	conifer cone bract	5463 ± 41	6230 (6340-6170)
Mazama	377-384.5	Mazama tephra age	-	7630 ± 25
OS-170037	482-483	Charred conifer needle	8280 ± 55	9270 (9430-9040)
OS-166896	511-512	pollen fraction	8700 ± 45 *	9860 (10120-9580)
OS-170038	513-514	conifer needle	8820 ± 65	9890 (10150-9610)
D-AMS-41114	579-580	bulk sediment > 150 um	9465 ± 34	10700 (10990-10580)

REFERENCES CITED

CHAPTER I

Freeman, S., Quillin, K., & Allison, L. (2013). *Biological Science* (5th ed.). Pearson.

Marchant, R., & Hooghiemstra, H. (2004). Rapid environmental change in African and South American tropics around 4000 years before present : a review. *Earth-Science Reviews*, *66*, 217–260. https://doi.org/10.1016/j.earscirev.2004.01.003

Nelson, D. B., Abbott, M. B., Steinman, B., Polissar, P. J., Stansell, N. D., Ortiz, J. D., … Riedel, J. (2011). Drought variability in the Pacific Northwest from a 6 , 000-yr lake sediment record, 1–6. https://doi.org/10.1073/pnas.1009194108/-/DCSupplemental.www.pnas.org/cgi/doi/10.1073/pnas.1009194108

Roberts, N. (1998). *The Holocene: An Environmental History* (second). Oxford: Blackwell Publishers Ltd.

Scheffer, M., Carpenter, S., Foley, J. A., Folke, C., & Walker, B. (2001). Catastrophic shifts in ecosystems, 591–596.

Scheffer, M., & Carpenter, S. R. (2003). Catastrophic regime shifts in ecosystems : linking theory to observation, *18*(12), 648–656. https://doi.org/10.1016/j.tree.2003.09.002

Schlesinger, W. H., & Bernhardt, E. S. (2013). *Biogeochemistry An Analysis of Global Change* (Third). Waltham: Elsevier.

Silva, L. C. R., Sternberg, L., Haridasan, M., Hoffmann, W. A., Miralles-Wilhelm, F., & Franco, A. C. (2008). Expansion of gallery forests into central Brazilian savannas. *Global Change Biology*, *14*(9), 2108–2118. https://doi.org/10.1111/j.1365-2486.2008.01637.x

Smith, R. J., & Mayle, F. E. (2018). Impact of mid- to late Holocene precipitation changes on vegetation across lowland tropical South America : a paleo-data synthesis. *Quaternary Research*, 134–155. https://doi.org/10.1017/qua.2017.89

Whittaker, R. H. (1975). *Communities and Ecosystems*. New York: Macmillan Publishing Co., Inc.

CHAPTER II

Abreu, R. C. R., Hoffmann, W. A., Vasconcelos, H. L., Pilon, N. A., Rossatto, D. R., & Durigan, G. (2017). The biodiversity cost of carbon sequestration in tropical savanna. *Science Advances*, *August*, 1–8.

Andreoni, M., & Londoño, E. (2019). Amid Outrage Over Rainforest Fires, Many in the Amazon Remain Defiant. *The New York Times*.

Austin, K. G., González-Roglich, M., Schaffer-Smith, D., Schwantes, A. M., & Swenson, J. J. (2017). Erratum: Trends in size of tropical deforestation events signal increasing dominance of industrial-scale drivers (2017 *Environ. Res. Lett.* **5** 054009). *Environmental Research Letters*, *12*(7), 079601. https://doi.org/10.1088/1748-9326/aa7760

Behling, H. (1998). Late Quaternary vegetational and climatic changes in Brazil. *Review of Palaeobotany and Palynology*, *99*(2), 143–156. https://doi.org/10.1016/S0034-6667(97)00044-4

Berhe, A. A., Harden, J. W., Torn, M. S., Kleber, M., Burton, S. D., & Harte, J. (2012). Persistence of soil organic matter in eroding versus depositional landform positions. *Journal of Geophysical Research: Biogeosciences*, *117*, 1–16. https://doi.org/10.1029/2011JG001790

Bird, B. W., Abbott, M. B., Vuille, M., Rodbell, D. T., Stansell, N. D., & Rosenmeier, M. F. (2011). A 2,300-year-long annually resolved record of the South American summer monsoon from the Peruvian Andes. *Proceedings of the National Academy of Sciences of the United States of America*, *108*(21), 8583–8588. https://doi.org/10.1073/pnas.1003719108

Bomfim, B., Silva, L. C. R., Doane, T. A., & Horwath, W. R. (2019). Interactive effects of land-use change and topography on asymbiotic nitrogen fixation in the Brazilian Atlantic Forest. *Biogeochemistry*, *142*(1), 137–153. https://doi.org/10.1007/s10533-018-0525-z

Bomfim, B., Silva, L. C. R., Marimon-Júnior, B. H., Marimon, B. S., Doane, T. A., & Horwath, W. R. (2020). Fire Affects Asymbiotic Nitrogen Fixation in Southern Amazon Forests. *Journal of Geophysical Research: Biogeosciences*, *125*(2). https://doi.org/10.1029/2019JG005383

Brannstrom, C., Jepson, W., Filippi, A. M., Redo, D., Xu, Z., & Ganesh, S. (2008). Land change in the Brazilian Savanna (Cerrado), 1986-2002: Comparative analysis and implications for land-use policy. *Land Use Policy*, *25*(4), 579–595. https://doi.org/10.1016/j.landusepol.2007.11.008

Capriles, J. M., Lombardo, U., Maley, B., Zuna, C., Veit, H., & Kennett, D. J. (2019). Persistent Early to Middle Holocene tropical foraging in southwestern Amazonia. *Science Advances*, *5*(4), eaav5449. https://doi.org/10.1126/sciadv.aav5449

Cruz, F. W., Burns, S. J., Karmann, I., Sharp, W. D., Vuille, M., Cardoso, A. O., Ferrari, J. A., Dias, P. L. S., & Viana, O. (2005). Insolation-driven changes in atmospheric circulation over the past 116,000 years in subtropical Brazil. *Nature*, *434*, 63–65. https://doi.org/10.1029/2003JB002684

Dexter, K. G., Pennington, R. T., Oliveira-filho, A. T., Bueno, M. L., Miranda, P. L. S. De, Neves, D. M., Osborne, C., Langan, L. J., & Dexter, K. G. (2018). Inserting Tropical Dry Forests Into the Discussion on Biome Transitions in the Tropics. *Frontiers in Ecology and Evolution*, *6*(July), 1–7. https://doi.org/10.3389/fevo.2018.00104

Didan, K. (2015). *MOD13A1 MODIS/Terra Vegetation Indices 16-Day L3 Global 500m SIN Grid V006.* NASA EOSDIS Land Processes DAAC. https://doi.org/10.5067/MODIS/MOD13A1.006

Duarte-guardia, S., Peri, P. L., Amelung, W., Sheil, D., Laffan, S. W., Borchard, N., Bird, M. I., & Peri, P. L. (2019). Better estimates of soil carbon from geographical data : a revised global approach. *Mitigation and Adaptation Strategies for Global Change*, 355–372.

Elbasiouny, H., Abowaly, M., Abu-Alkheir, A., & Gad, A. A. (2014). Spatial variation of soil carbon and nitrogen pools by using ordinary Kriging method in an area of north Nile Delta, Egypt. *Catena*, *113*, 70–78. https://doi.org/10.1016/j.catena.2013.09.008

Elias, F., Hur, B., Junior, M., Júnior, F., Oliveira, M. De, Carlos, J., Oliveira, A. De, & Schwantes, B. (2019). Soil and topographic variation as a key factor driving the distribution of tree fl ora in the Amazonia / Cerrado transition. *Acta Oecologica*, *100*(July), 103467. https://doi.org/10.1016/j.actao.2019.103467

Flores, B. M., Staal, A., Jakovac, C. C., Hirota, M., Holmgren, M., & Oliveira, R. S. (2019). Soil erosion as a resilience drain in disturbed tropical forests. *Plant and Soil*. https://doi.org/10.1007/s11104-019-04097-8

Frazer, G. W. (1999). *Gap Light Analyzer (GLA):*

Freitas, F. L. M., Sparovek, G., Berndes, G., Persson, U. M., Englund, O., Barretto, A., & Mörtberg, B. (2018). Potential increase of legal deforestation in Brazilian Amazon after Forest Act revision. *Nature Sustainability*, *1*(11), 665–670.

Garcia, E. S., Swann, A. L. S., Villegas, J. C., Breshears, D. D., Law, D. J., Saleska, S. R., & Stark, S. C. (2016). Synergistic Ecoclimate Teleconnections from Forest Loss in Different Regions Structure Global Ecological Responses. *PLOS ONE*, 1–12. https://doi.org/10.1371/journal.pone.0165042

Hare, V. J., Loftus, E., Jeffrey, A., & Ramsey, C. B. (2018). Atmospheric CO2 effect on stable carbon isotope composition of terrestrial fossil archives. *Nature Communications*, *9*. https://doi.org/10.1038/s41467-017-02691-x

Hoffmann, U., Hoffmann, T., Jurasinski, G., Glatzel, S., & Kuhn, N. J. (2014). Assessing the spatial variability of soil organic carbon stocks in an alpine setting (Grindelwald, Swiss Alps). *Geoderma*, *232–234*, 270–283. https://doi.org/10.1016/j.geoderma.2014.04.038

Hoffmann, W. A., Geiger, E. L., Gotsch, S. G., Rossatto, D. R., Silva, L. C. R., Lau, O. L., Haridasan, M., & Franco, A. C. (2012). Ecological thresholds at the savanna-forest boundary : how plant traits , resources and fire govern the distribution of tropical biomes. *Ecology Letters*, 759–768. https://doi.org/10.1111/j.1461-0248.2012.01789.x

Ladd, B., Laffan, S. W., Amelung, W., Peri, P. L., Silva, L. C. R., Gervassi, P., Bonser, S. P., & Navall, M. (2013). Estimates of soil carbon concentration in tropical and temperate forest and woodland from available GIS data on three continents. *Global Ecology and Biogeography*, 461–469. https://doi.org/10.1111/j.1466-8238.2012.00799.x

Ladd, B., Peri, P. L., Pepper, D. A., Silva, L. C. R., Sheil, D., Bonser, S. P., Laffan, S. W., Amelung, W., Ekblad, A., Eliasson, P., Bahamonde, H., Duarte-Guardia, S., & Bird, M. (2014). Carbon isotopic signatures of soil organic matter correlate with leaf area index across woody biomes. *Journal of Ecology*, *102*(6), 1606–1611. https://doi.org/10.1111/1365-2745.12309

Levy, M. C., Lopes, A. V., Cohn, A., Larsen, L. G., & Thompson, S. E. (2018). Land Use Change Increases Streamflow Across the Arc of Deforestation in Brazil. *Geophysical Research Letters*, *45*(8), 3520–3530. https://doi.org/10.1002/2017GL076526

Lombardo, U., Iriarte, J., Hilbert, L., Ruiz-Pérez, J., Capriles, J. M., & Veit, H. (2020). Early Holocene crop cultivation and landscape modification in Amazonia. *Nature*, *581*(7807), 190–193. https://doi.org/10.1038/s41586-020-2162-7

Lombardo, U., Ruiz-pérez, J., Rodrigues, L., Mestrot, A., Mayle, F., Madella, M., Szidat, S., & Veit, H. (2019). Holocene land cover change in south-western Amazonia inferred from paleoflood archives. *Global and Planetary Change*, *174*, 105–114.

Maezumi, S. Y., Robinson, M., Souza, J. de, Urrego, D. H., Schaan, D., Alves, D., & Iriarte, J. (2018). New insights from pre-Columbian land use and fire management in Amazonian dark earth forests. *Frontiers in Ecology and Evolution*, *6*(AUG), 111. https://doi.org/10.3389/fevo.2018.00111

Malhi, Y., Roberts, J. T., Betts, R. A., Killeen, T. J., Li, W., & Nobre, C. A. (2008). Climate Change, Deforestation, and the Fate of the Amazon. *Science*, *January*, 169–173.

Marchant, R., & Hooghiemstra, H. (2004). Rapid environmental change in African and South American tropics around 4000 years before present : a review. *Earth-Science Reviews*, *66*, 217–260. https://doi.org/10.1016/j.earscirev.2004.01.003

Marimon, B. S., Lima, E. S., Duarte, T. G., & Chieregatto, L. C. (2006). Observations on the vegetation of northeastern Mato Grosso, Brazil. IV. An analysis of the Cerrado-Amazonian Forest ecotone. *Edinburgh Journal of Botany*, *63*(2–3), 323–341.

Miranda, S. do C. de, Bustamante, M., Palace, M., Hagen, S., Keller, M., & Ferreira, L. G. (2014). Regional Variations in Biomass Distribution in Brazilian Savanna Woodland. *Biotropica*, *46*(2), 125–138.

Mishra, U., & Slater, B. (2009). Predicting Soil Organic Carbon Stock Using Profi le Depth Distribution Functions and Ordinary Kriging. *Soil Science Society of America Journal*, *73*(2). https://doi.org/10.2136/sssaj2007.0410

Nobre, C., & Lovejoy, T. E. (2018). Amazon Tipping Point. *Science Advances*, *0*(February), 1–2. https://doi.org/10.1126/sciadv.aat2340

Oliver, M. A., & Webster, R. (2014). Catena A tutorial guide to geostatistics : Computing and modelling variograms and kriging. *Catena*, *113*, 56–69. https://doi.org/10.1016/j.catena.2013.09.006

Pausas, J. G., & Bond, W. J. (2020). Alternative biome states in terrestrial ecosystems. *Trends in Plant Science*.

Posth, C., Nakatsuka, N., Lazaridis, I., Fehren-schmitz, L., Krause, J., Reich, D., Posth, C., Nakatsuka, N., Lazaridis, I., Skoglund, P., & Mallick, S. (2018). Reconstructing the Deep Population History of Central and South America Article Reconstructing the Deep Population History of Central and South America. *Cell (Cambridge)*, 1185–1197. https://doi.org/10.1016/j.cell.2018.10.027

Rosan, T. M., Aragão, L. E. O. C., Oliveras, I., & Phillips, O. L. (2019). Extensive 21st - Century Woody Encroachment in South America ' s Savanna. *Geophysical Research Letters*, 1–10. https://doi.org/10.1029/2019GL082327

Sanaiotti, T. M., Martinelli, L. A., Victoria, R. L., Trumbore, S. E., & Camargo, P. B. (2002). Past Vegetation Changes in Amazon Savannas Determined Using Carbon Isotopes of Soil Organic Matter1. *Biotropica*, *34*(1), 2. https://doi.org/10.1646/0006-3606(2002)034[0002:PVCIAS]2.0.CO;2

Sande, M. T., Gosling, W., Correa-Metrio, A., Prado-Junior, J., Poorter, L., Oliveira, R. S., Mazzei, L., & Bush, M. B. (2019). A 7000-year history of changing plant trait composition in an Amazonian landscape; the role of humans and climate. *Ecology Letters*, ele.13251. https://doi.org/10.1111/ele.13251

Santos, G. M., Southon, J. R., Drenzek, N. J., Ziolkowski, L. A., Druffel, E., Xu, X., Zhang, D., Trumbore, S., Eglinton, T. I., & Hughen, K. A. (2019). Blank Assessment for Ultra-Small Radiocarbon Samples: Chemical Extraction and Separation Versus AMS. *Radiocarbon*, *52*(2), 1322–1335.

Schmidt, M. W. I., Torn, M. S., Abiven, S., Dittmar, T., Guggenberger, G., Janssens, I. A., Lehmann, J., Manning, D. A. C., Nannipieri, P., Rasse, D. P., Kleber, M., & Ko, I. (2011). Persistence of soil organic matter as an ecosystem property. *Nature (London)*. https://doi.org/10.1038/nature10386

Silva, L. C. R., Doane, T. A., Corrêa, R. S., Valverde, V., Pereira, E. I. P., & Horwath, W. R. (2015). Iron-mediated stabilization of soil carbon amplifies the benefits of ecological restoration in degraded lands. *Ecological Applications*, *25*(5), 1226–1234.

Silva, L. C. R., & Lambers, H. (2018). Soil-plant-atmosphere interactions: ecological and biogeographical considerations for climate-change research. In *Climate Change Impacts on Soil Processes and Ecosystem Properties* (pp. 29–60).

Silva, L C R, & Anand, M. (2013). Historical links and new frontiers in the study of forest-atmosphere interactions. *Community Ecology*, *14*(2), 208–218. https://doi.org/10.1556/ComEc.14.2013.2.11

Silva, Lucas C. R., & Lambers, H. (2020). Soil-plant-atmosphere interactions: structure, function, and predictive scaling for climate change mitigation. *Plant and Soil*, 1–23. https://doi.org/10.1007/s11104-020-04427-1

Silva, Lucas C.R., Sternberg, L., Haridasan, M., Hoffmann, W. A., Miralles-Wilhelm, F., & Franco, A. C. (2008). Expansion of gallery forests into central Brazilian savannas. *Global Change Biology*, *14*(9), 2108–2118. https://doi.org/10.1111/j.1365-2486.2008.01637.x

Silva, Lucas C R. (2014). Importance of climate-driven forest – savanna biome shifts in anthropological and ecological research. *Proceedings of the National Academy of Sciences*, *111*(37), 3831–3832. https://doi.org/10.1073/pnas.1413205111

Silva, Lucas C R, Haridasan, M., & Hoffmann, W. A. (2010). Not all forests are expanding over central Brazilian savannas. *Plant and Soil*, 431–442. https://doi.org/10.1007/s11104-010-0358-6

Silva, Lucas C R, Hoffmann, W. A., Rossatto, D. R., Franco, A. C., Horwath, W. R., Plant, S., December, N., Haridasan, M., Franco, A. C., & Horwath, W. R. (2013). Can savannas become forests ? A coupled analysis of nutrient stocks and fire thresholds in central Brazil. *Plant and Soil*, *373*(1), 829–842.

Smith, T. & Smith, R. (2015). *Elements of Ecology* (Ninth). Pearson.

Smith, R. J., & Mayle, F. E. (2018). Impact of mid- to late Holocene precipitation changes on vegetation across lowland tropical South America : a paleo-data synthesis. *Quaternary Research*, 134–155. https://doi.org/10.1017/qua.2017.89

Soil Survey Staff. (2014). *Keys to Soil Taxonomy*.

Souza, J. G. De, Schaan, D. P., Robinson, M., Barbosa, A. D., Aragão, L. E. O. C., Hur, B., Jr, M., Marimon, B. S., Brasil, I., Khan, S. S., Nakahara, F. R., & Iriarte, J. (2018). Pre-Columbian earth-builders settled along the entire southern rim of the Amazon. *Nature Communications*, *9*, 1125. https://doi.org/10.1038/s41467-018-03510-7

Spracklen, D. V, Arnold, S. R., & Taylor, C. M. (2012). Observations of increased tropical rainfall preceded by air passage over forests. *Nature*. https://doi.org/10.1038/nature11390

Staal, A., Tuinenburg, O. A., Bosmans, J. H. C., Holmgren, M., Van Nes, E. H., Scheffer, M., Zemp, D. C., & Dekker, S. C. (2018). Forest-rainfall cascades buffer against drought across the Amazon. *Nature Climate Change*, *8*(6), 539–543. https://doi.org/10.1038/s41558-018-0177-y

Sternberg, L. D. S. L. (2001a). Savanna-forest hysteresis in the tropics. *Global Ecology and Biogeography*, *10*(4), 369–378. https://doi.org/10.1046/j.1466-822X.2001.00243.x

Sternberg, L. D. S. L. (2001b). Savanna-Forest Hysteresis in the Tropics. *Global Ecology and Biogeography*, *10*(4), 369–378.

Team, A. (2019). *Application for Extracting and Exploring Analysis Ready Samples (AppEEARS)*. NASA EOSDIS Land Processes Distributed Active Archive Center (LP DAAC), USGS/Earth Resources Observation and Science (EROS) Center, Sioux Falls, South Dakota, USA.

Trumbore, S. (2000). Age of soil organic matter and soil respiration: radiocarbon constraints on belowground C dynamics. *Ecological Applications*.

Trumbore, S. (2009). Radiocarbon and Soil Carbon Dynamics. *Annual Review of Earth and Planetary Sciences*, *37*, 47–66. https://doi.org/10.1146/annurev.earth.36.031207.124300

Veldman, J. W., Overbeck, G. E., Negreiros, D., Mahy, G., Le Stradic, S., Fernandes, G. W., Durigan, G., Buisson, E., Putz, F. E., & Bond, W. J. (2015). Where Tree Planting and Forest Expansion are Bad for Biodiversity and Ecosystem Services. *BioScience*, *65*(10), 1011–1018. https://doi.org/10.1093/biosci/biv118

Victoria, R. L., Fernandes, F., Martinelli, L. A., Cassia Piccolo, M., Camargo, P. B., & Trumbore, S. (1995). Past vegetation changes in the Brazilian Pantanal arboreal-grassy savanna ecotone by using carbon isotopes in the soil organic matter. *Global Change Biology*, *1*(3), 165–171. https://doi.org/10.1111/j.1365-2486.1995.tb00018.x

von Fischer, J. C., Tieszen, L. L., & Schimel, D. S. (2008). Climate controls on C3 vs. C4 productivity in North American grasslands from carbon isotope composition of soil organic matter. *Global Change Biology*, *14*(5), 1141–1155. https://doi.org/10.1111/j.1365-2486.2008.01552.x

Vuille, M., Burns, S. J., Taylor, B. L., Cruz, F. W., Bird, B. W., Abbott, M. B., Kanner, L. C., Cheng, H., & Novello, V. F. (2012). A review of the South American monsoon history as recorded in stable isotopic proxies over the past two millennia. *Climate of the Past*, *8*(4), 1309–1321. https://doi.org/10.5194/cp-8-1309-2012

Ward, B. M., Wong, C. I., Novello, V. F., Mcgee, D., Santos, R. V, Silva, L. C. R., Cruz, F. W., Wang, X., Edwards, R. L., & Cheng, H. (2019). Reconstruction of Holocene coupling between the South American Monsoon System and local moisture variability from speleothem d 18 O and 87 Sr / 86 Sr records. *Quaternary Science Reviews*, *210*, 51–63.

Wortham, B. E., Wong, C. I., Silva, L. C. R., McGee, D., Montañez, I. P., Troy Rasbury, E., Cooper, K. M., Sharp, W. D., Glessner, J. J. G., & Santos, R. V. (2017). Assessing response of local moisture conditions in central Brazil to variability in regional monsoon intensity using speleothem87Sr/86Sr values. *Earth and Planetary Science Letters*, *463*, 310–322. https://doi.org/10.1016/j.epsl.2017.01.034

Zemp, D. C., Schleussner, C., Barbosa, H. M. J., Hirota, M., Montade, V., Sampaio, G., Staal, A., Wang-erlandsson, L., & Rammig, A. (2017). Self-amplified Amazon forest loss due to vegetation-atmosphere feedbacks. *Nature Communications*, *8*, 1–10. https://doi.org/10.1038/ncomms14681

CHAPTER III

Abatzoglou, J. T., & Williams, A. P. (2016). Impact of anthropogenic climate change on wildfire across western US forests. *Proceedings of the National Academy of Sciences of the United States of America*, *113*(42), 11770–11775. https://doi.org/10.1073/pnas.1607171113

Abney, R. B., Sanderman, J., Johnson, D., Fogel, M. L., & Berhe, A. A. (2017). Post-wildfire Erosion in mountainous terrain leads to rapid and major redistribution of soil organic carbon. *Frontiers in Earth Science*, *5*(November), 1–16. https://doi.org/10.3389/feart.2017.00099

Abrahams, E. R., Kaste, J. M., Ouimet, W., & Dethier, D. P. (2018). Asymmetric hillslope erosion following wildfire in Fourmile Canyon, Colorado. *Earth Surface Processes and Landforms*, *43*(9), 2009–2021. https://doi.org/10.1002/esp.4348

Anders, S., & Huber, W. (2010). Differential expression analysis for sequence count data. *Genome Biology*. https://doi.org/10.1074/jbc.272.7.4310

Averill, C., & Hawkes, C. V. (2016). Ectomycorrhizal fungi slow soil carbon cycling. *Ecology Letters*, *19*(8), 937–947. https://doi.org/10.1111/ele.12631

BAER. (n.d.). Mapping Burn Severity for Burned Area Emergency Response (BAER) and Monitoring Trends in Burn Severity (MTBS). Retrieved from https://www.mtbs.gov/baer

Bird, M. I., Veenendaal, E. M., Moyo, C., Lloyd, J., & Frost, P. (2000). Effect of fire and soil texture on soil carbon in a sub-humid savanna (Matopos, Zimbabwe). *Geoderma*, *94*(1), 71–90. https://doi.org/10.1016/S0016-7061(99)00084-1

Bödeker, I. T. M., Lindahl, B. D., Olson, Å., & Clemmensen, K. E. (2016). Mycorrhizal and saprotrophic fungal guilds compete for the same organic substrates but affect decomposition differently. *Functional Ecology*, *30*(12), 1967–1978. https://doi.org/10.1111/1365-2435.12677

Bokulich, N. A., & Mills, D. A. (2013). Improved selection of internal transcribed spacer-specific primers enables quantitative, ultra-high-throughput profiling of fungal communities. *Applied and Environmental Microbiology*, *79*(8), 2519–2526. https://doi.org/10.1128/AEM.03870-12

Callahan, B. J., McMurdie, P. J., Rosen, M. J., Han, A. W., Johnson, A. J. A., & Holmes, S. P. (2016). DADA2: High-resolution sample inference from Illumina amplicon data. *Nature Methods*, *13*(7), 581–583. https://doi.org/10.1038/nmeth.3869

Caporaso, J. G., Kuczynski, J., Stombaugh, J., Bittinger, K., Bushman, F. D., Costello, E. K., … Knight, R. (2010). QIIME allows analysis of high-throughput community sequencing data. *Nature Methods*, *7*(5), 335–336. https://doi.org/10.1038/nmeth.f.303

Cotrufo, M. F., Ranalli, M. G., Haddix, M. L., Six, J., & Lugato, E. (2019). Soil carbon storage informed by particulate and mineral-associated organic matter. *Nature Geoscience*, *12*(12), 989–994. https://doi.org/10.1038/s41561-019-0484-6

Cotrufo, M. F., Wallenstein, M. D., Boot, C. M., Denef, K., & Paul, E. (2013). The Microbial Efficiency-Matrix Stabilization (MEMS) framework integrates plant litter decomposition with soil organic matter stabilization: Do labile plant inputs form stable soil organic matter? *Global Change Biology*, *19*(4), 988–995. https://doi.org/10.1111/gcb.12113

Fernandez, C. W., & Kennedy, P. G. (2016). Revisiting the "Gadgil effect": Do interguild fungal interactions control carbon cycling in forest soils? *New Phytologist*, *209*(4), 1382–1394. https://doi.org/10.1111/nph.13648

Ford, S. A., Kleinman, J. S., & Hart, J. L. (2018). Effects of wind disturbance and salvage harvesting on macrofungal communities in a Pinus woodland. *Forest Ecology and Management*, *407*(October 2017), 31–46. https://doi.org/10.1016/j.foreco.2017.10.010

Francos, M., Úbeda, X., Pereira, P., & Alcañiz, M. (2018). Long-term impact of wildfire on soils exposed to different fire severities. A case study in Cadiretes Massif (NE Iberian Peninsula). *Science of the Total Environment*, *615*, 664–671. https://doi.org/10.1016/j.scitotenv.2017.09.311

Ghannam, R. B., & Techtmann, S. M. (2021). Machine learning applications in microbial ecology, human microbiome studies, and environmental monitoring. *Computational and Structural Biotechnology Journal*, *19*, 1092–1107. https://doi.org/10.1016/j.csbj.2021.01.028

Harris, D., Horwáth, W. R., & van Kessel, C. (2001). Acid fumigation of soils to remove carbonates prior to total organic carbon or CARBON-13 isotopic analysis. *Soil Science Society of America Journal*, *65*(6), 1853–1856. https://doi.org/10.2136/sssaj2001.1853

Hobbie, E. A. (2006). Carbon allocation to ectomycorrhizal fungi correlates with belowground allocation in culture studies. *Ecology*, *87*(3), 563–569. https://doi.org/10.1890/05-0755

Hoggard, M., Vesty, A., Wong, G., Montgomery, J. M., Fourie, C., Douglas, R. G., … Taylor, M. W. (2018). Characterizing the human mycobiota: A comparison of small subunit rRNA, ITS1, ITS2, and large subunit rRNA genomic targets. *Frontiers in Microbiology*, *9*(SEP), 1–14. https://doi.org/10.3389/fmicb.2018.02208

Hrelja, I., Šestak, I., & Bogunović, I. (2020). Wildfire impacts on soil physical and chemical properties - A short review of recent studies. *Agriculturae Conspectus Scientificus*, *85*(4), 293–301.

Jordanova, N., Jordanova, D., & Barrón, V. (2019). Wildfire severity: Environmental effects revealed by soil magnetic properties. *Land Degradation and Development*, *30*(18), 2226–2242. https://doi.org/10.1002/ldr.3411

Juan-Ovejero, R., Molinas-Gonzàlez, C. R., Leverkus, A. B., Peinado, F. J. M., & Castro, J. (2021). Decadal effect of post-fire management treatments on soil carbon and nutrient concentrations in a burnt Mediterranean forest. *Forest Ecology and Management*.

Jupke, J. F., & Schäfer, R. B. (2020). Should ecologists prefer model- over distance-based multivariate methods? *Ecology and Evolution*, *10*(5), 2417–2435. https://doi.org/10.1002/ece3.6059

Kessy Abarenkov, R. Henrik Nilsson, Karl-Henrik Larsson, Ian J. Alexander, Ursula Eberhardt, Susanne Erland, Klaus Høiland, Rasmus Kjøller, Ellen Larsson, Taina Pennanen, Robin Sen, Andy F. S. Taylor, Leho Tedersoo, Björn M. Ursing, Trude Vrålstad, Kare L, U. K. (2010). The UNITE database for molecular identification of fungi – recent updates and future perspectives. *New Phytologist*, 264–266.

Keyser, A. R., & Westerling, A. L. R. (2019). Predicting increasing high severity area burned for three forested regions in the western United States using extreme value theory. *Forest Ecology and Management*, *432*(October 2018), 694–706. https://doi.org/10.1016/j.foreco.2018.09.027

Kirkby, C. A., Kirkegaard, J. A., Richardson, A. E., Wade, L. J., Blanchard, C., & Batten, G. (2011). Stable soil organic matter: A comparison of C:N:P:S ratios in Australian and other world soils. *Geoderma*, *163*(3–4), 197–208. https://doi.org/10.1016/j.geoderma.2011.04.010

Kurth, V. J., MacKenzie, M. D., & DeLuca, T. H. (2006). Estimating charcoal content in forest mineral soils. *Geoderma*, *137*(1–2), 135–139. https://doi.org/10.1016/j.geoderma.2006.08.003

Lavallee, J. M., Conant, R. T., Haddix, M. L., Follett, R. F., Bird, M. I., & Paul, E. A. (2019). Selective preservation of pyrogenic carbon across soil organic matter fractions and its influence on calculations of carbon mean residence times. *Geoderma*, *354*(July), 113866. https://doi.org/10.1016/j.geoderma.2019.07.024

Lavallee, Jocelyn M., Soong, J. L., & Cotrufo, M. F. (2019). Conceptualizing soil organic matter into particulate and mineral-associated forms to address global change in the 21st century. *Global Change Biology*, *26*(1), 261–273. https://doi.org/10.1111/gcb.14859

Lehmann, J., & Kleber, M. (2015). The contentious nature of soil organic matter. *Nature*, *528*(7580), 60–68. https://doi.org/10.1038/nature16069

Leverkus, A. B., Rey Benayas, J. M., Castro, J., Boucher, D., Brewer, S., Collins, B. M., … Gustafsson, L. (2018). Salvage logging effects on regulating and supporting ecosystem services — A systematic map. *Canadian Journal of Forest Research*, *48*(9), 983–1000. https://doi.org/10.1139/cjfr-2018-0114

Leys, B. A., Likens, G. E., Johnson, C. E., Craine, J. M., & Mclauchlan, K. K. (2016). Natural and anthropogenic drivers of calcium depletion in a northern forest during the last millennium Linked references are available on JSTOR for this article : https://doi.org/10.1073/pnas.1611402113

Martin, M. (2011). Cutadapt removes adapter sequences from high-throughput sequencing reads. *EMBnet.Journal*, *17*, 10–12.

Massman, W. J. (2012). Modeling soil heating and moisture transport under extreme conditions: Forest fires and slash pile burns. *Water Resources Research*, *48*(10), 1–12. https://doi.org/10.1029/2011WR011710

Massman, William J., Frank, J. M., & Mooney, S. J. (2010). Advancing Investigation and Physical Modeling of First-Oder Fire Effects on Soils, *6*(1).

Maxwell, T. (n.d.). Particle Size Analysis.

McMurdie, P. J., & Holmes, S. (2013). Phyloseq: An R Package for Reproducible Interactive Analysis and Graphics of Microbiome Census Data. *PLoS ONE*, *8*(4). https://doi.org/10.1371/journal.pone.0061217

Nguyen, N. H., Song, Z., Bates, S. T., Branco, S., Tedersoo, L., Menke, J., … Kennedy, P. G. (2016). FUNGuild: An open annotation tool for parsing fungal community datasets by ecological guild. *Fungal Ecology*, *20*, 241–248. https://doi.org/10.1016/j.funeco.2015.06.006

Parsons, A., Robichaud, P. R., Lewis, S. A., Napper, C., & Clark, J. T. (2010). Field guide for mapping post-fire soil burn severity. *USDA Forest Service - General Technical Report RMRS-GTR*, (243), 1–49.

Peay, K. G., Garbelotto, M., & Bruns, T. D. (2009). Spore heat resistance plays an important role in disturbance-mediated assemblage shift of ectomycorrhizal fungi colonizing Pinus muricata seedlings. *Journal of Ecology*, *97*(3), 537–547. https://doi.org/10.1111/j.1365-2745.2009.01489.x

PRISM. (2022). PRISM Climate Group, Oregon State University. Retrieved January 16, 2022, from https://prism.oregonstate.edu

Rincón, A., Santamaría, B. P., Ocaña, L., & Verdú, M. (2014). Structure and phylogenetic diversity of post-fire ectomycorrhizal communities of maritime pine. *Mycorrhiza*, *24*(2), 131–141. https://doi.org/10.1007/s00572-013-0520-0

RStudio Team. (2020). RStudio: Integrated Development for R.

Santín, C., Doerr, S. H., Kane, E. S., Masiello, C. A., Ohlson, M., de la Rosa, J. M., … Dittmar, T. (2016). Towards a global assessment of pyrogenic carbon from vegetation fires. *Global Change Biology*, *22*(1), 76–91. https://doi.org/10.1111/gcb.12985

Santos, F., Rice, D. M., Bird, J. A., & Berhe, A. A. (2021). Pyrolysis temperature and soil depth interactions determine PyC turnover and induced soil organic carbon priming. *Biogeochemistry*, *153*(1), 47–65. https://doi.org/10.1007/s10533-021-00767-x

Schoeneberger, P. J., Wysocki, D. A., Benham, E. C., & Broderson, W. D. (2002). Field Book for Describing and Sampling Soils. *National Soil Survey Center*, *33*(September), 1–228. Retrieved from http://lawr.ucdavis.edu/faculty/gpast/hyd151/soilsfieldguide.pdf

Schroth, A. W., Bostick, B. C., Graham, M., Kaste, J. M., Mitchell, M. J., & Friedland, A. J. (2007). Sulfur species behavior in soil organic matter during decomposition. *Journal of Geophysical Research: Biogeosciences*, *112*(4), 1–10. https://doi.org/10.1029/2007JG000538

Serrano-Ortiz, P., Marañón-Jiménez, S., Reverter, B. R., Sánchez-Cañete, E. P., Castro, J., Zamora, R., & Kowalski, A. S. (2011). Post-fire salvage logging reduces carbon sequestration in Mediterranean coniferous forest. *Forest Ecology and Management*, *262*(12), 2287–2296. https://doi.org/10.1016/j.foreco.2011.08.023

Thorn, S., Bässler, C., Brandl, R., Burton, P. J., Cahall, R., Campbell, J. L., … Müller, J. (2018). Impacts of salvage logging on biodiversity: A meta-analysis. *Journal of Applied Ecology*, *55*(1), 279–289. https://doi.org/10.1111/1365-2664.12945

Throop, H. L., Archer, S. R., Monger, H. C., & Waltman, S. (2012). When bulk density methods matter: Implications for estimating soil organic carbon pools in rocky soils. *Journal of Arid Environments*, *77*(1), 66–71. https://doi.org/10.1016/j.jaridenv.2011.08.020

USDA. (2019). *Inherent Factors Affecting Bulk Density and Available Water Capacity*.

Westerling, A. L. R. (2016). Increasing western US forest wildfire activity: Sensitivity to changes in the timing of spring. *Philosophical Transactions of the Royal Society B: Biological Sciences*, *371*(1696). https://doi.org/10.1098/rstb.2015.0178

CHAPTER IV

Ames, K. M. (2003) 'The Northwest Coast', *Evolutionary Anthropology*, 12(1), pp. 19–33. doi: 10.1002/evan.10102.

Arnaud, F. *et al.* (2012) 'Lake Bourget regional erosion patterns reconstruction reveals Holocene NW European Alps soil evolution and paleohydrology', *Quaternary Science Reviews*, 51, pp. 81–92. doi: 10.1016/j.quascirev.2012.07.025.

Bennett, K. and Willis, K. J. (2001) 'Pollen', in *Tracking Environmental Change Using Lake Sediments.*

Blaauw, M. (2010) 'Methods and code for "classical" age-modelling of radiocarbon sequences', *Quaternary Geochronology*, 5(5), pp. 512–518. doi: 10.1016/j.quageo.2010.01.002.

BRANTLEY, S. L. *et al.* (2011) 'Twelve testable hypotheses on the geobiology of weathering', *Geobiology*, p. 24. Available at: http://ridum.umanizales.edu.co:8080/jspui/bitstream/6789/377/4/Muñoz_Zapata_Adriana_Patricia_Artículo_2011.pdf.

Brown, E. T. (2015) 'Estimation of Biogenic Silica Concentrations Using Scanning XRF: Insights from Studies of Lake Malawi Sediments', (August), pp. 267–277. doi: 10.1007/978-94-017-9849-5_9.

Burn, M. J. and Palmer, S. E. (2014) 'Solar forcing of Caribbean drought events during the last millennium', *Journal of Quaternary Science*, 29(8), pp. 827–836. doi: 10.1002/jqs.2660.

Constantine, D. *et al.* (2016) *Shadow Lake Integrated Aquatic Vegetation Management Plan*. King County.

Crausbay, Shelley D *et al.* (2017) 'Fire catalyzed rapid ecological change in lowland coniferous forests of the Paci fi c Northwest over the past 14 , 000 years', 98(9), pp. 2356–2369.

Crausbay, Shelley D. *et al.* (2017) 'Fire catalyzed rapid ecological change in lowland coniferous forests of the Pacific Northwest over the past 14,000 years', *Ecology*, 98(9), pp. 2356–2369. doi: 10.1002/ecy.1897.

Cwynar, L. C. . (2019) 'Fire and the Forest History of the North Cascade Range', 68(4), pp. 791–802.

Davies, S. J., Lamb, H. F. and Roberts, S. J. (2015) 'Core Scanning in Palaeolimnology: Recent Developments', in *Micro-XRF Studies of Sediment Cores*, pp. 189–226.

Gavin, D. G. and Brubaker, L. B. (2013) 'Postglacial climate and fire-mediated vegetation change on the western Olympic Peninsula , Washington (USA)', 83(4), pp. 471–489.

Hallett, D. J. *et al.* (2003) '11 000 Years of fire history and climate in the mountain hemlock rain forests of southwestern British Columbia based on sedimentary charcoal', *Canadian Journal of Forest Research*, 33(2), pp. 292–312. doi: 10.1139/x02-177.

Halofsky, J. E., Peterson, D. L. and Harvey, B. J. (2020) 'Changing wildfire, changing forests: the effects of climate change on fire regimes and vegetation in the Pacific Northwest, USA', *Fire Ecology*, 16(1). doi: 10.1186/s42408-019-0062-8.

Klaus, M., Karlsson, J. and Seekell, D. (2021) 'Tree line advance reduces mixing and oxygen concentrations in arctic–alpine lakes through wind sheltering and organic carbon supply', *Global Change Biology*, 27(18), pp. 4238–4253. doi: 10.1111/gcb.15660.

Leopold, E. B. and Boyd, R. (1999) 'An ecological history of old prairie area, southwestern Washington', *Oregon State University Press*.

Lepofsky, D. *et al.* (2005) 'Climate Change and Culture Change on the Southern Coast of British Columbia 2400-1200 Cal. B.P.: An Hypothesis', *American Antiquity*, 70(2), pp. 267–293. doi: 10.2307/40035704.

Leys, B. A. *et al.* (2016) 'Natural and anthropogenic drivers of calcium depletion in a northern forest during the last millennium Linked references are available on JSTOR for this article ': doi: 10.1073/pnas.1611402113.

Liu, X. *et al.* (2013) 'Estimation of carbonate, total organic carbon, and biogenic silica content by FTIR and XRF techniques in lacustrine sediments', *Journal of Paleolimnology*, 50(3), pp. 387–398. doi: 10.1007/s10933-013-9733-7.

Melles, M. *et al.* (2014) '2 . 8 Million Years of Arctic Climate', 315(2012).

Meyers, P. A. and Lallier-Vergès, E. (1999) 'Lacustrine sedimentary organic matter records of Late Quaternary paleoclimates', *Journal of Paleolimnology*, 21(3), pp. 345–372. doi: 10.1023/A:1008073732192.

Meyers, P. A. and Teranes, J. L. (2001) 'Sediment Organic Matter', in *Tracking Environmental Change Using Lake Sediments*, pp. 239–269.

Millspaugh, S. H. and Whitlock, C. (1995) 'A 750-year fire history based on lake sediment records in central Yellowstone National Park, USA', *The Holocene*, 5(3), pp. 283–292. doi: https://doi.org/10.1177/095968369500500303.

Nelson, D. B. *et al.* (2011) 'Drought variability in the Pacific Northwest from a 6 , 000-yr lake sediment record', pp. 1–6. doi: 10.1073/pnas.1009194108/-/DCSupplemental.www.pnas.org/cgi/doi/10.1073/pnas.1009194108.

Phillips, J. D. and Marion, D. A. (2005) 'Biomechanical effects, lithological variations, and local pedodiversity in some forest soils of Arkansas', *Geoderma*, 124(1–2), pp. 73–89. doi: 10.1016/j.geoderma.2004.04.004.

Porter, S. C. and Swanson, T. W. (1998) 'Radiocarbon age constraints on rates of advance and retreat of the Puget Lobe of the Cordilleran Ice Sheet during the last glaciation', *Quaternary Research*, 50(3), pp. 205–213. doi: 10.1006/qres.1998.2004.

Price, J. R. and Velbel, M. A. (2003) 'Chemical weathering indices applied to weathering profiles developed on heterogeneous felsic metamorphic parent rocks', *Chemical Geology*, 202(3–4), pp. 397–416. doi: 10.1016/j.chemgeo.2002.11.001.

Prichard, S. J. *et al.* (2009) 'Holocene fire and vegetation dynamics in a montane forest, North Cascade Range, Washington, USA', *Quaternary Research*, 72(1), pp. 57–67. doi: 10.1016/j.yqres.2009.03.008.

PRISM (2022) *PRISM Climate Group*.

Schwörer, C. *et al.* (2017) 'Holocene tree line changes in the Canadian Cordillera are controlled by climate and topography', *Journal of Biogeography*, 44(5), pp. 1148–1159. doi: 10.1111/jbi.12904.

Talbot, M. R. (2001) 'Nitrogen Isotopes in Paleolimnology', in *Tracking Environmental Change Using Lake Sediments*, pp. 401–439.

Thompson, R. S. *et al.* (1993) 'Climatic Changes in the Western United States since 18,000 yr B.P.', in *Global Climates since the Last Glacial Maximum*.

Tsukada, M., Sugita, S. and Hibbert, D. M. (1981) *Paleoecology in the Pacific Northwest I. Late Quaternary vegetation and climate. Internationale Vereinigung Für Theoretische Und Angewandtelimnologie, 21, 730–737.*

Unkel, I., Björck, S. and Wohlfarth, B. (2008) 'Deglacial environmental changes on Isla de los Estados (54.4°S), southeastern Tierra del Fuego', *Quaternary Science Reviews*, 27(15–16), pp. 1541–1554. doi: 10.1016/j.quascirev.2008.05.004.

Wallin, M. *et al.* (2010) 'Temporal and spatial variability of dissolved inorganic carbon in a boreal stream network: Concentrations and downstream fluxes', *Journal of Geophysical Research: Biogeosciences*, 115(G2), p. n/a-n/a. doi: 10.1029/2009jg001100.

Walsh, M. K. *et al.* (2015) 'A Regional Perspective on Holocene Fire–Climate–Human Interactions in the Pacific Northwest of North America', *Annals of the Association of American Geographers*, 105(6), pp. 1135–1157. doi: 10.1080/00045608.2015.1064457.

Walsh, M. K., Duke, H. J. and Haydon, K. C. (2018) 'Toward a better understanding of climate and human impacts on late Holocene fire regimes in the Pacific Northwest, USA', *Progress in Physical Geography*, 42(4), pp. 478–512. doi: 10.1177/0309133318783144.

Whitlock, C. (1992) 'Vegetational and climatic history of the Pacific Northwest during the last 20 000 years: implications for understanding present-day biodiversity', *Northwest Environmental Journal*, 8(1), pp. 5–28.